

FSI Study of internal Multiphase Flow in Subsea Piping Components

A Thesis

Presented to

the Faculty of the Department of Mechanical Engineering Technology

University of Houston

In Partial Fulfillment

of the Requirements for the Degree

Master of Science

in Engineering Technology

by

Leonardo Chica

May, 2014

FSI Study of Internal Multiphase Flow in Subsea Piping Components

Leonardo Chica

Approved:

Chairman of the Committee
Dr. Raymond E. Cline, Jr.
Department of Information and Logistics
Technology Chair, College of Technology

Co-Chairman of the Committee
Rares Pascali
Instructional Associate Professor
Mechanical Engineering Technology

Dr. Burak Ozturk,
Group Technology Manager
Wood Group Kenny

Dr. Rupa Iyer
Associate Dean for Research and Graduate
Studies, College of Technology

Dr. Heidar Malki,
Department Chair, Department Engineering
Technology

FSI Study of Internal Multiphase Flow in Subsea Piping Components

An Abstract of A Thesis

Presented to

the Faculty of the Department of Mechanical Engineering Technology

University of Houston

In Partial Fulfillment

of the Requirements for the Degree

Master of Science

in Engineering Technology

by

Leonardo Chica

May, 2014

Abstract

Multi-phase petroleum wells usually produce different configurations of oil and gas with addition of water and sand particles depending on the reservoir characteristics. This four-phase flow introduces many challenges in understanding and analyzing its unpredicted and unsteady behavior, and it sometimes induces significant amplitude vibrations due to oscillating forces, in particular on bends of well jumpers.

It is currently an interest to investigate the effect of the oil-gas-water mixture on the structure of pipelines since a significant response would lead to potential fatigue damage, specifically when oil brings dense sand particles or slug flow develops in the flowline. Oil sands reservoirs might develop chunks or slugs acting as severe dynamic loads such that the pipe starts vibrating at a large magnitude and it collapses.

In this thesis, understanding this Flow Induced Vibration (FIV) phenomenon is important to identify the flow and geometry variables predicting the structural response, and therefore a screening methodology is proposed to examine the potential damage of the amplitude vibrations. FIV is also considered a lock-in mechanism in which it is important to avoid that the slug or fluid frequency falls within $\pm 20\%$ of the natural frequencies. The frequency spectra of the pressure and volume fraction were obtained as a screening technique to identify if the energy of the fluid excites one of the modes of the structure.

This work consists of numerical simulations using a fluid solver (STAR-CCM+) and a stress solver within STAR-CCM+. Computational Fluid Dynamics (CFD) simulations describe the flow patterns developed in the horizontal and vertical sections of the jumper for oil-gas flow, oil-gas-water flow, and oil-gas-water with sand particles. On the structural side, modal analysis was performed using Finite Element Method (FEM) to determine the modes of the structure with its respective natural frequencies. A Fluid Structure Interaction (FSI) methodology was also proposed to study in more detail the response of the system in terms of stresses and displacements if the FIV methodology fails to satisfy the design criteria.

Table of Contents

Abstract	iv
List of Figures	4
List of Tables	8
1. Introduction	9
1.1. Background and Problem Statement.....	9
1.2. Objective.....	10
2. Literature Review	12
2.1. Two-Phase Flow	12
2.2. Three-Phase Flow	16
2.3. Liquid-Solid Flow	18
3. Conservation Equations in Multi-phase Flow	20
3.1. Conservation of Mass	20
3.2. Conservation of Momentum	20
3.2.1. Surface Tension.....	21
3.2.2. Pressure Correction Term	21
3.3. Conservation of Energy	21
4. Conservation Equations in Solid Mechanics	23
4.1. Elasticity Equations	23
5. Fluid Structure Interaction	25
5.1. Flow Induced Vibration	25
5.2. Flow Induced Turbulence	27
6. Multi-phase Flow	29
6.1. Flow Regimes	29
6.1.1. Flow Patterns in Horizontal Pipes.....	30
6.1.2. Flow Patterns in Vertical Pipes.....	31
6.2. Volume fraction	32
6.3. Superficial Velocity	32
6.4. Two-Phase Flow	33
6.4.1. Pressure Difference in Stratified Flow.....	33
6.4.2. The Taitel & Duckler Horizontal Flow Model	35

6.4.3.	Slug Flow	36
6.5.	Three-Phase Flow	37
6.5.1.	Stratified Flow	38
6.5.2.	Slug Flow	40
6.6.	Liquid-Solid Flow	42
6.6.1.	Pressure Build up of Particles	42
6.6.2.	Minimum Required Velocity	43
7.	Subsea Pipe Model and Multi-phase Properties.....	45
7.1.	M-Shaped Jumper Geometry	45
7.2.	Multi-phase Properties	45
8.	Methodology.....	47
8.1.	Computational Fluid Dynamics	49
8.1.1.	Fluid Domain	50
8.1.2.	Turbulence Model	50
8.1.3.	Volume of Fluid (VOF)	51
8.1.4.	Lagrangian Multiphase	51
8.1.5.	Implicit Integration and Time Step	52
8.1.6.	Meshing.....	53
8.1.7.	Boundary Conditions	54
8.1.8.	CFD Physics Models.....	55
8.2.	Finite Element Analysis	55
8.2.1.	Meshing.....	55
8.2.2.	Boundary Conditions	56
8.3.	FSI Analysis.....	56
9.	Benchmark.....	58
10.	Phase I – FIV Results.....	62
10.1.	Modal Analysis	62
10.2.	Oil-Gas Flow.....	63
10.2.1.	Volume Fraction	64
10.2.2.	Pressure Fluctuations	74
10.3.	Oil-Gas-Water Flow.....	76
10.3.1.	Volume Fraction	77

10.3.2.	Pressure Fluctuations	82
10.4.	Oil-Gas-Water Flow with Sand Production	84
10.4.1.	Volume Fraction, Velocity, and Tracking of Sand Particles.....	85
10.4.2.	Pressure	90
10.5.	Summary of CFD Results	90
11.	Phase II – FIV Results	92
11.1.	Oil-Gas Flow (Case 5)	92
11.2.	Oil-Gas-Water Flow (Case 8)	98
12.	Conclusions.....	103
13.	Recommendations and Future Work	104
14.	Bibliography	105
Appendices		108
Appendix A:	Modes Shapes of the Jumper from ABAQUS.....	108
Appendix B:	Computational Performance	112
Appendix C:	Setting up the Mesh in Star-CCM+ for Sensitivity Analysis	116
Appendix D:	Setting up the Lagrangian Particles in STAR-CCM+	124

List of Figures

Figure 1. Stress Vectors in a Hexahedral Element (Source:www.solidworks.com)	23
Figure 2. Fluid Element of the Pipe with Forces and Moments	26
Figure 3. Structure Element of the Pipe with Forces and Moments	27
Figure 4. Turbulence Eddies in a Pipe (Source:www.isa.org).....	28
Figure 5. General Flow Pattern of Two-phase Flow.....	30
Figure 6. Flow Regimes in Horizontal Pipes (Source: https://build.openmodelica.org)	31
Figure 7. Flow Regimes in Vertical Pipes (Source: https://build.openmodelica.org)	32
Figure 8. Stratified Flow Diagram for Pressure Difference at Cross-section.....	34
Figure 9. Annular Two-phase Flow just before Switching to another Flow Regime (Source: Bratland, 2010)	35
Figure 10. Slug Length as a Function of the Diameter of the Pipe based on Scott’s Equation (Source: Bratland, 2010).....	37
Figure 11. Three-phase Flow Regime Map for Horizontal Pipes.....	38
Figure 12. Gas-oil-water Stratified Flow Configuration with Center of Gravity Points	39
Figure 13. Slug Behavior in Horizontal Gas-oil-water Flow.....	40
Figure 14. Slug Flow Configuration with Gas Entrainment in Oil and Water Layers	41
Figure 15. Friction Loss as a Function of the Mixture Velocity when Sand Particles Flow in the Pipeline (Source: Bratland, 2010).....	43
Figure 16. Free Body Diagram of Static Forces on a Sand Particle	44
Figure 17. M-shaped Jumper with Dimensions	45
Figure 18. Phase I – FIV Methodology to assess Risk of Multi-phase Flow in Subsea Pipe Component.....	48
Figure 19. Phase II – FIV Methodology to determine the Fatigue Life of a Subsea Pipe	49
Figure 20. Fluid Domain Partition for Jumper Model	50
Figure 21. Generalized Cylinder Mesh of the Fluid Domain	54
Figure 22. Hexahedral Mesh of the Structural Domain in ABAQUS	56
Figure 23. Flow Pattern Map of Crude Oil and Natural Gas at 68atm and 38C in Horizontal Pipe (Taitel & E., 1976).....	58
Figure 24. Volume Fraction of Oil for a Horizontal Pipe under 68 atm and 38°C: (a) Stratified Smooth (b) Stratified Wavy (c) Slug Flow (d) Annular Flow	60

Figure 25. Cross-section of Annular Flow in a Horizontal Pipe under 68 atm and 38°C	60
Figure 26. a) Mode 1 and b) Mode 2 of the M-shaped Jumper - Isometric View	63
Figure 27. Contour of Volume Fraction of Oil for 50% oil-50% Gas Flow (Case 2) in First Half of the Jumper.....	65
Figure 28. Contour of Volume Fraction of Oil for 50% oil-50% Gas Flow (Case 2) in Second Half of the Jumper	66
Figure 29. Contour of Volume Fraction of Oil for 20% oil-80% Gas Flow (Case 1) in First Half of the Jumper.....	67
Figure 30. Contour of Volume Fraction of Oil for 20% oil-80% Gas Flow (Case 1) in Second Half of the Jumper	67
Figure 31. Contour of Volume Fraction of Oil for 80% oil-20% Gas Flow (Case 3) in First Half of the Jumper.....	68
Figure 32. Contour of Volume Fraction of Oil for 80% oil-20% Gas Flow (case 3) in Second Half of the Jumper	69
Figure 33. Cross-Section Planes of Jumper for Extraction of Volume Fraction Time History	70
Figure 34. Time History of Volume Fraction for Case 2 – Cross-section Plane A	71
Figure 35. Time History of Volume Fraction for Case 2 – Cross-section Plane B	71
Figure 36. PSD of Volume Fraction of Oil for Case 2 – Plane Section B.....	72
Figure 37. Time History of the Pressure for the Bends of the Jumper (Case 3).....	75
Figure 38. PSD of Pressure Signatures at the 4 th Bend for Case 3	76
Figure 39. Contour of Volume Fraction of Oil for Oil-gas-water Flow in First Half of the Jumper for Case 7	77
Figure 40. Contour of Volume Fraction of a) Gas, b) Water for the First Section of the Jumper for Case 7	78
Figure 41. Contour of Volume Fraction of Oil for Oil-gas-water Flow in Second Half of the Jumper for Case 7	79
Figure 42. Time History of Volume Fraction for Case 7 – Cross-section Plane B	80
Figure 43. PSD of Volume Fraction of Oil for Case 7 – Plane Section B.....	81
Figure 44. Time History of the Pressure for the Bends of the Jumper (Case 7).....	83
Figure 45. PSD of Pressure Signatures at the 4th Bend for Case 7	84
Figure 46. Contour of Sand Particles Traveling along the Pipe from Inlet of the Jumper	85

Figure 47. Initial Accumulation of Sand Particles at First Bend of the jumper.....	86
Figure 48. Contour of Volume Fraction of Oil in Jumper for a) Case 8, b) Case 9 and c) Case 10 after 20 Seconds of Flow	87
Figure 49. Contour of Velocity for Cross-section Area at the First Bend of the Jumper	88
Figure 50. Tracking Sand Particles Flowing into 1st Vertical Section of the Jumper	88
Figure 51. Tracking Sand Particles Flowing into First Top Horizontal Section of the Jumper ...	89
Figure 52. Tracking Sand Particles Flowing towards the Fourth Bend of the Jumper	89
Figure 53. Maximum Displacement of Jumper at Midpoint for Case 5	93
Figure 54. Maximum Displacement (in X direction) at Bends for Case 5	93
Figure 55. Maximum Displacement (in Y direction) at Bends for Case 5	94
Figure 56. Maximum Principal Stress at Top Point of Inlet for Case 5.....	95
Figure 57. Maximum Principal Stress at Right Point of Inlet for Case 5	95
Figure 58. Maximum Principal Stress at Right Point of Outlet for Case 5	96
Figure 59. PSD of Displacement of Jumper for Case 5	97
Figure 60. PSD of Max. Principal Stress of Jumper for Case 5.....	98
Figure 61. Comparison of the Deformation of the Jumper due to Oil-gas Flow and the Second Mode Shape	98
Figure 62. Maximum Displacement of Jumper at Midpoint for Case 8	99
Figure 63. Maximum Displacement of Jumper at Bends for Case 8.....	99
Figure 64. Maximum Principal Stress at Top Point of Inlet for Case 8.....	100
Figure 65. Maximum Principal Stress at Right Point of Outlet for Case 8	101
Figure 66. PSD of Displacement of Jumper for Case 8.....	102
Figure 67. PSD of Max. Principal Stress of Jumper for Case 8.....	102
Figure 68. Mode-1 for M-shaped Jumper - Isometric View	108
Figure 69. Mode-2 for M-shaped Jumper - Isometric View	108
Figure 70. Mode-3 for M-shaped Jumper - Isometric View	109
Figure 71. Mode-4 for M-shaped Jumper - Isometric View	109
Figure 72. Mode-5 for M-shaped Jumper - Isometric View	110
Figure 73. Mode-6 for M-shaped Jumper - Isometric View	110
Figure 74. Mode-7 for M-shaped Jumper - Isometric View	110
Figure 75. Mode-8 for M-shaped Jumper - Isometric View	111

Figure 76. Computational Demanding using a AMD Linux Cluster versus a Windows Machine Intel (R) Core (TM) i7-2600, 64-bit OS	114
Figure 77. Comparison of Maximum Displacement using different number of mesh divisions along the jumper	123

List of Tables

Table 1. Geometry and Material Properties of Jumper	45
Table 2. Fluid Properties and Conditions for the Multiphase Flow	46
Table 3. Meshing Parameters for the CFD Model	54
Table 4. Parameters of Velocity of the Taitel and Duckler Model	61
Table 5. Natural Frequencies of the Jumper from ABAQUS	63
Table 6. CFD Simulation Cases for Two-phase Flow	64
Table 7. Range of Volume Fraction of Oil for Two-phase Flow Cases	72
Table 8. PSD Volume Fraction Frequencies for Case 1 & Case 4	73
Table 9. PSD Volume Fraction Frequencies for Case 2 & Case 5	73
Table 10. PSD Volume Fraction Frequencies for Case 3 & Case 6	74
Table 11. Maximum Pressure on Bends for Two-phase Flow Cases	74
Table 12. PSD Pressure Response Frequencies of two-phase flow cases	76
Table 13. Range of Volume Fraction of Oil for Three-phase Flow Cases	80
Table 14. PSD Volume Fraction Frequencies for Case 7 & Case 8	81
Table 15. Maximum Pressure on Bends for Three-phase Flow Cases	82
Table 16. PSD Pressure Response Frequencies of Three-phase Flow Cases	84
Table 17. CFD Simulation Cases for Four-phase Flow	85
Table 18. PSD Volume Fraction Frequencies for Case 8, Case 9, & Case 10	90
Table 19. Maximum Pressure on Bends for Oil-water-gas Flow with and without Sand Particles	90
Table 20. Summary of CFD Results for Multiphase Flow	91
Table 21. Computational Demand for a Simulation with Different Mesh and Time Step using a Local Machine (Intel (R) Core (TM) 2.4 GHz Processor and 8GB RAM Memory)	112
Table 22. Hardware Specifications of AMD Opteron based Linux Cluster	113
Table 23. Mesh sensitivity results varying the number of mesh divisions along the jumper	123

1. Introduction

1.1. Background and Problem Statement

In offshore, production fluid that flows from the reservoir to the surface of an oil well usually comes as a mixture of oil, gas and water. This fluid mixture is transported to onshore through long pipelines that are subjected to harsh environmental conditions. Given that high pressure and high temperature might cause the pipeline to have large expansions, jumpers are usually installed to accommodate these expansions and avoid the failure of the system. Jumpers are relatively short pipes connecting a manifold, where the well is located, to the export pipelines. The challenge of jumpers is to withstand the internal pressure and hydrodynamic loads from the internal multiphase flow and current respectively. Those are sources of significant vibrations that might affect the reliability and safety of the piping system.

As stated by Rob Swindel from Xodus Group, vibration due to internal flow has received less attention such that this threat has led up to 21% of pipework failures on topsides facilities. This vibration-induced fatigue phenomenon occurs when the interaction between the flow and the pipe causes the fluid frequency and natural frequencies of the pipe to lock in. This is known as Flow Induced Vibration (FIV). High flow rates are the main reason of this vibration; however, there is limited information or investigation on the vibration effect of having more than two phases on the system.

Multiphase flow separators are implemented to separate the fluids for oil processing and purification; this process is usually performed after transporting the production fluid to the platform or onshore facilities via pipelines. It is too costly to design and install the multiphase flow separator at earlier stages of the production in order to prevent the vibration of the pipe. In addition, sand particles are sometimes coming from the reservoir such that the flow can be blocked or restricted due to low flow rates. The solution in this case is to inject high pressure flow to flush down the sand from the jumper. If the sand volume fraction is significant, this solution might require to be executed constantly leading to high expenses over time.

There is a need to develop a screening methodology that helps to predict the likelihood of failure for subsea structures when internal multiphase flow is transported through the pipe. A correlation of inputs and outputs is recommended to identify if the fluid frequency falls close by the natural frequencies of the pipe. In fact, it is of high interest to understand the effect on the

response of the jumper by varying the flow rates, the volume fraction of the phases, and the number of phases.

It is desired that standard guidelines are available to oil and gas companies to assess FIV in subsea pipes. A FIV methodology will help to estimate the effect of multiphase flow on subsea pipes. This will benefit oil and gas companies/ operators to monitor the structure and control the oil production.

1.2. Objective

The purpose of this thesis is to provide a screening methodology for FIV in subsea piping components when internal multiphase flow (oil-gas, oil-gas-water, oil-gas-water with sand particles) is injected into a pipe. This methodology is divided into two phases:

- Phase I: Identify the level of risk based on the magnitude and frequency spectra of the volume fraction of oil and the pressure/forces. If there is a high risk of failure, Phase II is required.
- Phase II: Determine the response of the structure (displacements and stresses) when it is subjected to internal multiphase flow by performing a detailed Fluid Structure Interaction (FSI) analysis.

From phase I, this includes simulating the flow using the CFD tool (STAR-CCM+) and performing a modal analysis using the FEA code (ABAQUS) to compare a) the fluid frequency (ies) with the natural frequencies and b) the frequency spectra of the forces or pressure with the natural frequencies. Following the guidelines from the Energy Institute, the excitation frequency should not be within $\pm 20\%$ of the natural frequencies of the pipe. If this occurs, it is suggested to perform a two-way coupling simulation between the CFD tool and the structural FEM to estimate the stresses and displacements.

The ultimate goal is to determine the stress distribution along a lapse of operation time and predict the fatigue life of the jumper using an S-N based approach. This technique helps to identify the locations of high displacements and high stresses, which can then be used to calculate the frequency response at those critical locations and compare it to the natural frequencies of the structure. This method determines how close the response frequency falls within one of the natural frequencies such that it might intensify the vibration of the structure. By

plotting the deformation of the jumper, it is easy to identify the mode shape at which the jumper is excited if resonance occurs.

As a hypothesis, it is of interest to prove that the flow behavior and response of the jumper (in terms of fluid frequency, displacement, and stresses) differs at least by 10% if oil-gas-water is flowing instead of oil-gas flow.

2. Literature Review

2.1. Two-Phase Flow

Most of the literature review in internal multiphase flow in pipes deals with two-phase flow (usually gas and water) since it is the most common configuration to analyze and understand in terms of flow patterns, superficial velocity, and void fraction. These parameters are usually correlated to the natural frequency, induced forces or amplitude of pressures, and displacements. It is understood that the most critical flow regime is the slug flow since the pipe is likely to exhibit forces that might generate significant vibrations. According to some of the present studies, bends and tees are the locations where forces are expected to induce the highest vibrations on the pipe.

Jumpers are one of the subsea piping components which are exposed to multiphase flow induced vibration. It is then important to understand the response of this type of structure to two or more phases. For example, Pontaza investigated the flow-induced forces on a subsea M-shaped well jumper with calculation of the fatigue life by performing a numerical simulation of a transient internal two-phase flow in a jumper. According to his results, subsea piping is most likely to experience FIV when gas content oscillates between 50-60 percent. The dominant frequencies of FIV correspond to modes 1 through 4 with highest stresses produced in mid-life flow conditions when the volume fraction of gas is 55% (Pontaza & Menon, 2011).

Turning elements (i.e. tees, elbows, and bends) are the most sensitive locations to experience flow-induced forces due to the change of momentum of the fluid. Because of the transient phenomenon, these forces are fluctuating with time and can induce significant vibration depending on the proximity of the slug frequency to the natural frequency of the pipe. An experimental research found that these loads are mainly due to the multiphase flow passing through bends, in particular slug flow whose dynamics can excite the pipe easily. (Riverin, de Langre, & Pettigrew, 2006)

As shown in Pontaza & Menon's paper, displacements are expected to be higher at the middle point of the span while maximum stresses are most likely to occur at the Pipeline end manifold (PLEM) or Pipeline end termination (PLET).

Pontaza and Menon also developed a similar procedure to investigate and compare the FIV response and fatigue life of a well jumper using impact tees vs. one with short radius bends. The screening procedure consists of: a) performing a 3-D numerical simulation of unsteady flow

in the jumper, b) estimating the flow-induced forces on the turning elements and finding its spectra forces, c) predicting the structural response at the manifold connection based on time-domain stress signals, and d) determining the fatigue life of the jumper using a single slope S-N curve. When comparing the Power Spectral Density (PSD) of the flow-induced forcing, it was found that the spectrum of the jumper with tees falls in a broader range of frequencies than the one with short radius bends. In fact, well jumper with impact tees is expected to be excited at higher frequencies (Pontaza & et. al, 2013).

Looking at the stress cycle response, it was found that both well jumper configurations have similar stress ranges but with different energy spectral frequency. A stronger structural response signal at lower frequencies was found at the well jumper with short radius bends while the jumper with impact tees is excited at higher frequencies as confirmed by the flow-induced forces spectra results. Fatigue life of the jumper with short radius bends indicates an improvement by a factor of two with respect to the well jumper with impact tees. The present work applies a similar approach as Pontaza and Menon's research.

Riverin, de Langre, & Pettigrew also studied the effect of bends and tees on the amplitude of the fluctuating forces exerted on the structure. The magnitude of these forces varies depending on the number of phases, geometry, superficial velocities, etc. They proposed a formulation of the magnitude of the forces in relation with the local variation of the void fraction in the flow. An experiment was conducted to characterize the rms value of the forces due to alternating of two phases and the corresponding spectral density of those forces. The experimental set-up consists of an air-water loop made of PVC tube test section with two configurations. The first configuration is a horizontal U-tube attached to the straight sections using two sharp bends. The second configuration is a vertical pipe connected to a tee with two equal short branches of same diameter. A force sensor is attached on both configurations to measure the forces from the flow. The air void fraction and superficial velocity are the two parameters under investigation for the flow conditions (Riverin, de Langre, & Pettigrew, 2006).

According to the experimental results, it was found that forces on bends and on tee are similar for a particular void fraction and flow velocity when referring to an equivalent bend force. The flow induced forces at 50% and 75% void fraction have similar trend with superficial velocity, but different in magnitude.

In this study, the flow regimes are modeled as alternative slugs of liquid and gas to relate the force on the bend or tee to the differences in void fractions. The flow pattern is developed based on the flow velocity, density fraction at the inlet, outlet and inside the bend. The estimated forces from the slugs using a momentum equation are in close agreement with the experiments of Tay and Thorpe for horizontal pipes. For vertical flows as the configuration with a tee, it is more complex to find the momentum balance since the dynamics of the phases has more variation than in horizontal flows.

Riverin et.al performed a similar study on four different U-shaped piping elements to measure in-plane vibration and the dynamic reaction force on the elbows. According to the vibration response, the periodic fluctuating forces match with the vibration modes of the pipe resulting in a resonance scenario. A narrow-random response frequency of the excitation forces is exhibited, and their spectra show a predominant frequency that increases with fluid velocity for a given void fraction. It was concluded that a maximum force is reached when void fraction is between 50% and 60%. Regarding the U-shaped geometry, there was not major effect of the radius of curvature of the elbows on the excitation forces. A passage frequency of bubbles and droplets was calculated based on their minimum size to correlate to the force spectra, and it was found that peak frequency at low velocities coincides with the predominant frequency of the force spectra. This suggests that the bigger bubbles or droplets are one of the potential sources of the excitation forces on the elbow, which is related with the flow pattern present at the section of the pipe (Riverin & Pettigrew, 2007)

Computational Fluid Dynamics (CFD) plays an important role in analyzing multiphase flow in pipes as it has the capability of solving the interface between the phases with a technique such as Volume of Fluid (VOF) and Level Set Method (LSM).

Ramdin and Henkes (2011) conducted a CFD numerical study to simulate two-phase flow configurations such as the Benjamin bubble and the Taylor bubble. This type of analysis was modeled using VOF multiphase model in CFD as a method of validation of the experimental results and analytical formulations. A Benjamin bubble consists of a long bubble which enters a stagnant liquid in a horizontal pipe. On the other hand, a Taylor bubble is a long bubble that rises in a liquid in a vertical pipe. These types of bubbles can be considered as a slug flow pattern which usually occurs when transporting oil and gas through pipelines.

According to their results for the Benjamin bubble, there is a good agreement with the analytical results for the bubble velocity when the effects of viscosity and surface tension are neglected. When considering the effect of viscosity, the bubble velocity decreases with decreasing Reynolds number and when the bubble is traveling along the pipe. For the effect of surface tension, it was found that the bubble velocity decreases with increasing the surface tension.

Regarding the CFD results for the Taylor bubble, there was not agreement with the analytical solution when neglecting the effects of viscosity and surface tension. In fact, a small value of surface tension produces an agreement with the analytical value of the bubble velocity. When including the effect of viscosity and surface tension, the bubble velocity decreases with Reynolds number and with decreasing Eötvös, which is in agreement with the experimental results and the Wallis correlation (Appendix B). It was found that velocity of the Taylor bubble is steady along the pipe when considering the viscosity, which is contrary to the effect of viscosity on the Benjamin bubble (Ramdin & Henkes, 2011). This study was successful to validate most of the experimental data and analytical solutions. Surface tension and viscosity are then important parameters to define in CFD simulations since their values affect the interaction between phases and as a result the development of the slug flow regime.

Maya B. and Minguéz M. investigated the slugging effect on pipelines since it is the most critical flow patterns that can result in fatigue damage. They analyzed the effect of the flow characteristics and its pressure on a subsea M-shaped jumper connected from the PLET to the base of a riser. A numerical CFD 2D simulation was performed to correlate the amplitude of the pressure loads with different parameters such as the spool elevation, the slug length, or the fluid properties. In this case, gas and oil are injected in an alternating to simulate a slug development. Three different slug length configurations were supplied at the inlet to compare the variation of the pressure histogram on the bends. According to the results, it was found that maximum forces are obtained with the passing of the gas bubble tail at the second and fifth bend, which are the bends connecting the vertical sections. In general, the upward flow tends to disrupt as several short slugs are formed at the lower section of the jumper and then those are merged with the downstream long slug of the vertical section. This disassociation of bubbles is likely to generate smaller scales (or turbulence eddies) which could be an additional source of vibration. In fact, It was found that the ratio between the spool height and the gas pocket length determines if the slug

dissociates or not. This study still requires a validation of the 2D analysis with a 3D numerical simulation to compare the accuracy of the results.

2.2. Three-Phase Flow

Some studies simplify the three-phase flow as a two-phase flow with properties of the mixture. Other studies only consider a few patterns of the three-phase flow or the continuous liquid is not taken into account for the classification. These assumptions can lead to inaccurate results since missing a phase or flow characteristic can give inaccurate vibration response and consequently the incorrect score in likelihood of failure (LOF) (Energy Institute, 2008). When dealing with three-phase flow patterns, it is noticed that those are classified first depending on the gas-liquid relationship and second the liquid-liquid arrangement.

For example, Keskin et al. classifies three-phase gas-oil-water in horizontal pipes in twelve flow patterns depending on the interaction of gas-liquid and oil-water. The flow patterns dictate the pressure fluctuations, holdups, and potential erosion within the pipeline. In their literature review, they found that some research studies classify the flow patterns based on liquid-wall relationship, liquid-liquid relationship, and gas-liquid relationship. Another researcher classifies fifteen flow patterns which were based on three relationships: liquid-liquid, liquid-wall based on dispersed flow, and gas-liquid. In general, those studies combine the flow patterns of two-phase flow to identify the potential flow patterns in three-phase flow. Taken into account this information, Keskin, Zhang, and Sarica decided to conduct experiments in which air, refined mineral oil and tap water flow through a horizontal pipe at different superficial velocities and water fraction. Superficial velocities of gas, oil and water range from 0.1 m/s to 7.0m/s, 0.02 m/s to 1.5 m/s, and 0.01 m/s to 1.0 m/s respectively. The water cut was set to 20, 40, 50, 60 and 80 percent.

Their classification consists of two terms: the first one indicates for gas-liquid flow pattern and the second term refers to oil-water flow pattern. The following gas-oil-water flow patterns were identified in the experiment: stratified-stratified (ST-ST), stratified-dual continuous (ST-DC), stratified-oil continuous (ST-OC), stratified-water continuous (ST-WC), intermittent-stratified (IN-ST), intermittent-dual continuous (IN-DC), intermittent-oil continuous (IN-OC), intermittent-water continuous (IN-WC), annular-oil continuous (AN-OC), annular-water continuous (AN-WC), dispersed bubble-oil continuous (DB-OC), and dispersed bubble-water

continuous (DB-WC). Experimental results also showed that annular and dispersed bubble flows did not form in the test section.

It is characteristic in subsea piping such as risers and pipelines to find hilly sections in which accumulation of liquid phases are developed at the lowest section of the downward and upward hill, also known as terrain slugging. Slug flows can also be developed in horizontal sections due to preceding wavy flow at the gas-liquid interface as indicated by an experimental study conducted in the University of Tulsa. This research helps in understanding the three-phase slug flow in horizontal and curve sections of M-shaped jumpers. Basically, Ersoy G. et al. performed an experimental investigation of gas-oil-water flow in a hilly-terrain pipeline which includes horizontal, downward inclined and upward inclined sections. The purpose of this study was to analyze and compare the slug flow behavior in different sections of the pipeline and also to understand the effect of the water cut, gas velocity and liquid velocity on the flow pattern. The test section of the experiment is a transparent pipe which consists of a horizontal branch and a long branch with hilly sections connected with a U-shaped PVC bend. The pipe has a 50.8 mm inner diameter. Sensors, valves, and transducers are some of the equipment to measure the fraction distribution of the phases, total liquid holdup, temperature, and pressure. Cameras were also installed to visualize the three-phase flow pattern in the pipe.

Based on the identification of the flow patterns, it was observed that intermittent flow (IN) of gas-liquid is present in all the tests for the horizontal section. For low flow rates, intermittent-stratified flow (IN-ST) with segregated oil and water phases was observed for all water cut percentages. At relative higher flow rates, oil and water phases mix and dispersion of oil-in-water or water-in-oil occurs. A segregated water layer is even formed on top of the dispersed oil and water phases. This flow pattern is known as intermittent-water-in-oil and water (IN-W/O&W) for oil continuous and intermittent-oil-in-water and water for water continuous. When the slug is developed, an annular thin film of water or oil is formed depending on the amount of water cut. This segregated liquid film layer vanishes at higher flow rates when oil and water mix homogeneously. It was found that the three-phase flow in the downstream horizontal section was more mixed in comparison to the oil-water flow in the upstream horizontal section since the U-shaped section makes the oil and water phases to mix before flowing to the straight horizontal pipe (Ersoy, Sarica, Al-Safran & Zhang, 2011).

Regarding to the pressure, it is expected that the lower section of the inclined section to have a maximum pressure since this is the location of the pressure built-up zone where slugs are initialized. Slug length and frequency seems to be steady in all sections along the pipe for low flow rates. However, differences in slug length and frequency were identified for moderate and high flow rates, specifically between 20% and 80 % water cuts.

2.3. Liquid-Solid Flow

Coming out of the production in reservoirs, sand particles are introduced into the multiphase pipelines and it is important to control its transportation or production since it might affect the integrity of the structure when flow assurance problems such as erosion, corrosion, pressure built up, and critical flow patterns occur in oil and gas lines. One of the main concerns is the deposition of sand particles at the bottom of the pipe, which depends on the minimum critical velocity of the continuous flow, the sand volume fraction, and the flow regimes. Although sand management is important to optimize the performance and operation of the multiphase pipelines, there are only a few experimental investigations and insufficient analytical methods to predict the effect of sand particles. Al-lababidi et al. conducted experiments on the transportation of sand to analyze the deposition characteristics in horizontal and inclined pipelines. The purpose of this study is to estimate the minimum velocity required in sand-water and sand-air-water flows to transport the solid particles and prevent accumulation of sand (sand dunes).

Six different sand concentrations were used in tests with a sand particle approximately of 0.2 mm in diameter flowing in a 0.05 m pipe inner diameter. It was observed that the sand minimum transport condition (MTC) in horizontal and +5 deg inclined pipeline are similar in water flow test. For air-water experiments, while the MTC in horizontal pipes occurs in stratified wavy and hydrodynamic slug flow patterns, the MTC in the inclined pipe is the terrain slug flow regime. This last flow pattern is more likely to occur in this hilly pipe, and consequently the deposition of sand is prevented due to the turbulent motion of the continuous fluid. All of the previous criteria should be considered when designing a pipeline to avoid flow assurance issues that can cause a decrease in oil production or failure of the pipeline (Al-lababidi, Yan & Yeung, 2012).

In the designing of oil-gas-sand multiphase flow pipelines, sand holdup is one of the important conditions that can affect the mass flux, pressure drop and even flow regime. Most of

these parameters are influenced by liquid and solid characteristics such as sand particle weight, gas superficial velocity, and liquid superficial velocity. Bello, Reinicke and Teodoriu studied this effect of sand loading and the velocity of the phases by performing an experimental work that measure the local sand holdup in an air-water-sand three-phase slug flow. Static and dynamic pressure distributions were also measured. Particle size diameter is approximately 0.6 mm.

According to the results of the three-phase slug flow in the pipeline, the axial distribution (from bottom to top of the pipe) of sand holdup shows a non-linear behavior with its highest values at the walls and a peak at the center for gas superficial velocities of 0.505m/s and 0.606m/s. It was indicated that the sand particle distribution depends on the collision of gas bubbles and sand particles and the vortex motion of the slug. As expected, the sand holdup decreases with increasing superficial gas velocity (Bello, Reinicke & Teodoriu, 2005).

For the remaining contents, percentage of water and sediments are limited to 0.5 percent in crude oil transmission pipelines that comes with deposits of sand particles and oil. However, these sediments can contribute to a corrosive environment when water volume fraction exceeds 10 percent (Been, 2011).

3. Conservation Equations in Multi-phase Flow

As in single-phase flow, multi-phase flow follows the main three conservation principles. These principles apply for each phase; thus, 9 equations describe the oil-gas-water flow. However, simplifications are made or correlations are added to describe the interaction between phases and the wall. For example, the cross section of each phase is expected to change along the pipe due to the transient flow patterns with the presence of slugs, bubbles, sand particles, droplets, etc.

Conservation equations, also well-known as Navier-Stokes equations, include convection and diffusion terms. The convection terms describe the organized motion of the fluid particles and its transfer of properties with the motion. The diffusion terms describe the interaction between fluid particles due to the turbulent kinetic energy of the flow (National Aeronautics and Space Administration, 2008).

3.1. Conservation of Mass

Following the general principle of mass conservation, the mass of a system should be conserved over time. Its quantity must not change unless mass is added or removed. This principle should apply for each phase as follows (Bratland, 2010):

$$\frac{\partial(\alpha_k \rho_k)}{\partial t} + \frac{\partial}{\partial x}(\alpha_k \rho_k v_k) = \Gamma_{ki} + \Gamma_{kw} \quad \text{Eq. 3.1}$$

The first term refers to the accumulated mass inside the pipe, the second term means the total mass flow into the pipe, the third and four terms refer to the mass flow from other phases and other external sources respectively. In this study, the last term is zero since there is no flow through the pipe wall.

3.2. Conservation of Momentum

Similar to single-phase flow, multi-phase flow follows the Newton's second law in which the pressure, gravity, and friction forces are the main forces acting on a phase. However, additional forces need to be added to the conservative momentum law to account for the phase-to-phase interactions. In fact, these forces are responsible to change the flow pattern along the pipe. The sum of the forces acting between all phases should be equal to zero (Bratland, 2010):

$$\sum_{k=1}^N R_{ki} + S_{ki} + v_k \Gamma_{ki} = 0 \quad \text{Eq. 3.2}$$

where R_{ki} is the friction force from other phases, S_{ki} is the force due to surface tension from other phases, and $v_k \Gamma_{ki}$ is the mass transfer or momentum exchange.

3.2.1. Surface Tension

This is one of the important forces acting within each one of the phases, between phases, and from the wall. It is defined as the intermolecular forces that attract the molecules towards each other [1]. Even though it is small in comparison with many other forces, the surface tension is important in determining the flow regime as the difference in tension might indicate a momentum transfer from one phase to the other. Thus, the following forces act in one phase in the axial direction of the pipe:

$$\frac{1}{A} \frac{d}{dx} \sum F_k = F_{kpg} + F_{kg} + R_{ki} + R_{kW} + S_{ki} + S_{kW} \quad \text{Eq. 3.3}$$

From the right-hand side, the first term is the force due a pressure gradient along the pipe, the second term is the gravity force, the third and four terms are the friction forces, and the fifth and sixth terms are the forces due to surface tension. It is then expected that the sum of the forces would vary when changing from two phases to three phases.

3.2.2. Pressure Correction Term

The pressure correction term is critical in predicting the transition from stratified flow to slug flow. This term indicates the pressure difference between phases due to the elevation with respect to the bottom of the pipe. Even though this pressure difference is very small in comparison with the one along the pipe, it makes a significant contribution to the formation of wavy flow.

Numerical problems can occur when the pressure correction term is ignored by assuming the pressure to be equal in all phases of the cross-section. Analytical equations are shown later to account for the pressure in each phase.

3.3. Conservation of Energy

Similar to the mass and momentum conservation laws, the energy must be conserved over time. The energy can change in different forms, but it cannot be created or destroyed. Heat or work from the outside can be added or removed from the system. In this study, energy sources

coming from outside are ignored. Adding all the internal and external energy sources acting on the phases gives:

$$\frac{\partial}{\partial t}(\alpha_k E_k) = -\frac{\partial}{\partial x}[\alpha_k v_k(E_k + p_k)] + q_{ki} + q_{kW} + w_{ki} + w_{kW} + \Gamma_{ki}h_{ki} + \Gamma_{kW}h_{kW} \quad \text{Eq. 3.4}$$

where the first term refers to the internal energy, q represents the specific heat, w is the specific work, Γ is the specific mass flow term, and h is the specific enthalpy. Sub-index i and w represent the energy coming from other phases to a phase k and the energy coming from outside (i.e. wall) to the phase k respectively.

4. Conservation Equations in Solid Mechanics

Solid mechanics is one of the areas in physics that analyzes the characteristics of a solid when it is subjected to external loads.

4.1. Elasticity Equations

For fluid structure interaction, you might expect some elastic or plastic deformation of the solid structure due to the forces induced by the flow. It is usually desirable that the material exhibits elastic behavior such that it returns to its original shape or arrangement after applying a load. At this stage, stress is known to vary linearly with strain.

Under the continuum mechanics, an elastic deformable solid must follow the conservation law in which the sum of the forces should be equal to zero. These forces generate a distribution of stress to the surface area. If large forces are exerted, the material might exceed the elastic region and it will fail either by fracture or plastic behavior. Stress varies depending on the location where the forces are applied. Thus, discretizing the elastic body into very small elements is usually the approach to solve the stress components such as the normal stress and two shear stresses as shown in Figure 1.

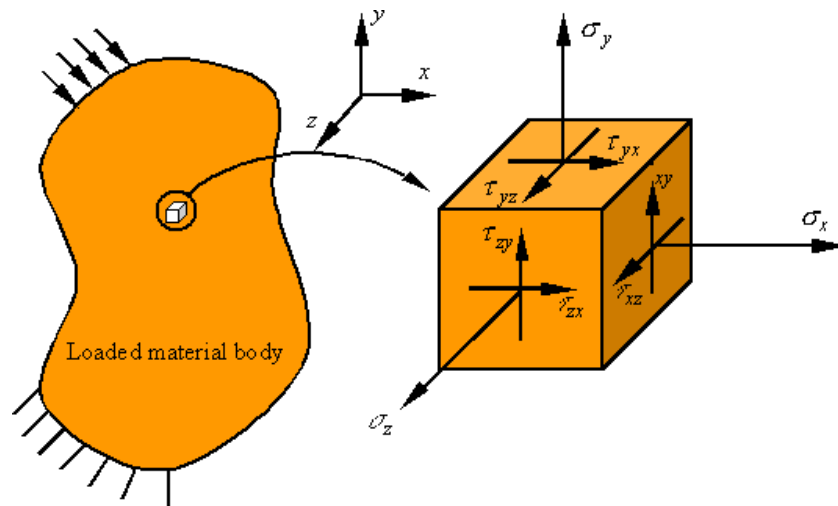


Figure 1. Stress Vectors in a Hexahedral Element (Source:www.solidworks.com)

Adding all of the forces in x, y, and z directions on the small element, the following equations are obtained by applying Newton's first law of motion (Timoshenko & Goodie, 1970):

$$\frac{\partial \sigma_x}{\partial x} + \frac{\partial \tau_{xy}}{\partial y} + \frac{\partial \tau_{xz}}{\partial z} + X_b = 0 \quad \text{Eq. 4.1}$$

$$\frac{\partial \tau_{xy}}{\partial x} + \frac{\partial \sigma_y}{\partial y} + \frac{\partial \tau_{yz}}{\partial z} + Y_b = 0 \quad \text{Eq. 4.2}$$

$$\frac{\partial \tau_{xz}}{\partial x} + \frac{\partial \tau_{yz}}{\partial y} + \frac{\partial \sigma_z}{\partial z} + Z_b = 0 \quad \text{Eq. 4.3}$$

where σ is the normal stress, τ is the shear stress, X_b , Y_b , and Z_b are body forces per unit volume. In this case, the gravitational force is the only body force acting on the system. There are a total of 9 stress components acting on the infinitesimal cube.

This physics describes the fundamentals of the Finite Element Method (FEM). The structure domain is divided into infinitesimal elements to solve equations 4.1 – 4.3 in each element. The solution is more accurate with increasing the number of elements. However, it takes more computational effort and time to find the solution since the cpu needs to solve greater number of partial differential equations. It is then important to find an appropriate balance between the number of elements (also known as mesh) and the computational time to have an accurate and quick solution.

5. Fluid Structure Interaction

Fluid Structure Interaction (FSI) is the subject in charge of studying the pressure fluctuations effect of the flow on the structure in terms of deformation and stresses. This multiphysics area also analyzes if the deformation of the solid structure is too large to modify the behavior of the flow.

5.1. Flow Induced Vibration

When dealing with the transportation of fluid in a pipe, vibrations can occur if large pressure fluctuations are imposed on the pipe wall. This FSI phenomenon is known as flow induced vibration (FIV). Instability of the pipe due to these vibrations depends on the end condition of the pipe. A straight pipe with both ends fixed is likely to fail first due to buckling when the critical velocity is exceeded:

$$v_c = \frac{\pi}{L} \left(\frac{EI}{\rho A} \right)^{1/2} \quad \text{Eq. 5.1}$$

where EI is the constant flexural rigidity, ρ is the density of the fluid, A is the internal area of the pipe, and L is the length of the pipe. The M-shaped jumper has a span equal to the distance from the PLET end to the PLEM end, and its maximum deflection is most likely to occur at the middle section when pipe is supported in both ends. Adding all the forces acting on a fluid element in the vertical direction shown in Figure 2 , the following relation applies:

$$F - \rho A \frac{\partial^2 Y}{\partial t^2} = \rho A \left(\frac{\partial}{\partial t} + v \frac{\partial}{\partial x} \right)^2 Y \quad \text{Eq. 5.2}$$

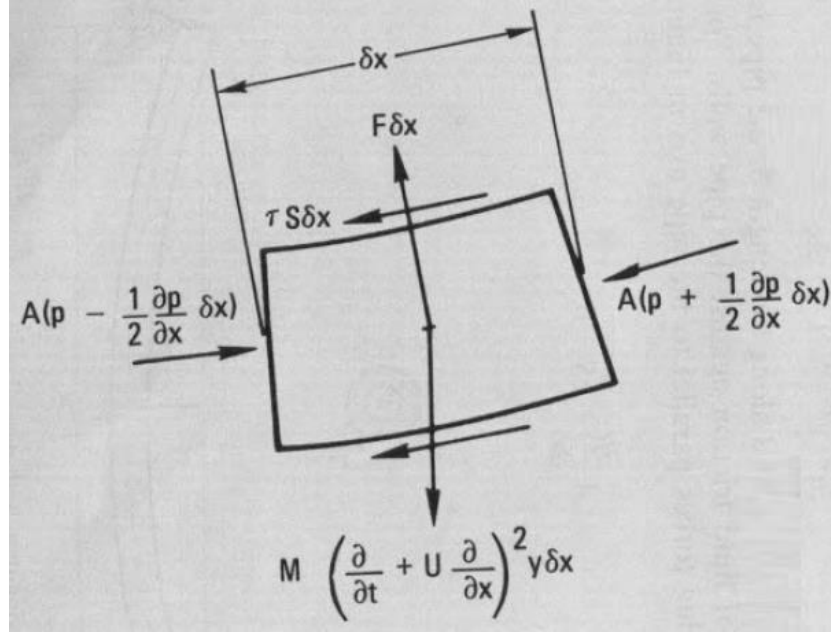


Figure 2. Fluid Element of the Pipe with Forces and Moments

The centrifugal force due to the curvature of the pipe opposes the vertical component of the fluid pressure and the force F applied by the wall on the fluid. Adding forces in the axial direction of the pipe, pressure gradient $\frac{\partial p}{\partial x}$ along the length of the pipe opposes the fluid friction τS against the pipe walls as follows:

$$A \frac{\partial p}{\partial x} + \tau S = 0 \quad \text{Eq. 5.3}$$

As mentioned in previous chapter, the solid can be exposed to shear and normal forces due to the flow with additional forces and moments such as the tension of the pipe, bending moment, Coriolis force (force required to rotate fluid element and align with local pipe axis), gravitational forces and inertia forces. Summing all the forces of the pipe element shown in Figure 3, the equation of motion gives:

$$EI \frac{\partial^4 Y}{\partial x^4} + \rho A v^2 \frac{\partial^2 Y}{\partial x^2} + 2\rho A v \frac{\partial^2 Y}{\partial x \partial t} + M \frac{\partial^2 Y}{\partial t^2} = 0 \quad \text{Eq. 5.4}$$

where the first term is the pipe stiffness, the second term refers to the centrifugal force, the third term is the Coriolis force, and the fourth term is the inertia of the pipe.

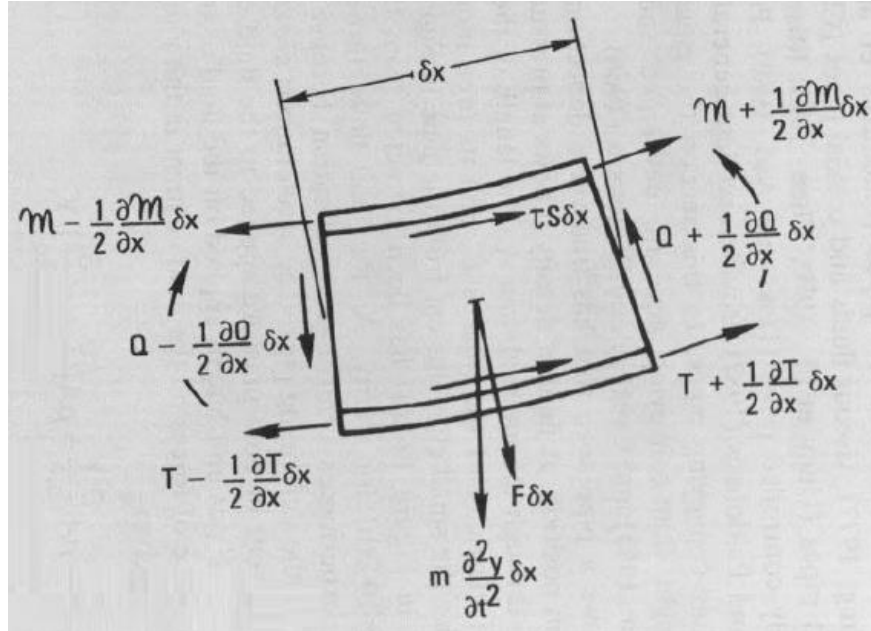


Figure 3. Structure Element of the Pipe with Forces and Moments

These formulations are applied in the FSI procedure to determine the shear and normal stresses on the pipe. The response of the structure depends on the velocity of the flow and its effect on the natural frequency of the pipe. According to Blevins, the lowest natural frequency of the pipe goes to zero when the velocity of the flow equals the critical velocity v_c . When $v = v_c$, the Coriolis force exceeds the stiffness of the pipe and it fractures.

As mentioned in chapter 2.1, the vibration response can increase if bends are included in the system since the highest induced forces occur on these sections of the jumper. It is also important to consider the resonance condition which occurs when the natural frequencies of the pipe matches with the fluid frequency. This occurrence can generate high levels of vibrations and cause a failure of the structure.

5.2. Flow Induced Turbulence

Turbulence flow is usually generated by high flow rates or the presence of flow discontinuities such as bends or tees. The flow at the center of the pipe usually has a high kinetic energy in the form of large eddies, and it dissipates into the turbulent boundary layer of the pipe in form of small eddies with heat and potential energy (Figure 4). This energy is then transferred

to the wall in form of pressure. In the turbulent zone, a broadband excitation of the kinetic energy occurs, but with low frequency. This increases the chances that the excitation frequency falls at the system's natural frequencies, which can generate significant vibrations.

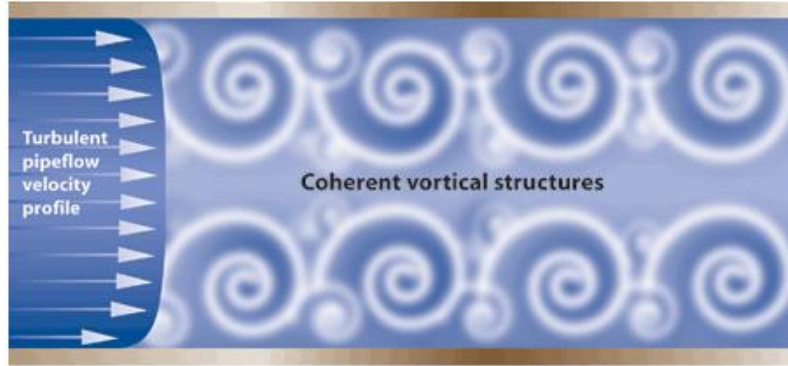


Figure 4. Turbulence Eddies in a Pipe (Source:www.isa.org)

Resolving the small scales of the turbulence becomes important when the viscosity has a significant effect. The dissipation rate ϵ of the kinetic energy and the viscosity ν are the two factors that determine the scales at which the energy is dissipated (McMurtry). Kolmogorov came with a relationship to relate these two variables to the smallest scale in turbulent flows:

$$\eta = \left(\frac{\nu}{\epsilon}\right)^{1/4} \quad \text{Eq. 5.5}$$

This is called the Kolmogorov length scale. He also found a relationship with the largest length scales as follows:

$$\eta = \left(\frac{\nu^3 L}{U^3}\right)^{1/4} \quad \text{Eq. 5.6}$$

where U is the kinetic energy of the flow. A special turbulence model was used to resolve in a good approximation the scales in the free stream and near wall where the sub viscosity boundary layer is located. This turbulence model is described in chapter 8.1.2.

Although it is expected that the effect of flow induced turbulence is much less than the effect of multi-phase flow, the methodology of this study considers both phenomena to prevent any high score in likelihood of failure.

6. Multi-phase Flow

It is common that the production fluid coming from the reservoir comes with water and sand particles making the flow multi-phase. It is understood that this three-phase or four-phase flow mixture might develop a potential slug (Cooper, Burnett, & Nash, 2009). The presence of sand is usually most concerned when dealing with erosion; however, if the amount of sand is greater than a minimum safety volume fraction, the accumulation at the bottom of the pipe might affect the flow or even block the pipe. A minimum fluid velocity mixture is required to keep the particles flowing through the pipe. The theory of this liquid-solid mixture will be explained in more detail later.

For multi-phase flow, some of the basic parameters that are considered to define the characteristics of flow are the number of phases, the volume fraction, and the velocity of each phase. In this chapter, the flow patterns developed in horizontal and vertical pipes will be defined. Next, the description of two-phase flow, three-phase flow, and liquid-solid flow are presented to understand how they differ from each other. Although three phases can sometimes be treated as two-phase flow, it is first important to compare their difference in the response of the structure before making this assumption.

6.1. Flow Regimes

Flow regime maps are the most common way to classify and identify the flow patterns either in horizontal or vertical pipes. These maps usually classify the flow patterns based on superficial velocity of each phase. Those are expected to change with the fluid phases, pipe diameter, surface tension, inclinations and other flow parameters. It is important to identify the flow regimes that can create fatigue issues or instabilities of the structure. Engineers can then control the flow conditions to prevent the development of unsafe flow patterns such as slug flow.

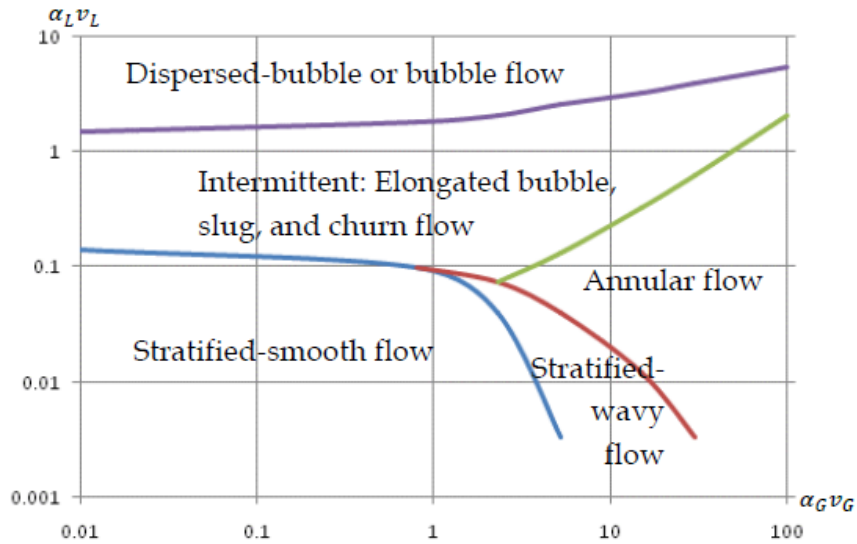


Figure 5. General Flow Pattern of Two-phase Flow

6.1.1. Flow Patterns in Horizontal Pipes

Most of the oil pipelines are horizontal or inclined pipes where two or more phases interact to develop a flow pattern. For liquid-gas flow, five potential flow regimes exist (Bratland, 2010):

- Dispersed bubble flow: tends to form with higher superficial velocity of liquid where the bubbles are distributed along the pipe and large bubbles are located on top of the pipe as shown in Figure 6 (a).
- Stratified flow: is the most common flow pattern where the superficial velocity of the gas and liquid are very low. The denser fluid (usually liquid) seats at the bottom of the pipe, and the gas is located on top of the liquid separated by the interface as shown in Figure 6 (b).
- Wavy flow: Superficial velocity of gas increases and waves starts forming at the interface boundary due to surface tension as shown in Figure 6 (c).
- Slug flow: discontinuous elongated gas bubbles separated by chunks of liquid that blocks the pipe (Figure 6 (d)).
- Annular flow: When superficial velocity of gas is very high in comparison to the liquid, the gas occupies the center of the pipe surrounded by a thin film layer of liquid at the wall of the pipe. A few droplets flow through the center of the pipe as shown in Figure 6 (e).

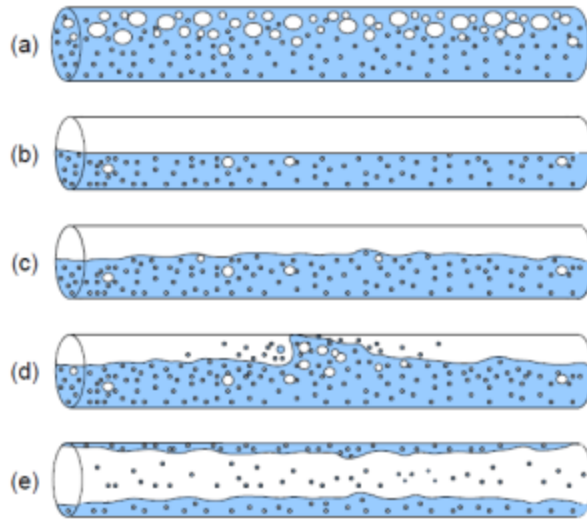


Figure 6. Flow Regimes in Horizontal Pipes (Source: <https://build.openmodelica.org>)

6.1.2. Flow Patterns in Vertical Pipes

In oil and gas industry, vertical pipes such as risers or jumpers can also developed similar flow patterns as the horizontal pipes with the exception of the stratified flow and wavy flow. Besides the surface tension and superficial velocity, the density of the phases is another parameter that has an effect on the formation of a particular vertical flow regime. There are four flow patterns that might be formed in vertical pipes:

- Dispersed bubble flow: gas bubbles are distributed through a continuous liquid flow with large bubbles located at the center of the pipe as shown in Figure 7 (a).
- Slug flow: Elongated gas bubbles are separated by slugs of liquid as shown in Figure 7 (b). When flowing upwards, the gas bubbles push the liquid slugs because of the difference in density. In contrast, the gas can prevent the passage of the liquid slugs when the flow is going downwards.
- Churn flow: Disorganized flow pattern as shown in Figure 7 (c) that can be treated as an intermediate regime between slug flow and annular flow.
- Annular flow: similar to the flow developed in horizontal pipes, in which a thin film layer of liquid forms at the wall while the gas flows at a very high velocity at the center of the pipe. Figure 7 (d) shows that a few droplets are dragged by the gas.

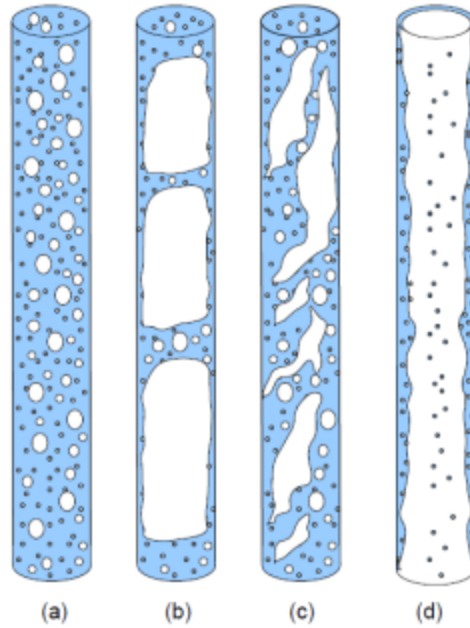


Figure 7. Flow Regimes in Vertical Pipes (Source: <https://build.openmodelica.org>)

6.2. Volume fraction

In the oil and gas industry, the ratio of the volume of the gas coming out of the well at room temperature, to the volume of oil produced at the same environmental conditions is reported as GOR or gas-oil ratio, which is usually measured in cubic feet of gas per barrel unit (Encyclopedia, 1979). The volume fraction or area fraction of a phase is the cross-section occupied by this particular phase. The sum of the volume fraction of all phases in cross-section should be equal to one. This is used in conjunction with the velocity of the phases.

6.3. Superficial Velocity

The area fraction of a phase is expected to change in space and time, so the average velocity of the flow varies depending on the volume fraction of each phase and its respective velocity. In this case, the average velocity of each phase is defined at its part of the cross-section as (Bratland, 2010):

$$\alpha_G v_G = \frac{Q_G}{A} \tag{Eq. 6.1}$$

The volumetric flow rate Q_G at the whole cross-section area A determines the superficial velocity of the phase. This tends to be lower than the average velocity of the flow.

6.4. Two-Phase Flow

Two-phase flow exists in oil pipelines as a combination of oil and gas. As mentioned in chapter 3, multi-phase flow must solve all the conservation equations. It is sometimes convenient to simplify the two-phase model to eliminate the forces or pressures that have small effect on the flow. First, this chapter describes a simplified model of a stratified flow in which some assumptions are made to estimate the oil-gas flow. It considers the effect of the pressure correction term. Second, this chapter explains the well-known Taitel & Duckler model which shows relationships of the transition between flow patterns. Third, a simplified model of slug flow is presented to find the formulations of slug frequency and slug length.

6.4.1. Pressure Difference in Stratified Flow

Assuming that the pressure is equal in a cross-section would prevent the formation of surface waves at the interface surface. Consequently, the system would be unreal and then numerical problems might occur.

To determine the pressure difference at cross-section, the following assumptions are made:

- a) The phases flow at a very low velocity, so the flow is stratified.
- b) The gas cannot be dissolved in the liquid.
- c) The fluids cannot flow through the pipe wall.
- d) The flow is isothermal.

The Bernoulli-effect is considered to take into account the difference in average velocity between phases. This is correlated to the pressure difference at different heights of the cross-section. As shown in Figure 8, the interface surface is taken as the reference level to find the pressure difference between the two phases. The pressure difference is calculated as (Bratland, 2010):

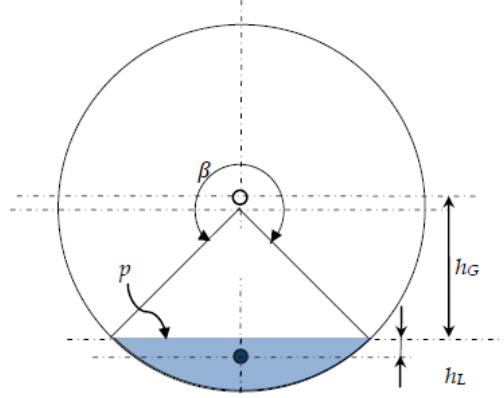


Figure 8. Stratified Flow Diagram for Pressure Difference at Cross-section

$$\Delta p_G = p_G - p = -\rho_G g h_G \quad \text{Eq. 6.2}$$

$$\Delta p_L = p_L - p = \rho_L g h_G \quad \text{Eq. 6.3}$$

where p_G and p_L are the pressures at the center of gravity of the gas and liquid respectively. ρ_G is the density of the gas, and ρ_L is the density of the liquid. The static pressure at the center of gravity of each one of the phases is distant from the surface interface as follows:

$$h_L = \left[-\frac{1}{2} \cos\left(\pi - \frac{\beta}{2}\right) + \frac{1}{3\pi\alpha_L} \left(\sin\left(\pi - \frac{\beta}{2}\right)\right)^3 \right] d \cos \theta \quad \text{Eq. 6.4}$$

$$h_G = \left[\frac{1}{2} \cos\left(\pi - \frac{\beta}{2}\right) + \frac{1}{3\pi\alpha_G} \left(\sin\left(\pi - \frac{\beta}{2}\right)\right)^3 \right] d \cos \theta \quad \text{Eq. 6.5}$$

These relationships are valid when the inclination angle θ of the pipe is nearly horizontal in which waves can be generated by the gravity. Biberg also proposed an approximation of the angle β as a function of the fraction of liquid α_L , and it is accurate within ± 0.002 rad (Bratland, 2010):

$$\beta = 2\pi - 2 \left\{ \pi\alpha_L + \left(\frac{3\pi}{2}\right)^{1/3} \left[1 - 2\alpha_L + \alpha_L^{1/3} - (1 - \alpha_L)^{1/3} \right] \right\} \quad \text{Eq. 6.6}$$

6.4.2. The Taitel & Duckler Horizontal Flow Model

A formulation was developed by Taitel & Dukler in 1976 for steady-state two-phase flow in horizontal pipes. A stratified flow is analyzed to find if the flow will be changed to another flow regime. This model is valid in small diameters and $\pm 10^\circ$ inclined pipes. For circular pipes, the Bernoulli effect takes place when a transition occurs from stratified flow to other flow regimes. This transition is initiated at a velocity (Bratland, 2010):

$$v_{GB^*} = \left(1 - \frac{h_L}{d}\right) \left[\frac{(\rho_L - \rho_G)g \cos \theta A_G}{\rho_G S_{GL}} \right]^{0.5} \quad \text{Eq. 6.7}$$

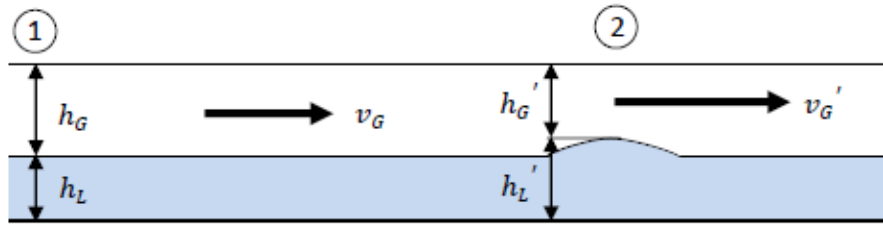


Figure 9. Annular Two-phase Flow just before Switching to another Flow Regime (Source: Bratland, 2010)

If the velocity of the gas v_G is less than the v_{GB^*} , the flow stays stratified. Some of the parameters that have an effect on the transition between flow patterns are the height of the stratified liquid h_L , the area occupied by the gas A_G , and the distance of the boundary between phases S_{GL} . Other condition that might create surface waves at a lower velocity is stated by Jeffrey. He proposed a formulation to include the effect of the wave propagation when the velocity of the gas is much larger than the waves' propagation velocity (Bratland, 2010):

$$v_{Gw^*} = \left[\frac{4\mu_L(\rho_L - \rho_G)g \cos \theta}{s\rho_L\rho_G v_L} \right]^{0.5} \quad \text{Eq. 6.8}$$

Considering equations 6.7 and 6.8, the following conclusions can be drawn regarding the surface interface:

- Stratified flow if $v_G \leq v_{Gw^*}$
- Wavy flow if $v_{Gw^*} < v_G \leq v_{GB^*}$
- Slug flow, annular flow, or other if $v_G > v_{GB^*}$

For the last configuration, it is possible to estimate the type of flow based on the difference of the velocity between phases and volume fraction of each phase. Slug flow tends to form when the velocity of the gas is not significant than the gas velocity. On the other hand, annular flow is expected to develop at very high gas and low liquid flow rates; the liquid level is low at this flow condition since the wave tends to reach the bottom of the pipe. In fact, the liquid level is important to determine if annular flow or slug flow is developed as follows (Bratland, 2010):

$$\begin{aligned} \text{Annular flow if } v_G > v_{GB^*} \text{ and } h_L < 0.35d \\ \text{Slug flow if } v_G > v_{GB^*} \text{ and } h_L > 0.35d \end{aligned} \quad \text{Eq. 6.9}$$

6.4.3. Slug Flow

As mentioned in chapter 6.1.1, slug flow is an intermittent flow of Taylor or elongated bubbles and liquid slugs. In horizontal pipes, the Taylor-bubbles travel in the upper section of the pipe as shown in Figure 6. Slug flow is a critical pattern since it can create significant pressure fluctuations, flooding issues, or corrosion. There are three mainly types of slugs:

- Hydrodynamic slugs: short slugs that are developed due to instability at the surface interface when the hydrodynamic force of the gas exceeds the surface tension at the interface, and the liquid reaches the top of the pipe
- Terrain slugs: accumulation of long liquid slugs at the lowest sections of a pipe due to the inclined angle. This type of slugs can continue for hours.
- Operational induced slugs: this usually happens in pigging operations when the production is shut down. The accumulated liquid at the low points is transported out of the line as a slug.

In nature, it is very difficult to find a constant or steady slug flow, but an average slug flow can be taken as a reference to describe some empirical relationships to find average slug length and frequency. Zabarar formulated a correlation of the slug frequency (f_s) based on pipe diameters ranging from 0.0254m to 0.20m and elevation angles from 0° to 11° (Bratland, 2010):

$$f_s = 0.0226 \left(\frac{\alpha_L v_L}{gd} \right)^{1.2} \left[\frac{64.8}{\alpha_G v_G + \alpha_L v_L} + 3.281(\alpha_G v_G + \alpha_L v_L) \right]^{1.2} [0.836 + 2.75(\sin \theta)^{0.25}] \quad \text{Eq. 6.10}$$

α_G and α_L are volume fractions averaged over the whole slug. This slug frequency is also dependent on the slug length. Using the empirical relationship from Scott et al., the slug length can be estimated as a function of the diameter d with the following formulation (Bratland, 2010):

$$l_s = \max \left\{ 30d, \exp \left\{ -26.8 + 28.5 \left[\ln \left(\frac{d}{0.0254} \right) \right]^{0.1} \right\} \right\} \quad \text{Eq. 6.11}$$

Figure 10 shows the plot of this relationship. For these hydrodynamic slugs, it is clearly seen that the average slug length is about 300d for diameters above 0.5 m.

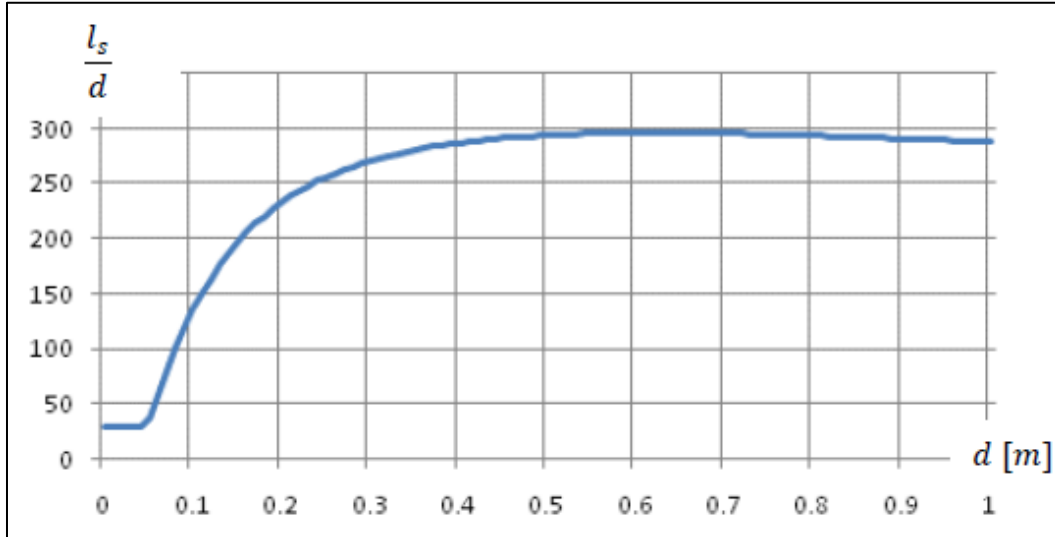


Figure 10. Slug Length as a Function of the Diameter of the Pipe based on Scott's Equation
(Source: Bratland, 2010)

Similarly, other empirical formulation correlates the slug frequency with the pipe length measured from the inlet. It is based on a curve fitting that shows fair agreement with laboratory and field test data:

$$f_s = \frac{0.47(\alpha_L v_L)^{0.75}}{d^{1.2} l_{in}^{0.55}} \quad \text{Eq. 6.12}$$

There are a couple empirical formulations available used to predict the slug frequency and length; however, there is not a general or correlation that predicts clearly the slugging behavior due to its unsteady complexity. For this reason, CFD simulations are now becoming the technique to understand and model this fluid dynamic problem.

6.5. Three-Phase Flow

Ignoring sand particles in subsea pipelines, it is a real situation to find that water comes with oil and gas. Three-phase flow must obey the same conservation equations for two-phase flow. However, it is expected to find more flow regimes besides the gas-liquid flow and liquid-

liquid flow as demonstrated in the chapter 2.2. Figure 11 shows a general flow regime map for three-phases with the possible flow regimes depending on the volume fraction and velocity of each phase. It is then possible to find dispersion of one liquid in the other, the Taylor-bubbles separated by two-phase slugs, or the elongated bubble with two-liquid layer at the bottom section of the pipe. This section will describe the mechanism and formulation when stratified flow and slug flow are traveling along horizontal and inclined pipelines.

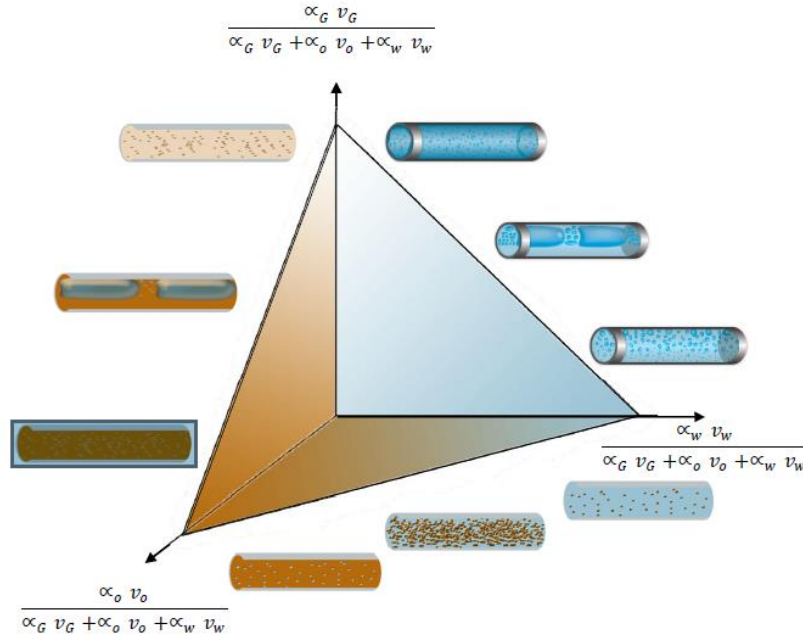


Figure 11. Three-phase Flow Regime Map for Horizontal Pipes

6.5.1. Stratified Flow

When considering three phases, there are still all forces such as friction, surface tension, and pressure correction term. This last term is estimated taking into account that there are two interfaces (gas-oil, oil-water). As shown in Figure 12, the pressure p is defined at the boundary between the gas and the denser liquid. The gas pressure correction term is the same as for two-phase gas liquid flow:

$$\Delta p_G = p_G - p = -\rho_G g h_G \quad \text{Eq. 6.13}$$

For the liquid correction terms, the center of gravity of each liquid phase is taken as a reference to measure the oil and water pressure correction terms as follows:

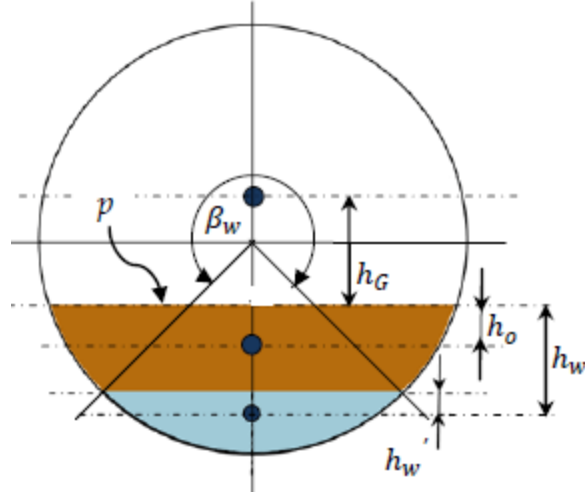


Figure 12. Gas-oil-water Stratified Flow Configuration with Center of Gravity Points

$$\Delta p_o = p_o - p = \rho_o g h_o \quad \text{Eq. 6.14}$$

$$\Delta p_w = p_w - p = \Delta p_o + \rho_w g h_w \quad \text{Eq. 6.15}$$

where h_o is the distance from the center of gravity of oil to the oil-gas interface, and h_w is the distance from the center of gravity of water to the oil-gas interface. The Interfacial frictions can also be calculated using the following empirical equation proposed by Petalas & Aziz ignoring the effect of wall friction, turbulence, and velocity profile (Bratland, 2010):

$$f_{GL} = (0.004 + 0.5 \times 10^{-6} Re_{SL}) Fr_L^{1.335} \frac{\rho_L d g}{\rho_G v_G^2} \quad \text{Eq. 6.16}$$

where Re_{SL} is the Reynolds number of the oil phase, and Fr_L is the liquid's Froude number. It is also dependent on the diameter of the pipe d , gravity g , velocity of each phase, and density of each phase. The Froude number is used to define the gravitational effects on the liquid velocity v_L , and it can be defined as (Bratland, 2010):

$$Fr_L = \frac{v_L}{\sqrt{g h_L}} \quad \text{Eq. 6.17}$$

Nobody has investigated if this system of equations is hyperbolic to understand if numerical problems can occur such that the simulations may crash. An eigenvalue analysis or perturbation methods are needed to find the hyperbolicity of these formulations.

6.5.2. Slug Flow

Regarding the modeling and analysis of slugs in three-phase flow, it can be treated in two ways:

1. Liquid phases (oil and water) are treated as a single phase with mixture properties of both liquids, and it is combined with gas such that it can be solved as a two-phase flow
2. Both liquid phases are separated into two layers with the denser liquid (oil) at the top and gas entrainment in the oil as shown in Figure 13.

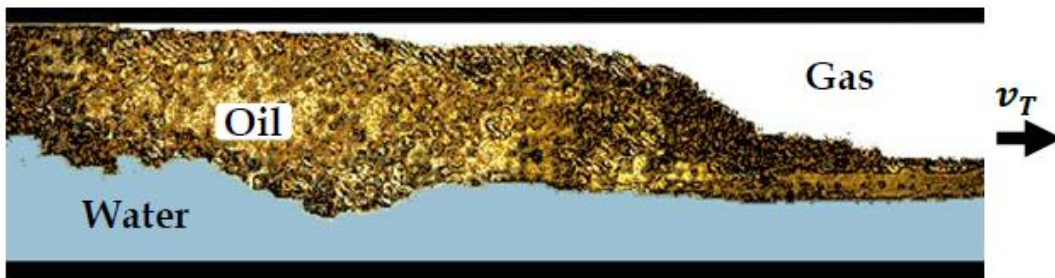


Figure 13. Slug Behavior in Horizontal Gas-oil-water Flow

Slugs are known to have a transient dynamic behavior with random frequency and superficial velocity varying in space and time. It is then very complex to solve these differential equations of momentum and mass. Assuming a simplified steady-state stratified flow with no liquid entrainment in the gas, the following relationship can be applied:

$$(1 - \alpha_{WGS})(1 - \alpha_{oS})(v_T - v_{oS}) = \alpha_{oT}(v_T - v_{oT}) \quad \text{Eq. 6.18}$$

where the first term corresponds to the fraction of oil slug with bubbles, the second term is the fraction of water of the oil-water slug without bubbles, and the third term corresponds to the difference in velocity between the Taylor gas bubbles and the oil fraction of the slug.

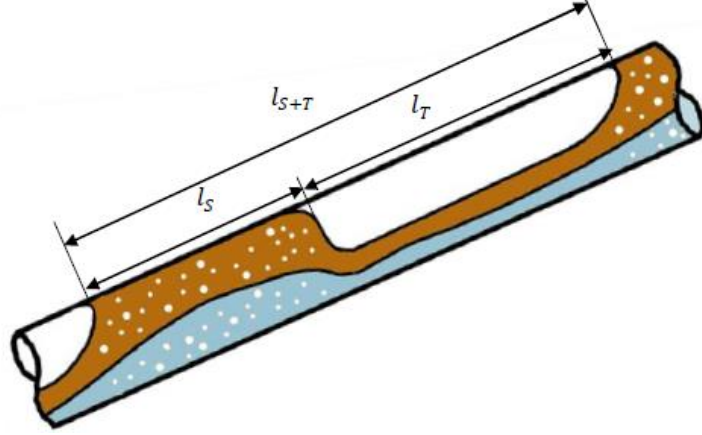


Figure 14. Slug Flow Configuration with Gas Entrainment in Oil and Water Layers

To derive formulation that it can be useful to compare with experimental and numerical solutions, it is convenient to use the mixture as a steady-state flow with its velocity defined as:

$$v_M = \alpha_G v_G + \alpha_o v_o + \alpha_w v_w \quad \text{Eq. 6.19}$$

With the development of a slug and Taylor bubbles, their mixture velocity can be estimated respectively using the following closure relationships:

$$v_M = (1 - \alpha_{wGS})v_{oS} + \alpha_{wGS}v_{wS} \quad \text{Eq. 6.20}$$

$$v_M = \alpha_{oT}v_{oT} + \alpha_{wT}v_{wT} + (1 - \alpha_{oT} - \alpha_{wT})v_{GT} \quad \text{Eq. 6.21}$$

The volume fraction of each phase in the slug can help to determine the flow rate or amount of each phase if fatigue damage occurs on the structure. Therefore, the average of oil, water, and gas in the slug portion of the flow can be expressed as:

$$\alpha_o v_o = \frac{l_S}{l_{S+T}}(1 - \alpha_{wGS})(1 - \alpha_{oS})v_{oS} + \frac{l_T}{l_{S+T}}\alpha_{oT}v_{oT} \quad \text{Eq. 6.22}$$

$$\alpha_w v_w = \frac{l_S}{l_{S+T}}\alpha_{wGS}(1 - \alpha_{wS})v_{wS} + \frac{l_T}{l_{S+T}}\alpha_{wT}v_{wT} \quad \text{Eq. 6.23}$$

$$\alpha_G v_G = \frac{l_S}{l_{S+T}}[(1 - \alpha_{wGS})\alpha_{oS}v_{oS} + \alpha_{wGS}\alpha_{wS}v_{wS}] + \frac{l_T}{l_{S+T}}(1 - \alpha_{oT} - \alpha_{wT})v_{GT} \quad \text{Eq. 6.24}$$

As shown in Figure 14, l_{S+T} represents the total slug length. Steady state momentum equations can be applied to describe the Taylor bubbles and water behavior in the slug including

the shear stresses between phases, the velocity and mass of each phase within the slug unit length. These relationships can be found in more detailed in Pipe Flow 2 book Chapter 15 from Bratland.

6.6. Liquid-Solid Flow

It is possible to have sand particles to be coming out of the oil-gas transporting pipelines. The most common sand production problem is the erosion of the pipe. However, sand particles might also affect the stability and integrity of the structure by blockage of the pipe due to the accumulation of those particles. This type of flow assurance issue can be treated by:

- avoiding the sand production at the wells with downhole sand exclusion systems , or
- preventing the sand accumulation with control of the sand transportation

The first method can lead to an extra pressure drop due to the inclusion of this system. On the other hand, the second method is less costly and more productive if the flow conditions can be controlled. The particle size and volume fraction of sand are the two major factors to consider for sand built up. From crude oil production, sand production is usually designed to keep it below 0.05 (Bratland, 2010). Regarding the size, the diameter of the sand particles is usually smaller than 1mm (Bello, 2008).

Particles can be classified into different categories depending on their diameter (Stour, 1988):

- very fine (0.05 - 0.1 mm)
- fine (0.1 - 0.25 mm)
- medium (0.25 - 0.5 mm)
- coarse (0.5 - 1 mm)
- very coarse (1 - 2 mm)

The most critical flow regime in pipelines is stratified flow since the particles tend to accumulate at the bottom section of the pipe (in this case at the bends). As a consequence of the transporting of sand particles, the pressure loss increases even though the liquid-gas flow has enough velocity to prevent sand build up. If the velocity is too low, the sand might block or reduce the area of the multi-phase flow and production will then decrease.

6.6.1. Pressure Build up of Particles

If the sand starts building up in the pipe, this implies that the pressure and friction loss also increases depending on the mixture velocity of the flow. It is important to assess how these solids might affect the oil and gas production. Assuming that there is no sand in the pipeline, the

friction loss starts increasing quadratically with the velocity of the mixture. With sand flowing in the line, the friction loss is much higher even though the particles are carried by the fluid. The pressure drop increases dramatically when high flow rates are exhibited as shown in Figure 15.

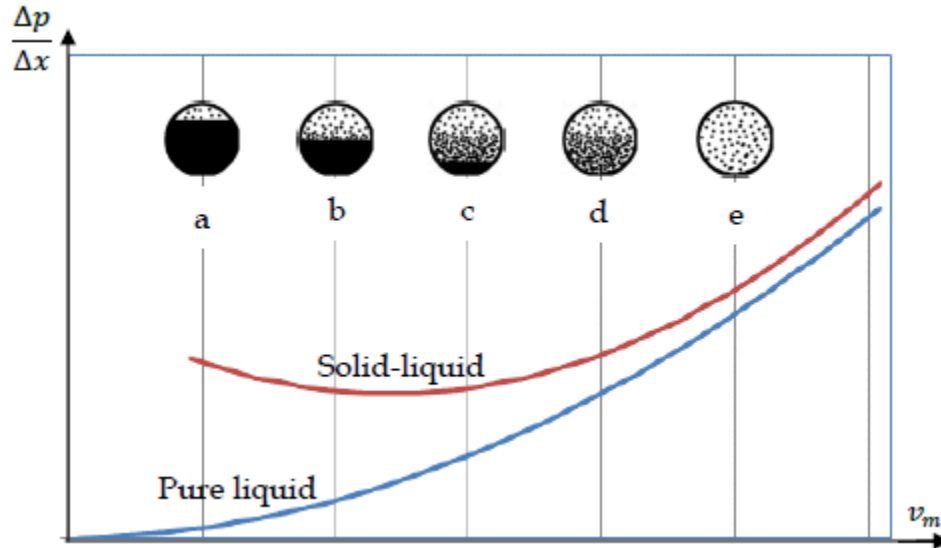


Figure 15. Friction Loss as a Function of the Mixture Velocity when Sand Particles Flow in the Pipeline (Source: Bratland, 2010)

The solid-liquid curve in Figure 15 shows how the pressure drop decreases with the reduction of the flow velocity. At this region, some sand particles can accumulate at the lower section of the pipe and the rest keep circulating. However, if the mixture velocity keeps decreasing, there is a high probability that the sand buildup increases and as a result the pressure drop increases again. The main idea is basically to maintain a balance in the velocity to avoid the blockage of the pipeline and high pressure drop.

6.6.2. Minimum Required Velocity

The main parameter that has an effect on the sand buildup is the velocity of the mixture. This is the minimum required velocity to keep a sand particle moving with the flow. Before developing a formulation of this minimum velocity, the following assumptions are established:

1. Sand particles are spherical and have the same average diameter
2. The volume fraction of sand is very low in comparison to the liquid flow
3. Pipe is assumed to be horizontal or has very small pipe inclinations

Considering the static forces between the particles and gravity force as shown in Figure 16, the critical velocity to push a grain of sand is found to be (Bratland, 2010):

$$v_{L^*} = \sqrt{\frac{16(\rho_S - \rho_L)}{3f\rho_L} g d_S \left[\frac{\sin\left(\theta + \frac{\pi}{6}\right) + \mu_{fS} \cos\left(\theta + \frac{\pi}{6}\right)}{\cos\left(\frac{\pi}{6}\right) - \mu_{fS} \sin\left(\frac{\pi}{6}\right)} \right]} \quad \text{Eq. 6.25}$$

where ρ_S is the density of the solid particle, ρ_L is the density of the liquid, f is the friction due the flow, g is the gravity, d_S is the diameter of a solid particle, θ is the inclination of the pipe, and μ_{fS} is the friction coefficient between grains . Assuming the sand particles are rolling rather than sliding, then $\mu_{fS} = 0$. Also, if the pipe wall is almost smoothly as the grains, these particles will slide along the wall and the angle $\frac{\pi}{6}$ changes to 0, and equation 6.25 changes to (Bratland, 2010):

$$v_{L^*} = \sqrt{\frac{16(\rho_S - \rho_L)}{3f\rho_L} g d_S [\sin \theta + \mu_{fS} \cos \theta]} \quad \text{Eq. 6.26}$$

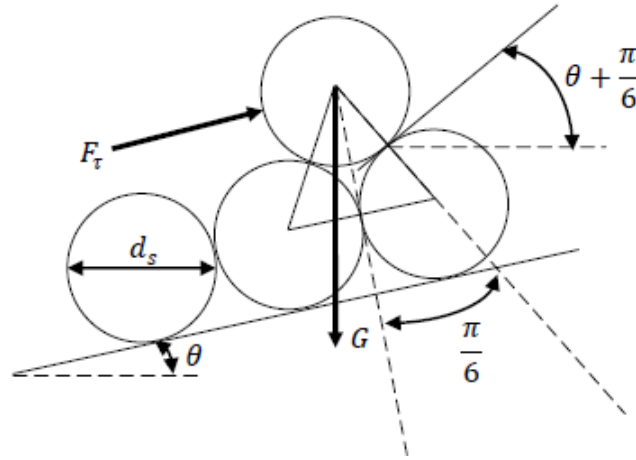


Figure 16. Free Body Diagram of Static Forces on a Sand Particle

In case of vertical pipes, the sand particles are treated as bubbles or droplets distributed across the pipe's cross section.

7. Subsea Pipe Model and Multi-phase Properties

7.1. M-Shaped Jumper Geometry

The geometry consists of an M-shaped pipe with the flow starting in a horizontal section, and the jumper has a 102 ft (31.1 m) suspended span. It has 7 bends with a radius of $5D$ as shown in Figure 17. Table 1 indicates the geometry and material properties of the jumper model. Rigid jumpers are usually made of carbon steel with yield strength of 65 ksi or 448 MPa.

Table 1. Geometry and Material Properties of Jumper

Geometry and Material Properties	Value
OD (mm)	273.05
ID (mm)	209.55
Density (kg/m ³)	7850
Young's Modulus (GPa)	210
Poisson's ratio	0.3
M (m, ft)	31.09 [102]
A (m, ft)	3.66 [12]
B (m, ft)	7.32 [24]
C (m, ft)	7.92 [26]

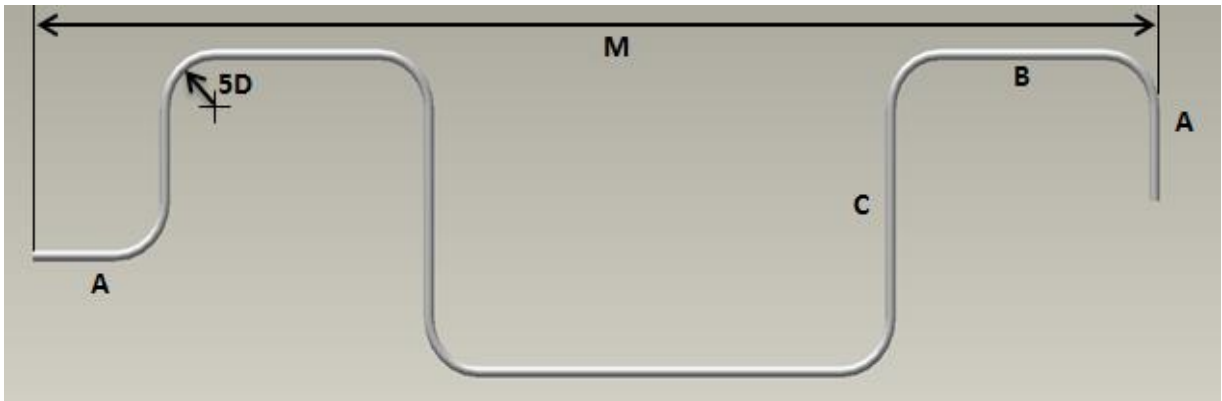


Figure 17. M-shaped Jumper with Dimensions

7.2. Multi-phase Properties

The properties of the multi-phase flow inside the pipe vary depending on the pressure and temperature of each well and reservoir. Experimental and common values available in research studies and private information from oil and gas companies were collected to specify the flow conditions and the properties of each phase. For a good prediction of the real conditions, the

surface tension between oil and gas is set to an approximate value of two liquids with similar viscosities as water and oil.

Table 2. Fluid Properties and Conditions for the Multiphase Flow

Fluids	Oil	Gas	Water
Density (kg/m ³)	835	73	1020
Dynamic Viscosity (Pa-s)	0.0044	0.000015	0.0006
Flow rate (m ³ /s)	0.04968	0.1404	0.03496
surface tension (N/m)	*oil-gas: 0.031 oil-water: 1E-6	*oil-gas: 0.031 gas-water: 0.074	oil-water: 1E-6 gas-water: 0.074

For the four-phase flow, the properties of the sand are set to the sample particles used in the experimental work performed by Bello, Reinicke, and Teodoriu. The average particle diameter is 0.6 mm with a density of 2600 kg/m³.

8. Methodology

There is not a standard procedure or methodology to analyze FIV in subsea pipelines. It is sometimes analyzed based on very conservative guidelines for vibration induced fatigue in onshore piping. The challenge is to create a methodology that engineers can follow to identify the risk of failure based on preliminary flow analysis and then perform a more detailed assessment that tells if the flow conditions need to be modified. Figure 18 shows the procedure to perform a Phase I – screening of FIV in a subsea pipe. If the actual flow conditions do not meet the criteria, a Phase II is required which consists of a FSI analysis to determine the life of the pipe. This last approach is preferred due to its accuracy, but it usually takes long computation time even with availability of good computational resources. A FSI process is presented to solve the interaction between multi-phase and structure as indicated in Figure 19. The FSI analysis is explained in chapter 8.3.

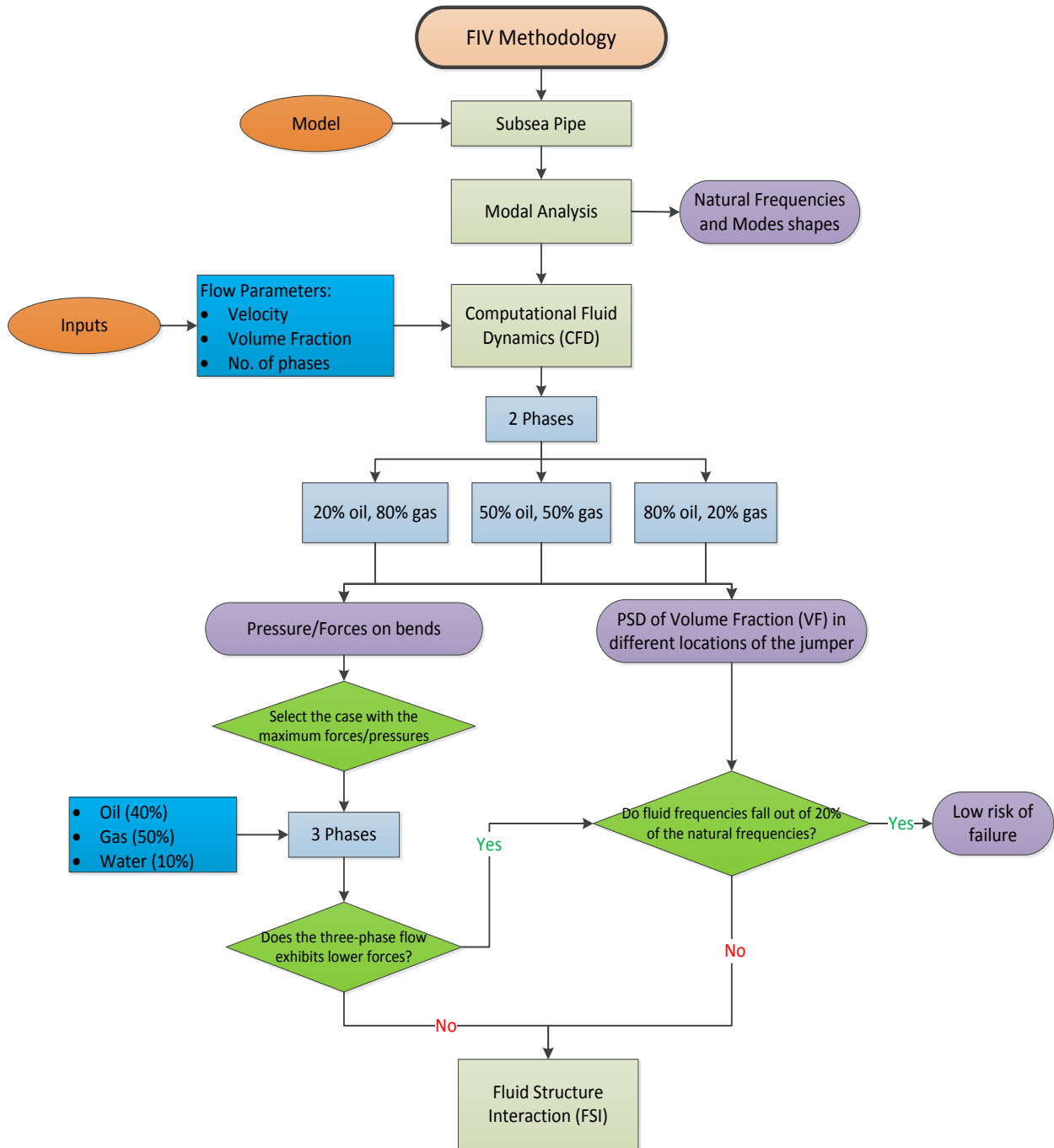


Figure 18. Phase I – FIV Methodology to assess Risk of Multi-phase Flow in Subsea Pipe Component

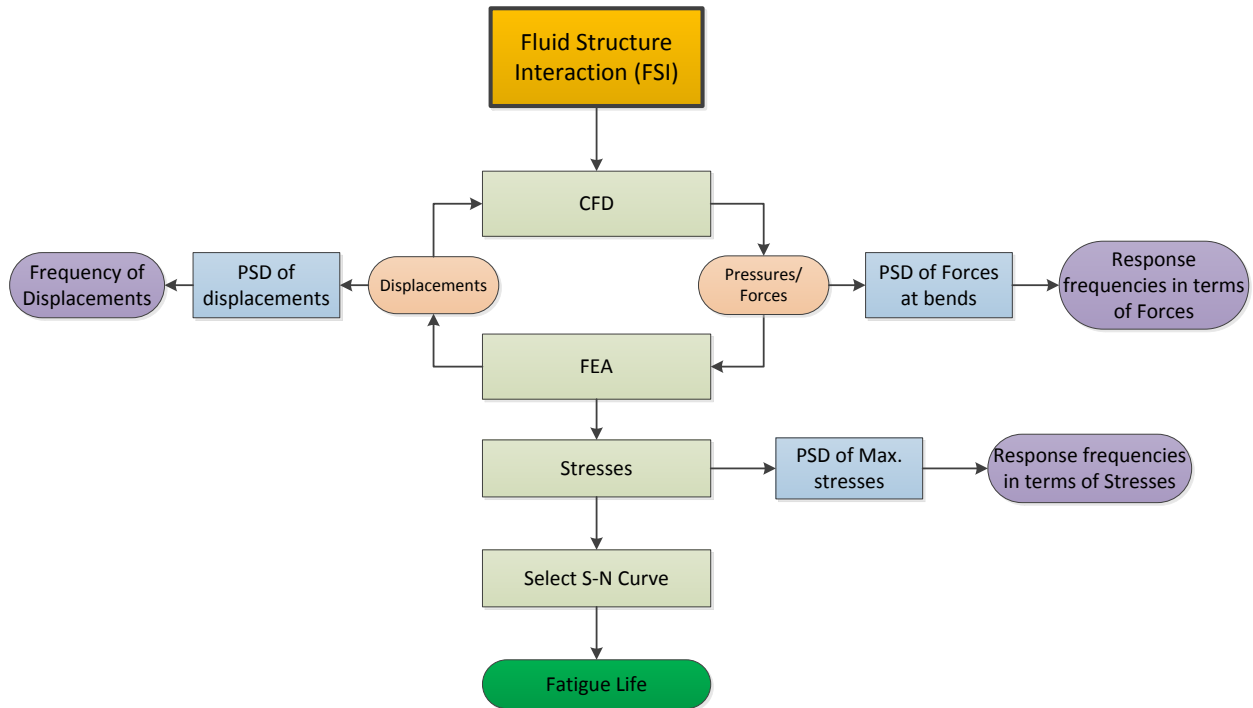


Figure 19. Phase II – FIV Methodology to determine the Fatigue Life of a Subsea Pipe

8.1. Computational Fluid Dynamics

As solutions to multi-phase flow are very complex and comprehensive, Computational Fluid Dynamics (CFD) is implemented as a numerical method to simulate realistic flow conditions and achieve accurate results. It has the advantage of capturing multiple flow outputs in the same analysis for a better understanding. CFD can reduce the cost and limitation that experimental tests have with its difficult setup and calibration of the equipment.

CFD tools, in this case STAR-CCM+, usually follow work flow to perform flow simulations:

- Create CAD model and import the geometry.
- Specify the boundary conditions (i.e. type of boundary: velocity inlet, or pressure outlet)
- Select the appropriate meshing models and mesh size
- Select the physics of the model (turbulent models, flow regime, multi-phase or single phase, steady or unsteady).
- Specify the time step and physical time of the simulation
- Create reports and plots to monitor the solution and then run the solution
- Analyze the results

8.1.1. Fluid Domain

The M-shaped jumper was modeled in Pro Engineer and it was then exported to Abaqus and Star CCM+.

The internal fluid volume was extracted from the CAD model since this is the only domain of interest. The jumper was divided into 15 sections to refine the mesh on bends, improve the quality of the mesh, and mesh each section separately. For the boundary conditions, the left end is defined as velocity inlet while the right end is set as pressure outlet.

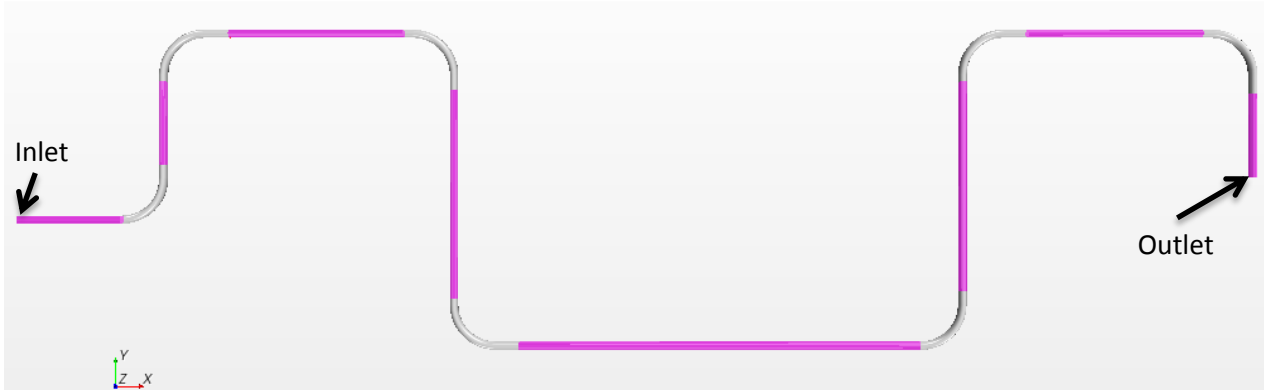


Figure 20. Fluid Domain Partition for Jumper Model

8.1.2. Turbulence Model

Turbulence models are available to solve the unclosed system with mean flow equations. In other words, it is only necessary to account the effect of the turbulence on the mean flow without resolving the turbulent fluctuations of the system. The Reynolds stresses term appears in the Navier-Stokes equation after solving the Reynolds average. Therefore, a turbulence model is necessary to solve the transport equations for the stresses and extra transport equations from the turbulent dissipation rate and turbulent kinetic energy (Izarra, 2009). From the three turbulent methods available, the Reynolds-Averaged Navier-Stokes (RANS) is the most efficient due to its balance between simulation time and accuracy. RANS solves the Navier-Stokes (NS) equations into its time-averaged (\bar{u}_i) and fluctuating term (u_i'). Therefore, the instantaneous velocity can be expressed as:

$$u_i = \bar{u}_i + u_i' \quad \text{Eq. 8.1}$$

A two-equation turbulence model is implemented to determine the turbulent velocity and length scales. The SST k- ω model is selected to resolve the flow since it has the advantage of two models by providing an accurate formulation to solve the all y^+ treatment:

- The viscous near-wall region (for pressure gradients) , and
- The free-stream flow in the far field

This model solves two extra transport equations with the variables k and ω defined independently as follows in a simple form:

$$\text{Turbulent Kinetic Energy} \quad k = \frac{3}{2} (I v)^2 \quad \text{Eq. 8.2}$$

$$\text{Specific turbulent dissipation rate} \quad \omega = \frac{\sqrt{k}}{L \cdot \beta^{1/4}} \quad \text{Eq. 8.3}$$

where v is the local velocity magnitude, I is the turbulence intensity, L is turbulent length scale, and β is the coefficient of the model. Those parameters are usually defined at a recommended default values in the CFD tool based on the stability of the PDE.

8.1.3. Volume of Fluid (VOF)

This is a multiphase model that simulates the interaction between two or more phases. It solves the interface between phases using numerical grids that track the volume fraction of each phase at each small volume. The transport equation is solved for each phase within the finite volumes using a segregated flow model for mildly compressible flow or incompressible flow. VOF is an Eulerian method in which the grid is fixed while the flow material passes through the mesh.

8.1.4. Lagrangian Multiphase

Multiphase flows with solid particles are modeled and solved using a different method from the Eulerian method. In fact, there are two methods to model particles of sand in Star CCM+:

- a) Lagrangian Method and
- b) Discrete Element Method (DEM).

A Lagrangian phase is a dispersed phase modeled in a Lagrangian framework such as sand particles. This involves the transport of particles, liquid droplets or gas bubbles (disperse phases) by a gaseous or liquid continuous phase. The Lagrangian method allows selecting the phase models and setting the phase boundary conditions. If interaction of particles with the continuous phase dominates their motion, the dispersed phases are dilute (STAR CCM+, 2013).

For this multiphase modeling, parcels (particle-like elements) are followed through the continuous phase. This method gives the option to select the physical behavior of the particles: material particles or massless particles. In addition, this modeling provides the boundary conditions, the two-way coupling interaction between particles, and drag.

The lagrangian method is recommended for very small particle sizes such that the only interest is to capture the effect of the cloud of particles on the continuous flow rather than the particle-particle interaction. The Lagrangian method is also more appropriate to prevent long computational times.

Alternatively, the DEM is an extension of the Lagrangian Multiphase model in which each particle is modeled to account for the interaction forces between particles. The interaction of the particles with the continuous phase (oil, gas, water) is as important as the interaction between the dense particles. This model resolves the interaction very accurate but it is time computational intense. Some of the applications include sand, food particles, powders, capsules, and slurries.

For the purpose of the present work, the lagrangian method was implemented to simulate only the interaction of continuous flow-particle since particle-particle interaction has minor damage effects on the life of the structure.

8.1.5. Implicit Integration and Time Step

Solving complex problems requires to select the appropriate numerical method that considers how both accurate and stable the solution needs to be. Numerical solutions are either explicit or implicit. Explicit solutions take into account the quantities at the previous time steps to estimate the values of the variables for the current time step. It is usually implemented for time-dependent problems in which the time step should be set such that it advances less than one cell distance due to the potential of numerical instabilities. Neighboring cells have no information about the variables at this stage such that it is impractical if the time step jumps to these cells (Science Flow, 2013).

On the other hand, implicit method applies iterations through steps to compute the variables based on the known and unknown values at the cells of the current (n) and forward time step (n+1). This method is more computational intensive, but it allows large time steps. In this case, all cells are coupled together such that it is more stable due to its independency on the time step.

In this CFD model, the implicit integration is applied to achieve faster convergence and avoid instability issues. The amount of variables in the Navier-Stokes equations makes this transient problem more robust using the implicit method.

A time step sensitivity analysis was performed to estimate the appropriate time step based on the Courant number (CFL). This is used as an estimate of the time step depending on the mesh size Δx and average velocity u as follows:

$$\Delta t < \frac{CFL \cdot \Delta x}{u} \quad \text{Eq. 8.4}$$

The purpose is to converge the solution at a faster rate. CFL is recommended to be no more than 1. Therefore, a balance between the mesh size and the time step must be achieved. The recommended time step based on this criterion is 0.005 seconds.

8.1.6. Meshing

A Finite Volume Method is usually implemented for fluid simulations to discretize the differential form of the conservation equations. This approach has the advantage of having a conservative discretization both locally and globally. This method can also be applied to irregular meshes such as polyhedrals in 3D problem as happens with this FIV problem.

There are two types of mesh that can be assigned to solve the multi-phase flow: Eulerian mesh and Lagrangian mesh. The Eulerian mesh has a fixed grid with the flow moving through the mesh. This type of mesh is the most common for single flow or multiphase mixture flows. The Lagrangian mesh deforms or moves with the flow as it can happen with the modeling of solid particles.

The generalized cylinder mesher was selected based on its effectiveness in reducing the number of cells and computational time with respect to other meshing techniques. This technique consists of extruding polyhedral (14 faces) cells or volumes from the inlet of the pipe along the length of the pipe as shown in Figure 21. The user has the option to specify the number of layers along the pipe. It is also important to capture the velocity gradient and turbulence close to the wall, so the prism layer mesh creates thin layers of elements by the wall. It is recommended to use at least 4 thin layers for turbulence flows (STAR CCM+, 2013). For some of the analyses, the number of layers was reduced to prevent the distortion of the mesh due to the displacements of the FEA tool.

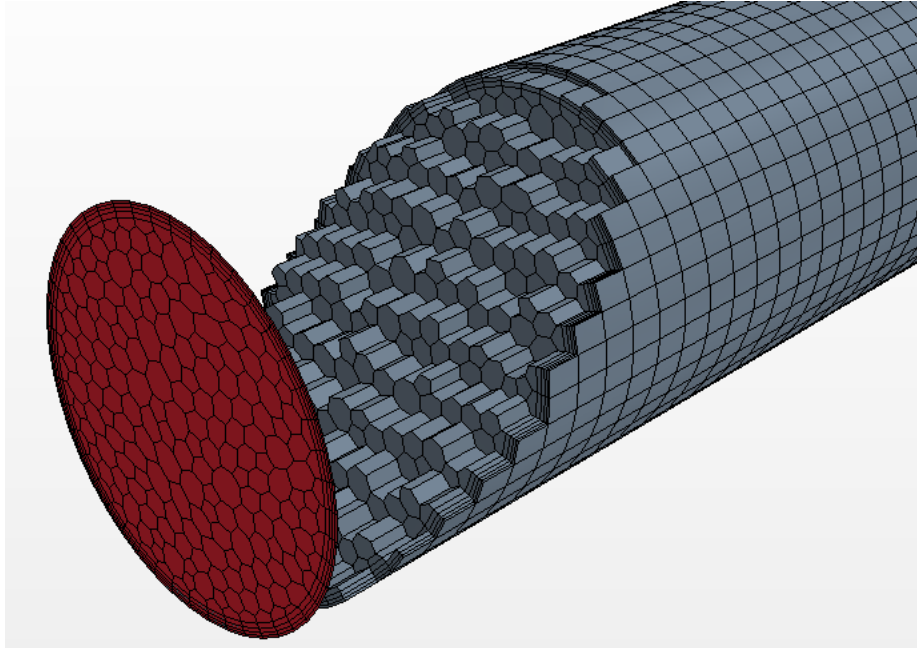


Figure 21. Generalized Cylinder Mesh of the Fluid Domain

Table 3 shows some of the mesh parameters and its reference values for the CFD simulations.

Table 3. Meshing Parameters for the CFD Model

Mesh Parameters	Value
Base size (mm)	15
Number of prism layers	4
Prism Layer Stretching	1.3
Prism Layer Thickness (mm)	7.5

Bend sections were refined to capture the circulation flow and pressure fluctuations.

For the FSI analysis, the mesh was modified to have a better control on the number of cells along the length of the jumper and proximity to the wall. A directed mesh was applied at the inlet of the jumper and then this surface mesh is extruded along the length of the jumper similar to the process of the generalized cylinder mesher. Appendix C shows a step-by-step to generate this directed mesh.

8.1.7. Boundary Conditions

For the flow in a pipe, the following boundary conditions are specified:

- Velocity Inlet: an initial velocity is provided at the entrance of the pipe
- Pressure outlet: a static pressure is specified at the exit of the pipe

- Wall: the inner surface of the pipe is treated as a no-slip smooth wall

8.1.8. CFD Physics Models

The physics models selected for solving the multi-phase flow are:

- Three Dimensional
- Implicit Unsteady: iterative time-dependent analysis
- Multiphase Mixture: composed of oil, gas, and water
- Eulerian Multiphase
- Volume of Fluid (VOF)
- Segregated Flow: solve the momentum and continuity equations in an uncoupled manner
- Lagrangian Multiphase: this option is enabled if solid particles are modeled.
- Gravity

8.2. Finite Element Analysis

The Finite Element Method (FEM) is an approach to solve linear and non-linear structural problems. This numerical method helps to determine how a structure responds when a load or displacement is applied to it. This is based on discretizing the structural domain in small elements to solve partial differential equations described in Chapter 4.1. The formulation of the FEM is generated to satisfy the equilibrium condition of work when forces are applied to the object which undergoes a displacement. Basically, this method is based on a spring system in which the stiffness of the material dictates the amount of force required to deform the spring to a specific distance.

The jumper structure is studied using a FEA tool to perform two types of analysis:

- Modal Analysis: dynamic response of the structure to find the frequencies at which resonance might occur
- Dynamic Coupling Analysis: FSI simulation coupled with the fluid solver to determine the stresses and displacements due to the multiphase flow pressure

8.2.1. Meshing

The jumper model was meshed using linear elastic stress hexahedral elements (8-node brick). A good roundness of the inner surface is important to avoid a large gap between the CFD and FEA mesh such that unrealistic large displacement might take place and cause a distortion of the mesh. At least 30 nodes were allocated to the inner surface of the pipe as shown in Figure 22.

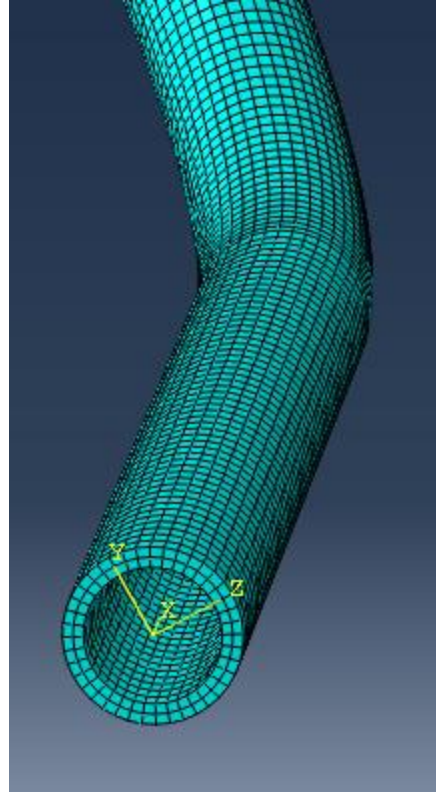


Figure 22. Hexahedral Mesh of the Structural Domain in ABAQUS

8.2.2. Boundary Conditions

For conservatism, it was assumed that the jumper has a fixed-fixed boundary condition such that the stresses range might be of large magnitude. The fatigue life might not satisfy the minimum required life due to overestimate the dynamic motion. It is then important to assess the high conservatism of the boundary conditions and perform further analysis if required.

8.3. FSI Analysis

Fluid Structure Interaction is a multi-physics analysis in which the structure is elastically or plastically deformed due to the induced forces of the fluid. This FSI simulation is performed by coupling within the CFD program the fluid solver and the stress solver to capture the effects of the internal multi-phase flow on the structure. The two solvers can be coupled in a loose or tightly manner depending on the magnitude of the displacements.

One-way coupling is a loose manner such that the pressures from the fluid in STAR CCM+ are mapped and exported to the structural model in ABAQUS to calculate the displacements and stresses. The geometry of the fluid domain is not updated since the displacements are too small that the structure of the flow remains the same.

The two-way coupling simulation is a tightly method of solving the same analysis with the difference that the fluid and stress solvers exchange information at least once every time step, and the geometry of the fluid is updated since it is expected an alteration of the flow due to the large deformations. For this dynamic co-simulation, the information can exchange at each iteration within the time step, known as implicit coupling, or at the end of every step, known as explicit coupling. The implicit coupling is preferred when the deformation of the mesh is significant, so the solution is more stable. This FSI two-way coupling simulation was performed within STAR-CCM+.

An important factor to control the deformation of the mesh is the morphing. The purpose is to stretch or move the mesh to provide a good quality fluid grid that adapts to the motion of the solid structure. The shapes of the cells are changing over time due to the iterative displacements coming from the structural solver.

9. Benchmark

A flow pattern map was calculated based on Taitel and Duckler theoretical model and according to equations 6.7 to 6.9. A 5cm-diameter horizontal pipeline at operating conditions of 68 atm and 38° C carries oil and natural gas with a density of 0.65 g/cm³ and 0.05 g/cm³ respectively. Figure 23 indicates the different flow patterns developed depending on the superficial velocity of the gas (U_G^S) and superficial velocity of the oil (U_L^S). A numerical model was used to validate the flow patterns identified on the map. The following flow patterns with its corresponding superficial velocity points taken from the map were analyzed using a CFD tool:

1. Stratified smooth, $U_L^S = 0.05 \text{ m/s}$ and $U_G^S = 0.1 \text{ m/s}$, $h_L = 0.5d$
2. Stratified wavy, $U_L^S = 0.4 \text{ m/s}$ and $U_G^S = 1 \text{ m/s}$, $h_L = 0.5d$
3. Slug flow, $U_L^S = 1.0 \text{ m/s}$ and $U_G^S = 0.5 \text{ m/s}$, $h_L > 0.35d$ from Eq. 6.9
4. Annular flow, $U_L^S = 0.1 \text{ m/s}$ and $U_G^S = 10 \text{ m/s}$, $h_L < 0.35d$ from Eq. 6.9

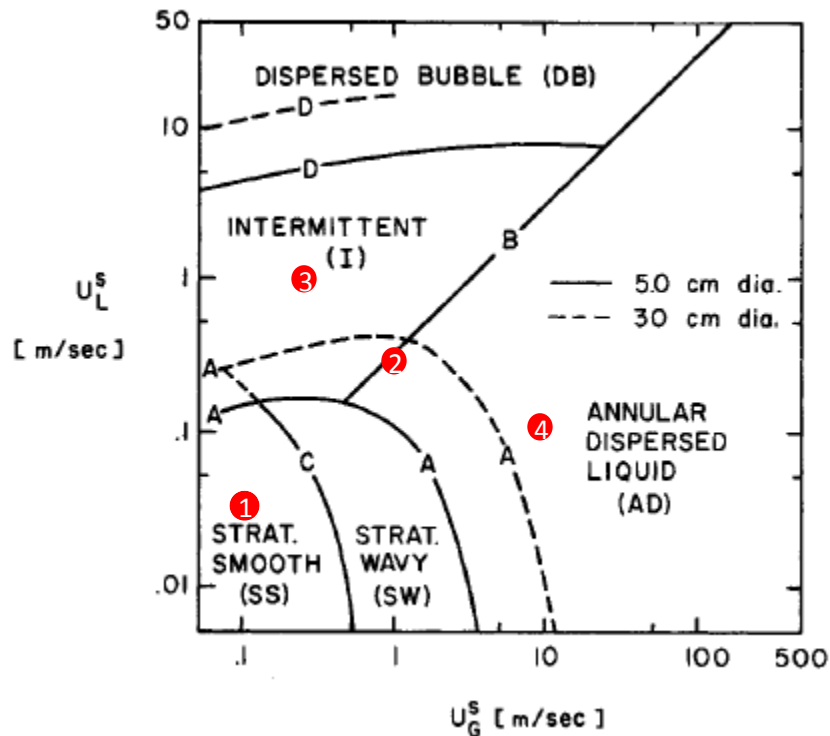


Figure 23. Flow Pattern Map of Crude Oil and Natural Gas at 68atm and 38C in Horizontal Pipe (Taitel & E., 1976)

Figure 23 indicates the different flow patterns developed depending on the superficial velocity of the phases and height of the oil. The red dots represent the selected points to benchmark the flow regimes in a 5 cm diameter pipe.

As shown in the contour of the numerical analysis in Figure 24, the results have a good agreement according to the theoretical flow pattern map of Taitel and Duckler. It is expected to have a smooth stratified flow at very low flow rates (See Figure 24 (a)). As the velocity of the gas starts increasing, a disruption between the liquid and gas phases occurs such that waves are developed on the surface (See Figure 24 (b)). If the velocity of the gas keeps increasing such that the ratio of the velocity of the gas to the velocity of the liquid is very large (above 50), annular flow can developed as illustrated in Figure 24 (d). As stated in Equation 6.9, the height of the oil should be below 0.35 the diameter of the pipe to develop this type of flow regime as confirmed by the CFD results. Similarly, a blockage of the pipe happens at the beginning of the pipeline, which represents the condition where a slug was developed as predicted by Taitel and Duckler theoretical model.

In general, there is a good agreement between the theoretical solution by Taitel and Duckler and the numerical results. Wavy flow is the only point of the numerical analysis which falls outside of the stratified wavy flow region of the map. In fact, this point is located at the boundary with the intermittent flow (slug) which is a potential flow regime after waves reach the top of the pipe.

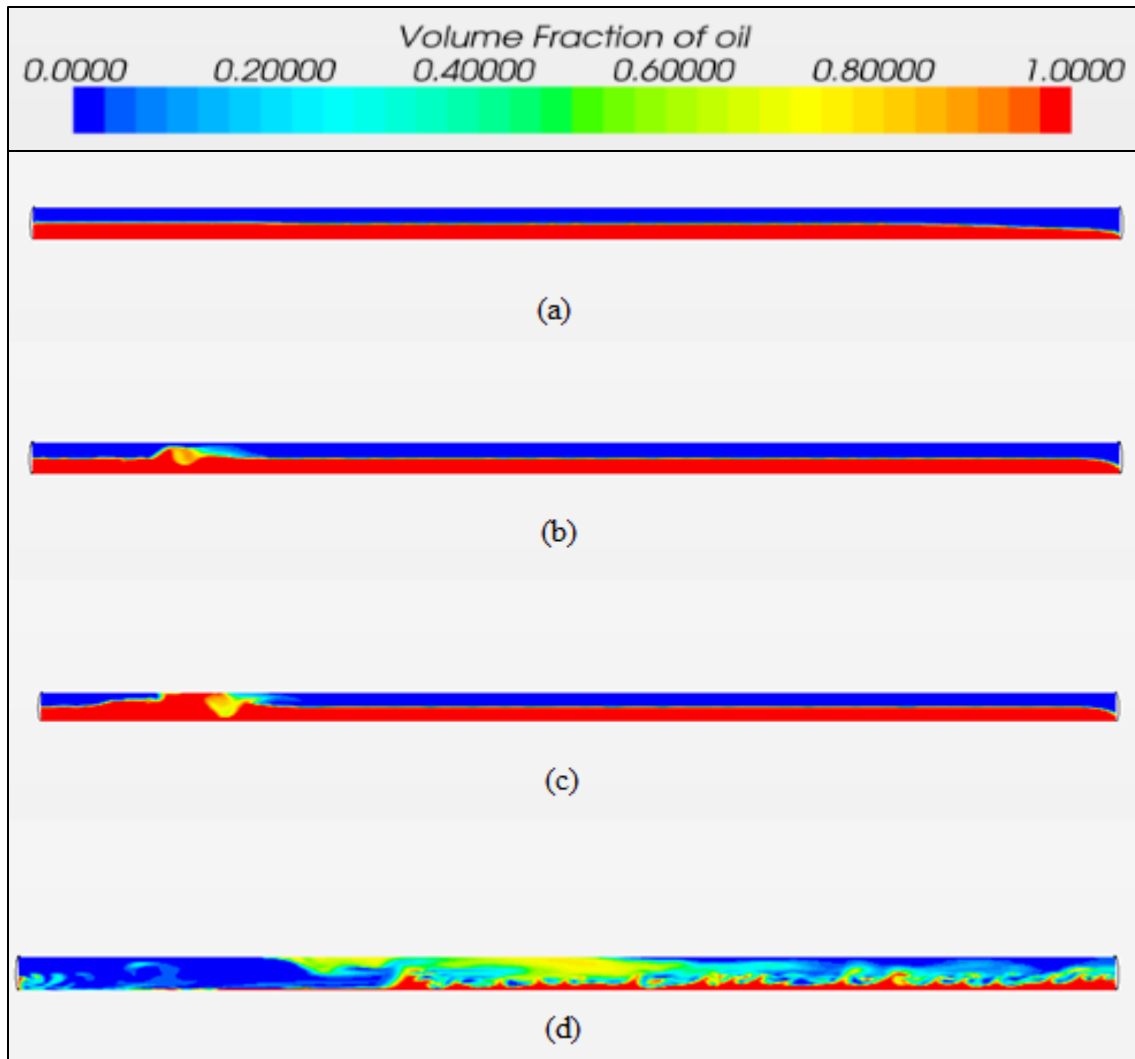


Figure 24. Volume Fraction of Oil for a Horizontal Pipe under 68 atm and 38°C: (a) Stratified Smooth (b) Stratified Wavy (c) Slug Flow (d) Annular Flow

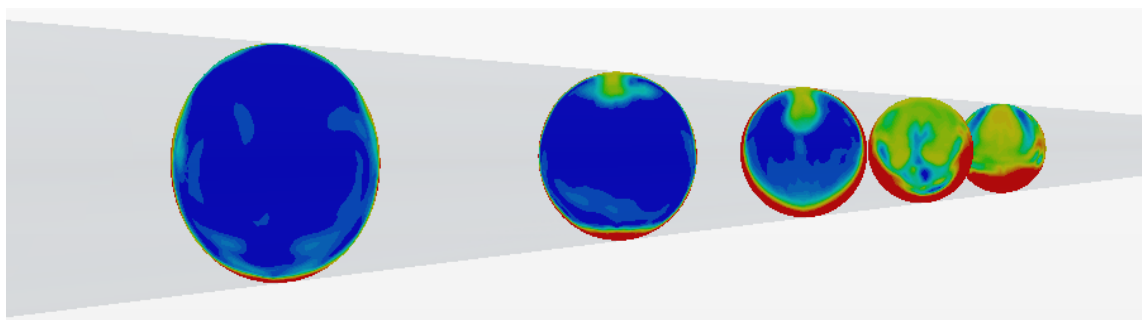


Figure 25. Cross-section of Annular Flow in a Horizontal Pipe under 68 atm and 38°C

Equations 6.7-6.9 were implemented to determine the velocity at which a transition from stratified to wavy occurs. Similarly, these set of equations will apply to the transition from wavy

to slug flow or annular flow. Table 4 shows the transition velocities and velocity of the gas for the selected points in the numerical analysis. According to the criteria, stratified flow and slug flow agree to be within the appropriate range of velocities. However, the velocity of the gas for the wavy flow falls out of the range according to the theoretical model from Taitel and Duckler. A possible reason for this discrepancy is the unknown surface tension value between the oil and natural gas since this parameter determines the equilibrium at the interphase between the two phases and the transition from a wavy flow to slug flow.

Table 4. Parameters of Velocity of the Taitel and Duckler Model

Flow Pattern	$V_{Gw}^*(m/s)$	$V_G(m/s)$	$V_{GB}^* (m/s)$
Stratified Flow	0.60	0.1	0.76
Wavy Flow	0.30	1.0	0.76
Slug Flow	0.19	10	0.76

10. Phase I – FIV Results

As specified in the FIV methodology, a modal analysis is performed as a first step to extract the natural frequencies. After that, CFD cases are described and explained in general for each configuration in terms of the volume fraction. The time and frequency domains of pressure and volume fraction of oil were obtained as screening to assess the risk of failure. As a validation and verification method, a numerical analysis was performed to benchmark the expected flow patterns of a two phase flow in a straight pipe using a theoretical flow pattern map.

10.1. Modal Analysis

Significant vibrations can occur when internal flow induces forces on the structure of a pipe if this external source is vibrating at the same frequency of the natural frequencies of the pipe. When a load is applied to a system and then release to vibrate freely, the object oscillates at particular frequencies depending on the mass and stiffness. This vibration analysis tells how the energy is transferred along the structure. The estimation of the natural frequencies and its respective mode shapes are derived from the equation of motion with the damping ignored, resulting in the following general form (Clough & Penzien, 1993):

$$[M][\ddot{U}] + [K][U] = [0] \quad \text{Eq. 9.1}$$

where M is the mass matrix, \ddot{U} is the acceleration, and K is the stiffness matrix. Using ABAQUS (FEM solver), a modal analysis was performed to determine the natural frequencies and its mode shapes. These are the dominant modes of vibration of rigid structures such as jumpers. The added mass due to the external current is accounted for the modal analysis. It is assumed that this added mass is equivalent to the displaced volume of the seawater occupied by the pipe.

Table 5 indicates the frequencies for the first eight modes and compares the results with and without added mass.

Figure 26 b) shows the first two mode shapes of the jumper with the black frame indicating the undeformed shape. Refer to Appendix A to see the remaining mode shapes obtained from ABAQUS.

Table 5. Natural Frequencies of the Jumper from ABAQUS

Mode	Frequency (Hz)	Frequency with added mass (Hz)	% Difference
1	0.656	0.571	13.9
2	1.125	0.981	13.7
3	1.611	1.403	13.8
4	1.890	1.646	13.8
5	2.125	1.851	13.8
6	2.370	2.065	13.8
7	3.068	2.673	13.8
8	6.517	5.678	13.8

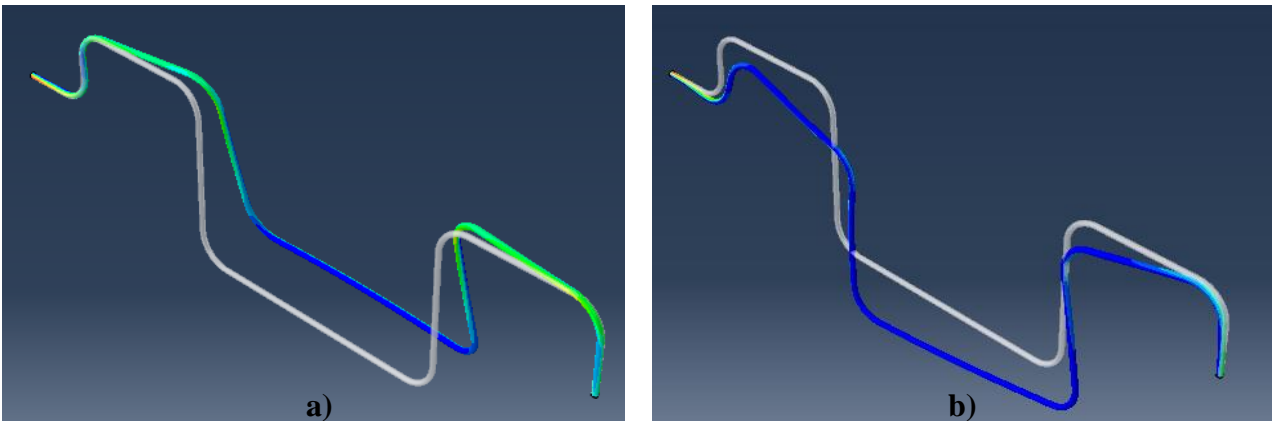


Figure 26. a) Mode 1 and b) Mode 2 of the M-shaped Jumper - Isometric View

10.2. Oil-Gas Flow

For the two-phase flow, oil and gas were initialized as a stratified flow. The simulation of this multiphase flow is allowed to run at least until the flow reaches the outlet of the pipe (PLET end). The volume fraction of the phases and superficial velocity are the two parameters that are analyzed in this work since those are expected to have a significant effect on the flow and the structure. As initial conditions, it was assumed that the jumper is filled with gas. Table 6 indicates the cases of oil-gas flow in the M-shaped jumper that were modeled and analyzed.

Table 6. CFD Simulation Cases for Two-phase Flow

Case	Inlet Velocity (m/s)	Volume Fraction of Oil	Volume Fraction of Gas
1	1	0.2	0.8
2		0.5	0.5
3		0.8	0.2
4	2	0.2	0.8
5		0.5	0.5
6		0.8	0.2

10.2.1. Volume Fraction

As described in Pontaza's study, 50-60% gas flow should be the most critical case regarding to FIV, which corresponds to mid-life production (case 2 in Table 6). This percentage of gas corresponds to the mid-life production.

The mid-life flow condition is initialized at the inlet with 50 percent of the denser fluid (in this case oil) at the bottom of the pipe as shown in Figure 27 Section A. The stratified flow reaches the first bend without any mixing, and then the oil starts accumulating until backflow occurs due to the effect of gravity. At this moment, the oil blocks partially the passage of gas into the vertical section and pressure builds up as the gas keeps flowing from the inlet. The gas pushes the oil to flow upwards and a wavy flow is developed at the bend since a high tension at the interface is generated when the gas accelerates. At the first vertical section, some small droplets of oil initially are forced to flow up, and then both fluids start mixing. Even though a dispersed flow or slug tends to develop at a specific period of time in vertical sections, churn flow is the dominant pattern during the entire simulation (see Section B in Figure 27) Once the two-phase flow reaches the horizontal top section of the jumper, the oil mixed with a small percentage of gas seats at the bottom of the pipe due to gravity as shown in Section C from Figure 27. When the flow reaches the third bend, the thick-layer of stratified oil flow changes to a thin stream (see Section D in Figure 27) that impacts the bend. The oil-gas flow is then induced to flow downwards, and it is expected the oil to push the gas downwards in particular when long gas bubbles forms. The reason of this flow behavior is the difference in density between phases. In this vertical section, flow transition occurs between dispersed bubble flow and churn flow (see Section E in Figure 27). Due to the high disturbance or turbulence of the flow, slugs are difficult to develop even though accumulations of oil are formed at an instance of a specific location of the jumper as shown in Section F from Figure 27. As the disorganized oil-gas flow moves downwards, the kinetic energy keeps increasing.

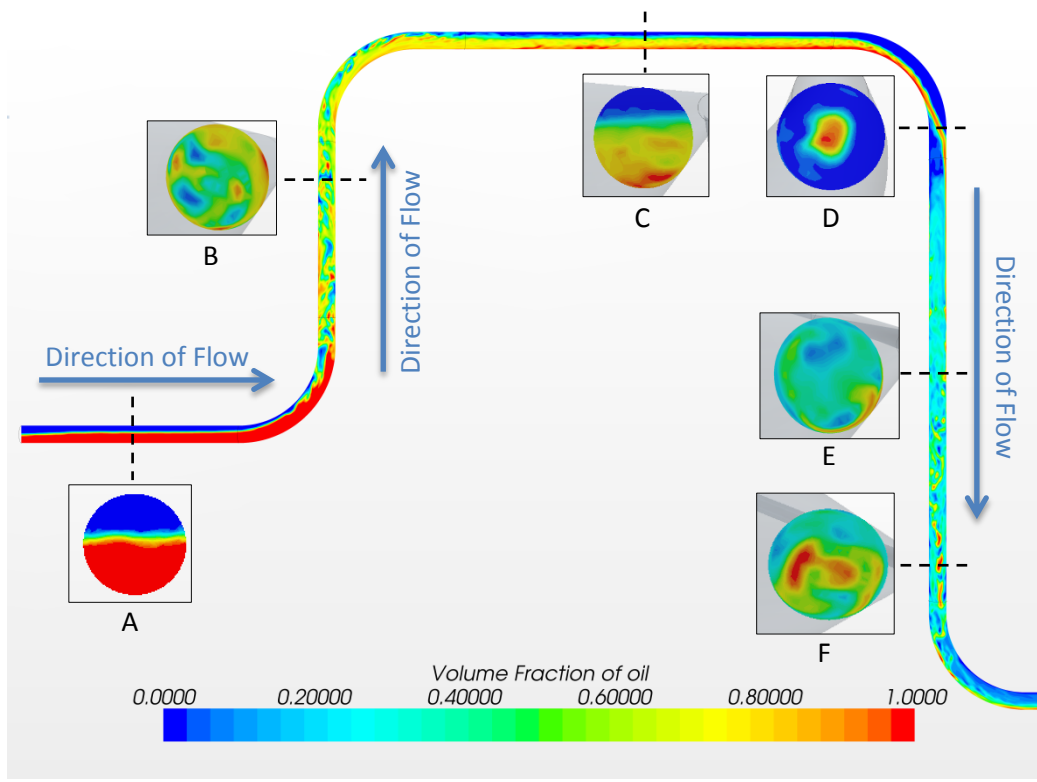


Figure 27. Contour of Volume Fraction of Oil for 50% oil-50% Gas Flow (Case 2) in First Half of the Jumper

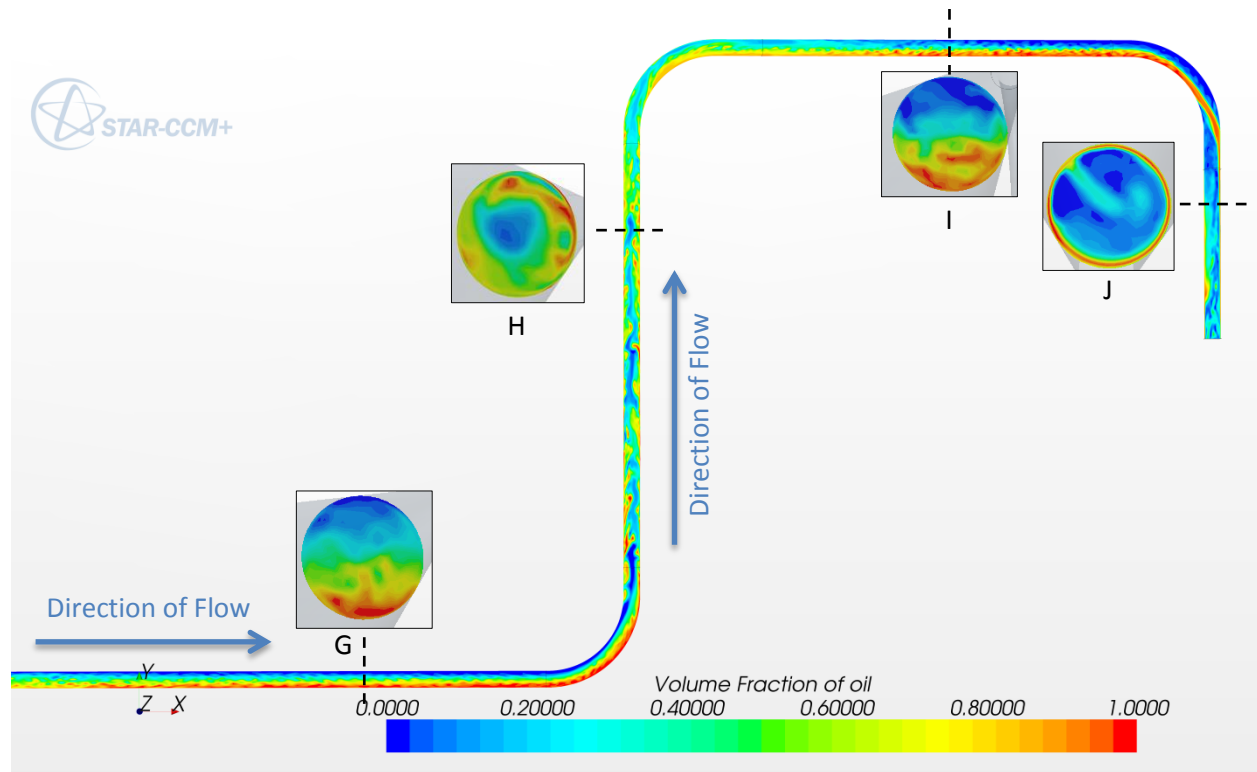


Figure 28. Contour of Volume Fraction of Oil for 50% oil-50% Gas Flow (Case 2) in Second Half of the Jumper

After the flow leaves the first half of the jumper, the flow patterns of the second half are very similar. A stratified oil-gas layer is again developed at the long horizontal section with the oil settled at the bottom as shown in Section G from Figure 28. The two-phase flow reaches the fifth bend and the same physical flow behavior as the first bend occurs at this location. The oil-gas flow then moves upwards with the development of churn flow and particularly elongated bubbles at the center of the pipe as illustrated in Section H from Figure 28. The horizontal section at the top makes the flow to stratify again, and finally it goes to the last vertical section where annular flow is formed as a consequence of the change in momentum due to the curvature of the last bend. This two-phase flow exits the jumper to feed into the main pipeline.

For the 20% oil and 80% gas flow, it is found that similar flow regimes as the 50 % oil flow are developed. The oil is dragged down along the jumper and it only blocks the gas slightly from flowing freely at the bends. Figure 29 and Figure 30 show that the flow transition from stratified to churn flow occurs as a consequence of the flow moving from a horizontal section to a vertical section. Some droplets or isolated small chunks of oil are also transported by the continuous flow of gas.

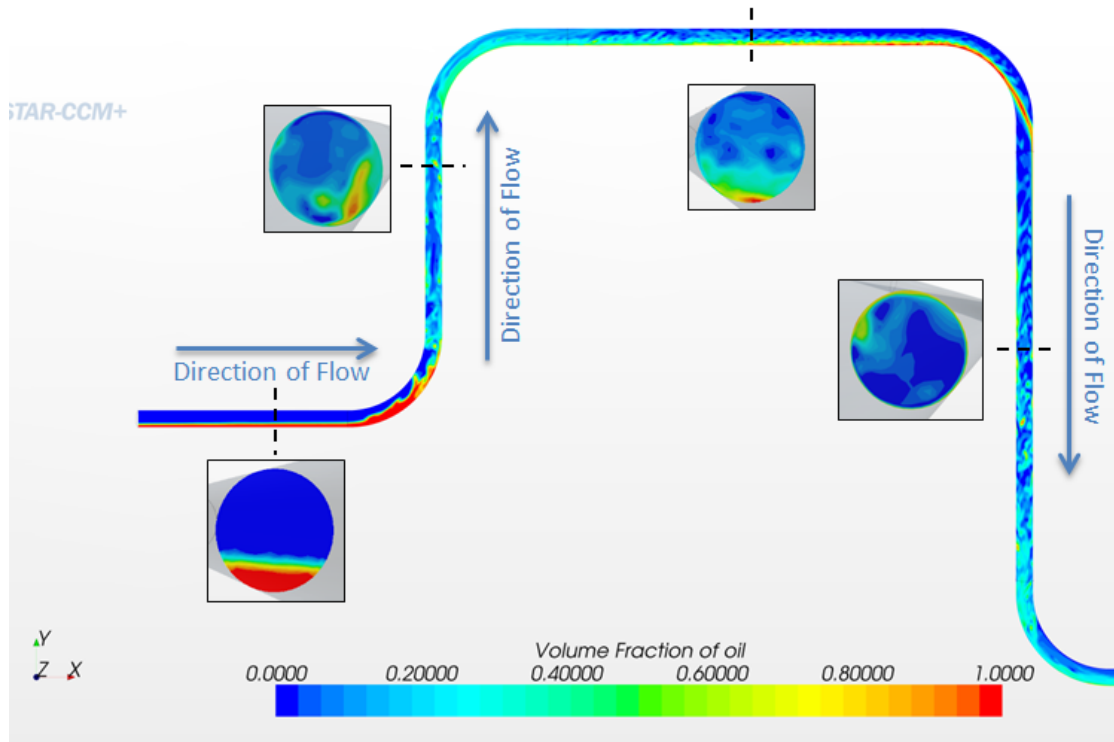


Figure 29. Contour of Volume Fraction of Oil for 20% oil-80% Gas Flow (Case 1) in First Half of the Jumper

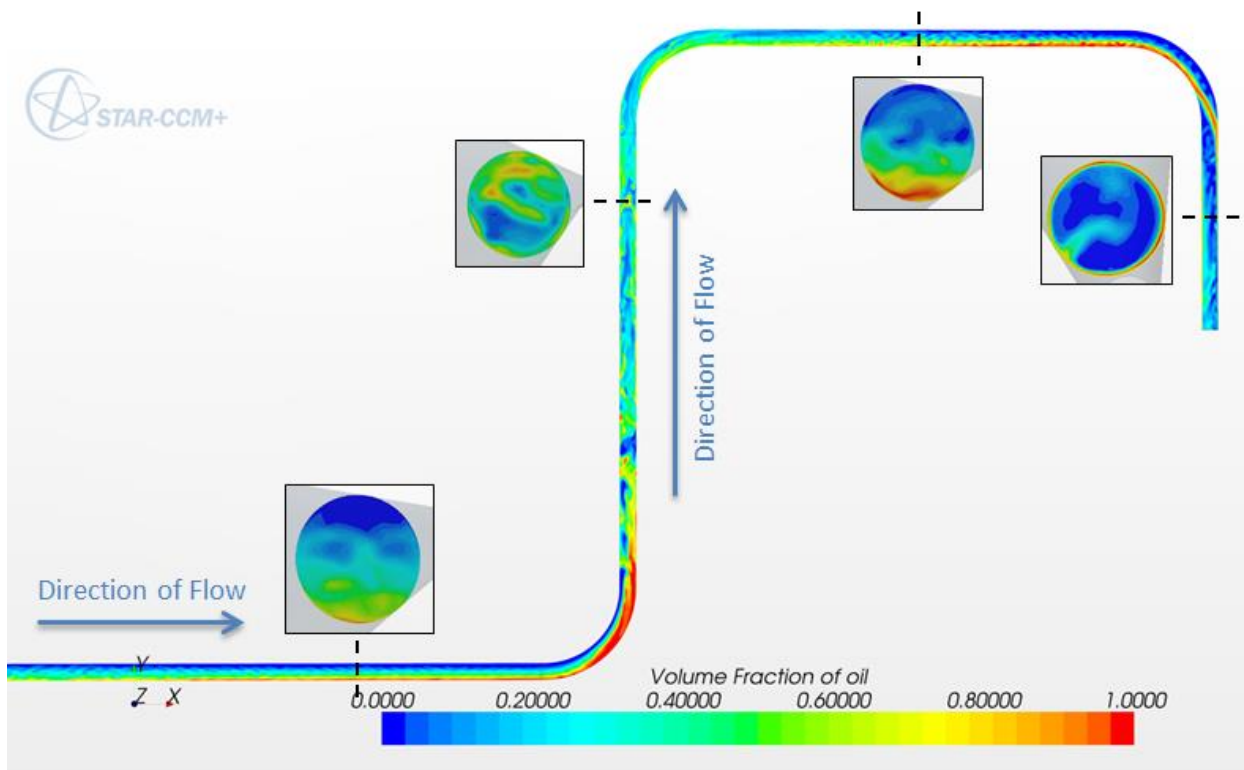


Figure 30. Contour of Volume Fraction of Oil for 20% oil-80% Gas Flow (Case 1) in Second Half of the Jumper

It was found that case 3, which is 80% oil and 20% gas, tends to have some changes in the flow regimes due to the difference in volume fraction with case 1, specifically in the vertical sections of the jumper. The first vertical section seems to have the two phases separate with only slight mixing. In fact, small pockets of gas struggle to move the oil upwards as illustrated in Figure 31. It is observed that the horizontal sections of this case have a thick layer of oil covering more than half of the area of the cross section (See Section C from Figure 31). The chaotic and turbulent behavior of the flow after the third bend makes a greater mixing of the two phases. Churn flow still dominates the behavior of the flow with random formation of tiny slugs in this vertical region.

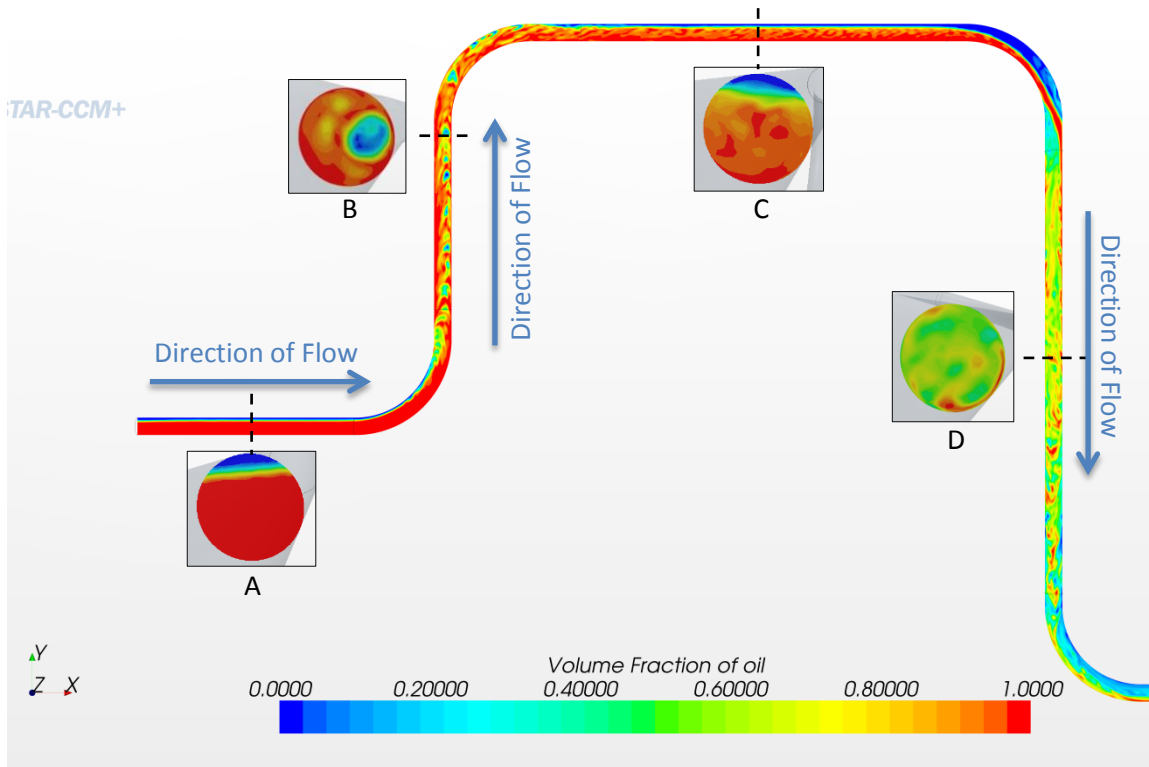


Figure 31. Contour of Volume Fraction of Oil for 80% oil-20% Gas Flow (Case 3) in First Half of the Jumper

In the second half of the jumper, the flow regimes are very similar in almost all regions except for the vertical section where the flow goes upwards. In this region, elongated chunks of oil are formed with small dispersed bubbles of gas as illustrated in Figure 32. It is important to assess the impact of this intermittent flow regime on the structure.

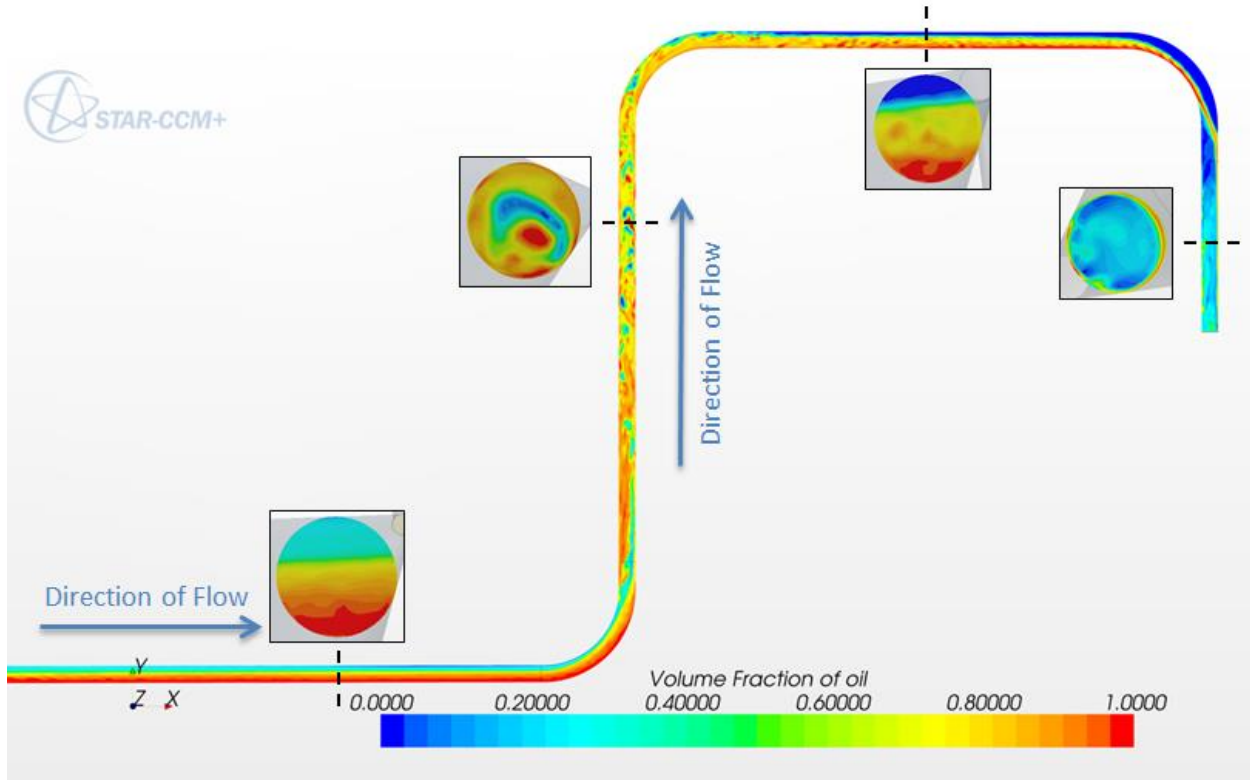


Figure 32. Contour of Volume Fraction of Oil for 80% oil-20% Gas Flow (case 3) in Second Half of the Jumper

As a screening method, it is important to estimate the fluid frequencies along the entire fluid domain to compare with the structural natural frequencies. Contrary to the assumption of previous studies in which the fluid frequency (or slug frequency) was input from the inlet, the flow is initialized as a stratified flow and then the two phases start mixing until slugs are naturally developed if the flow conditions fall into the slug region zone. In this case, it was not clear evidence that slugs were developed. Therefore, it was considered that the best method to extract the fluid frequencies is in terms of the time history of volume fraction. Figure 33 shows the locations in the jumper where the volume fraction was quantified for the entire simulation time.

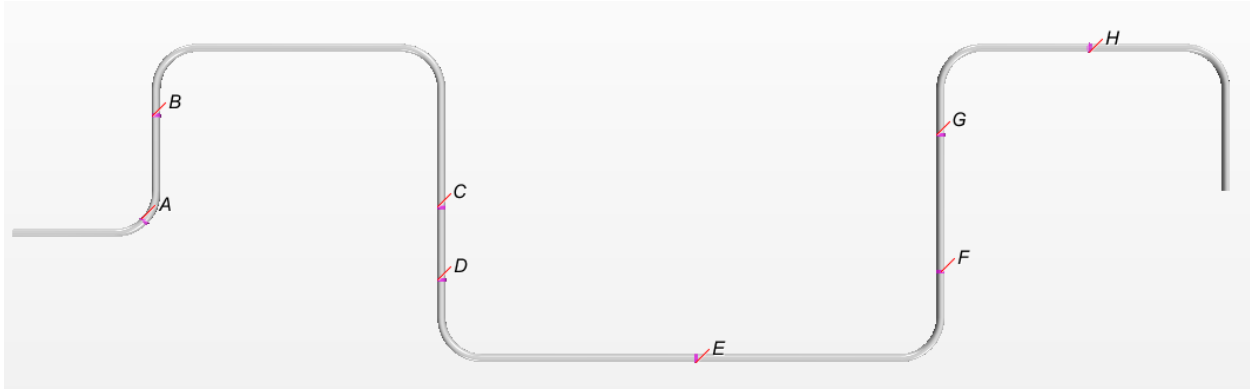


Figure 33. Cross-Section Planes of Jumper for Extraction of Volume Fraction Time History

It is expected that oil starts accumulating at the first bend due to the action of the gravitational force on the flow. Therefore, at least 70% of oil accumulates in the bend in all cases as indicated in Figure 34, in which the volume fraction oil varies between 0.75 and 0.95 at cross-section plane A. For the rest of the cross section planes, the range of percentage of oil depends on the amount of volume fraction specified as initial conditions. For example, the volume fraction is less than 0.35 for the cases where the flow is initiated as 20% of oil. The volume fraction of oil falls between 0.35 and 0.70 for cases in which the flow initiates as 50% of oil (See Figure 35) while it is greater than 0.60 for case 3 and 6 in which oil starts flowing at 80% of the inlet cross section. Table 7 summarizes the volume fraction of oil at different locations for each one of the cases described before.

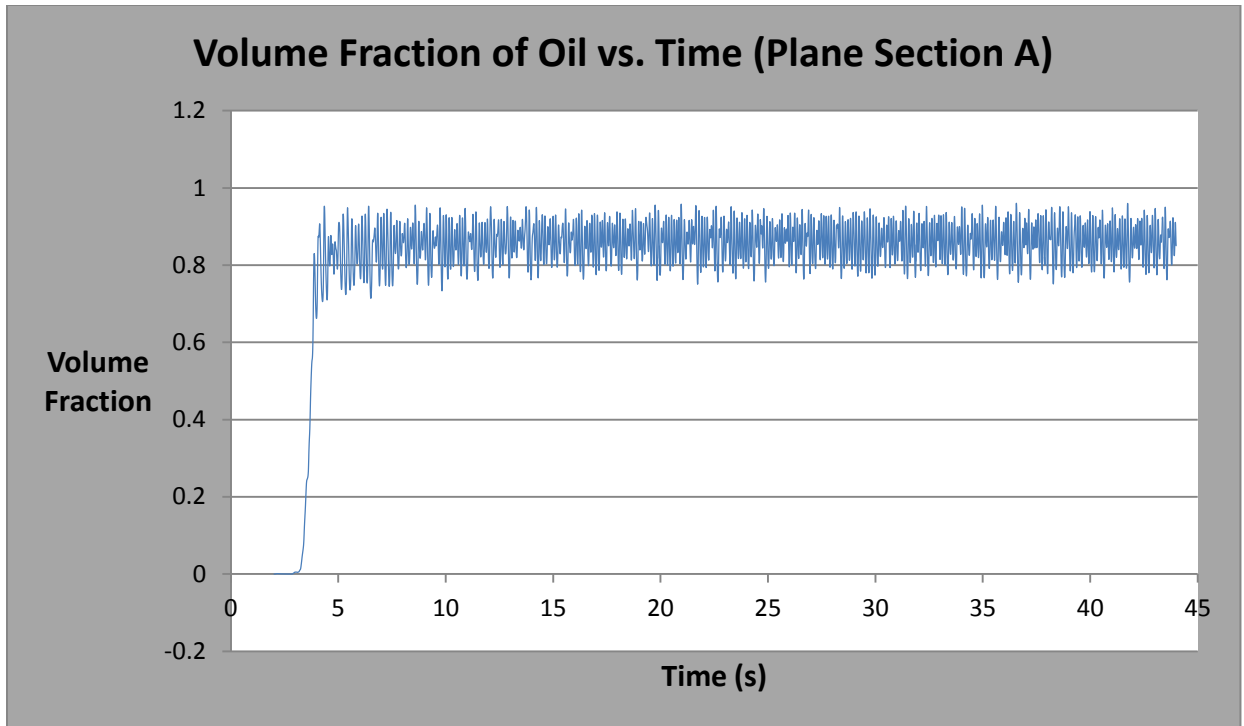


Figure 34. Time History of Volume Fraction for Case 2 – Cross-section Plane A

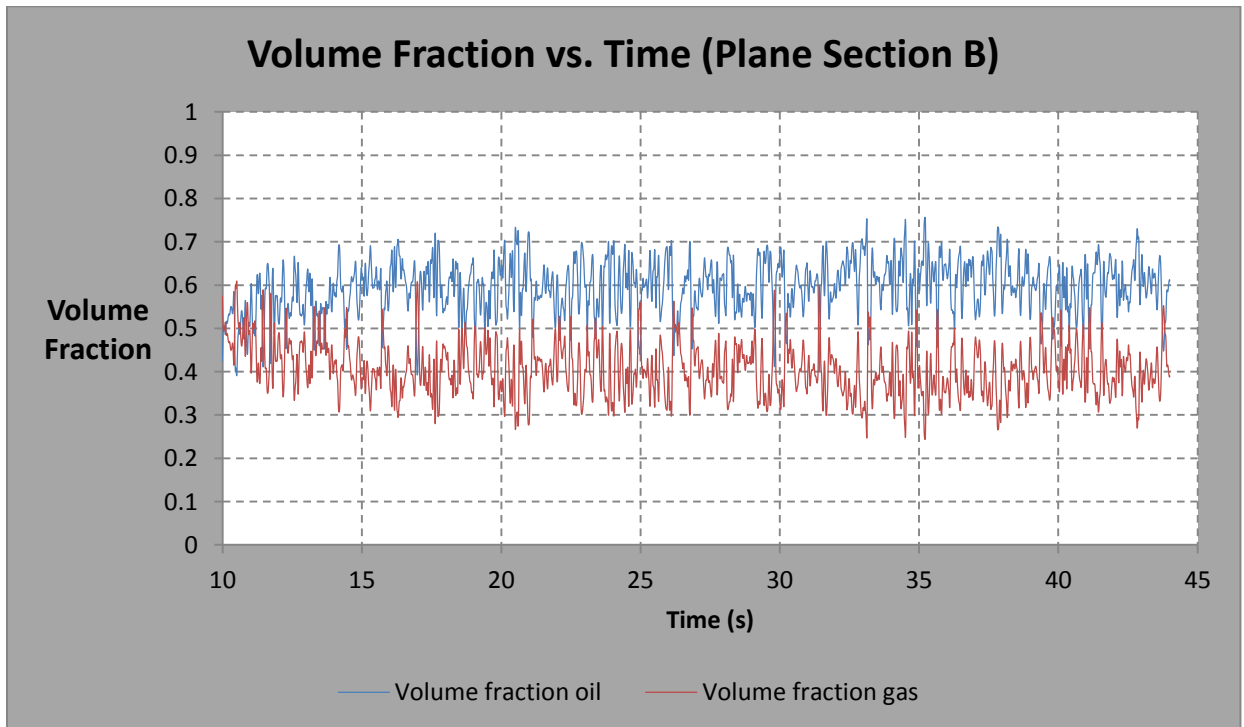


Figure 35. Time History of Volume Fraction for Case 2 – Cross-section Plane B

Table 7. Range of Volume Fraction of Oil for Two-phase Flow Cases

Ranges for Volume Fraction of Oil – Two-phase flow							
Cases	Section A	Section B	Section C	Section D	Section E	Section F	Section G
1	0.70-0.90	0.16-0.25	0.12-0.20	0.12-0.21	0.25-0.30	0.26-0.36	0.27-0.35
2	0.75-0.95	0.50-0.70	0.35-0.50	0.35-0.45	0.45-0.55	0.45-0.60	0.40-0.58
3	0.94-0.97	0.84-0.93	0.68-0.78	0.60-0.70	0.69-0.70	0.74-0.82	0.61-0.78
4	0.55-0.80	0.16-0.24	0.12-0.24	0.14-0.28	0.26-0.29	0.25-0.50	0.27-0.38
5	0.78-0.87	0.50-0.64	0.26-0.45	0.30-0.47	0.42-0.48	0.45-0.60	0.45-0.57
6	0.93-0.95	0.86-0.93	0.45-0.68	0.48-0.61	0.58-0.63	0.61-0.74	0.55-0.68

The time history of the volume fraction was transformed into frequency domain to identify the frequency (ies) at which the energy of the fluid is distributed. For each of the cases in Table 7, power spectral density (PSD) was extracted and plotted to estimate broadband or narrow frequency content. It was found that most of the volume fraction signatures appear to be broadband with two or three dominated frequencies as shown in Figure 36.

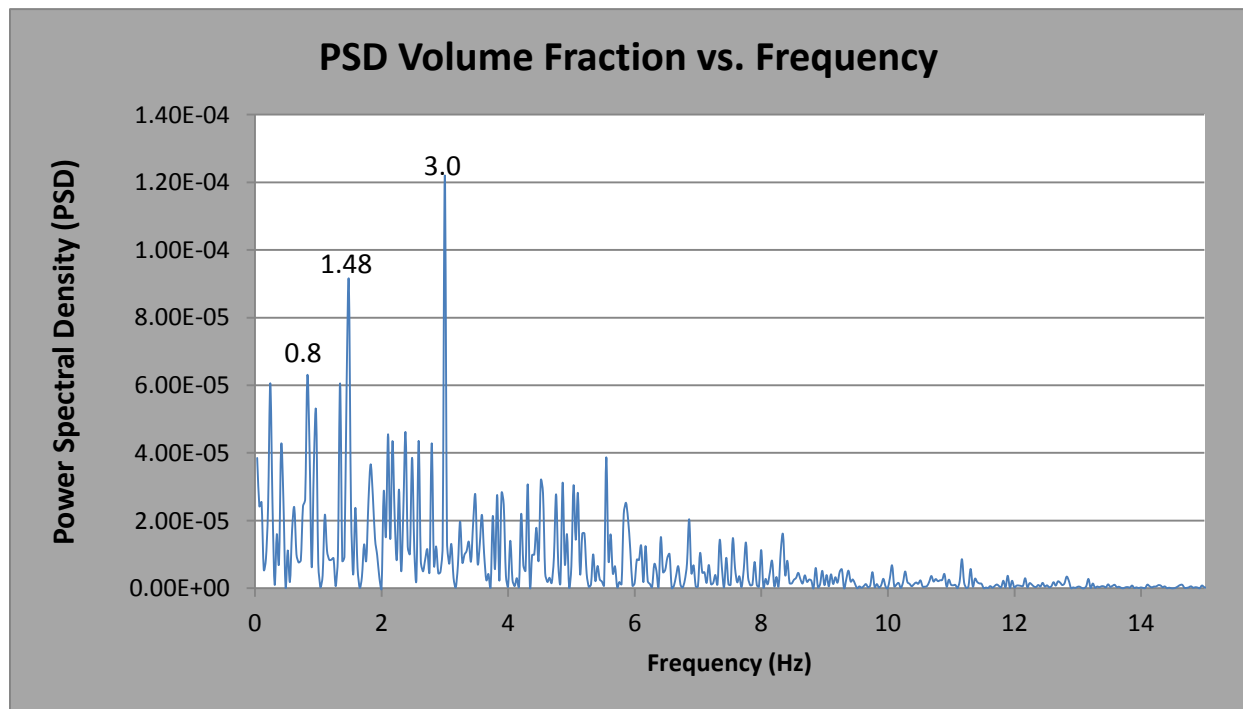


Figure 36. PSD of Volume Fraction of Oil for Case 2 – Plane Section B

It was also found that the fluid frequency varies along the jumper such that there is not a unique fluid (or slug) frequency which is contrary to the unrealistic assumption of inputting a

particular slug frequency as denoted in other research studies. Table 8 – Table 10 indicate the two strongest frequencies of the volume fraction of oil for each one of the two-phase flow cases at locations Section A – Section G.

The wide range of fluid energy content makes the jumper sensitive to vibrate at the structural modes. However, this broadband signal might be unimportant such that it is too weak to cause damage since the energy is spread along different frequencies. Some of these frequencies fall within 20 percent of the natural frequencies, so it is then recommended to perform an FSI simulation to assess in more detail the effect of the two-phase flow. These cases are highlighted in Table 8 – Table 10 depending on the level of the vibration. If the fluid frequencies differ by less than 10 percent with respect to the natural frequencies, there is a high risk of high amplitude vibration. If the fluid frequencies fall between 10 percent and 20 percent, there is a moderate risk of high amplitude vibration. This range difference is based on the guidelines for the avoidance of vibration induced fatigue in process pipework from the Energy Institute which recommends to avoid the excitation frequencies to be within $\pm 20\%$ of the structural natural frequencies.

HIGH RISK	
LOW RISK	

Table 8. PSD Volume Fraction Frequencies for Case 1 & Case 4

PSD for cases with 0.20 volume fraction of oil							
Case 1	Section A	Section B	Section C	Section D	Section E	Section F	Section G
1 st Frequency	5.4	0.5	0.288	0.205	0.237	0.15	2.93
2 nd Frequency	6.05	1.08	2.02	1.82	0.395	1.35	1.93
Case 4	Section A	Section B	Section C	Section D	Section E	Section F	Section G
1 st Frequency	2.355	0.952	2.078	1.166	0.3103	0.346	0.2608
2 nd Frequency	4.73	1.262	3.788	2.833	0.069	0.154	0.4346

Table 9. PSD Volume Fraction Frequencies for Case 2 & Case 5

PSD for cases with 0.50 volume fraction of oil							
Case 2	Section A	Section B	Section C	Section D	Section E	Section F	Section G
1 st Frequency	8.1	3	0.33	0.29	0.316	0.83	2.44
2 nd Frequency	8.36	1.48	1.83	0.67	1	2.38	5.99
Case 5	Section A	Section B	Section C	Section D	Section E	Section F	Section G
1 st Frequency	10.33	0.977	3.946	1.189	0.1818	2.867	1.11
2 nd Frequency	9.042	0.349	2.657	1.108	0.3635	1.7	0.222

Table 10. PSD Volume Fraction Frequencies for Case 3 & Case 6

PSD for cases with 0.80 volume fraction of oil							
Case 3	Section A	Section B	Section C	Section D	Section E	Section F	Section G
1 st Frequency	10.65	8.05	0.182	0.273	0.519	0.278	0.483
2 nd Frequency	14.3	8.2	0.333	0.333	NA	NA	0.621
Case 6	Section A	Section B	Section C	Section D	Section E	Section F	Section G
1 st Frequency	15.02	1.089	0.974	1.081	0.212	0.633	1.392
2 nd Frequency	13.9	1.466	2.025	0.351	0.242	2.33	3.39

10.2.2. Pressure Fluctuations

Another screening is to assess the impact of the flow by finding the critical locations where the maximum forces occur. The maximum pressure in each one of the bends was extracted. It was found that the maximum force was exhibited on case 3 where the velocity is 1 m/s and the volume fraction of oil is 0.8 (See Figure 37) . As indicated in Table 11, the pressure increases with increasing the volume fraction of oil; however, there is not a clear trend with the effect of velocity on the pressure because it also depends on the interaction of the velocity with the volume fraction. For the cases of 0.2 as the volume fraction of oil, the pressure increases as the initial velocity of the flow increases. On the other hand, the 0.5 and 0.8 volume fraction cases exhibit a decrease in pressure as the velocity increases.

For each one of the cases, the 4th bend and the 5th bend are the sections where the highest forces are exerted and therefore significant vibrations might occur. The velocity of the flow is at the highest value due to the effect of the gravity such that the impact force or pressure of the flow is much more significant. Table 11 summarizes the results of the maximum pressure on the bends.

Table 11. Maximum Pressure on Bends for Two-phase Flow Cases

Case	Max. Pressure 3 rd Bend (Pa)	Max. Pressure 4 th bend (Pa)	Max. Pressure 5 th bend (Pa)	Max. Pressure 6 th bend (Pa)
1	13600	24400	20890	4140
2	17870	36575	33686	3169
3	29100	45720	43230	5440
4	15800	27300	24030	4830
5	17270	35130	32310	5780
6	28990	40950	38370	6977

This two-phase flow is a transient phenomenon in which the pressure or force varies with time as shown in Figure 37. The amplitude of the pressure fluctuations is approximately 1,000 Pascal and its pressure signature appear to be broadband with two or three response frequencies. As observed from the volume fraction signature, PSD of the pressure seems to have broadband frequency content ranging from 0 to 2 Hz as shown in Figure 38. This range falls in the first five natural frequencies of the jumper such that the oil-gas flow can excite one of the modes transitorily and moderately.

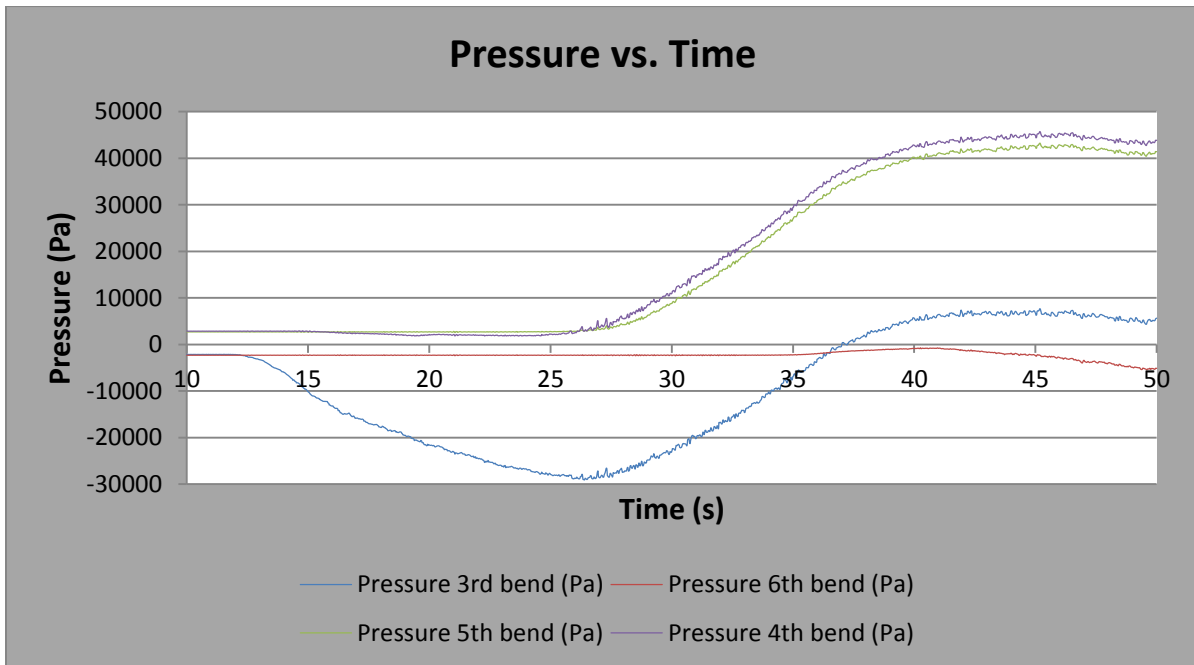


Figure 37. Time History of the Pressure for the Bends of the Jumper (Case 3)

Table 12 summarizes the pressure response frequencies indicating the first three excitation frequencies for each case with its respective broadband frequency range. The range for the 2m/s is about twice the range of the 1m/s. Given the uncertainty of the magnitude of the vibrations due to the broadband energy of the pressure signature, it is suggested to determine the life of the jumper by performing a co-simulation between CFD and FEA tools.

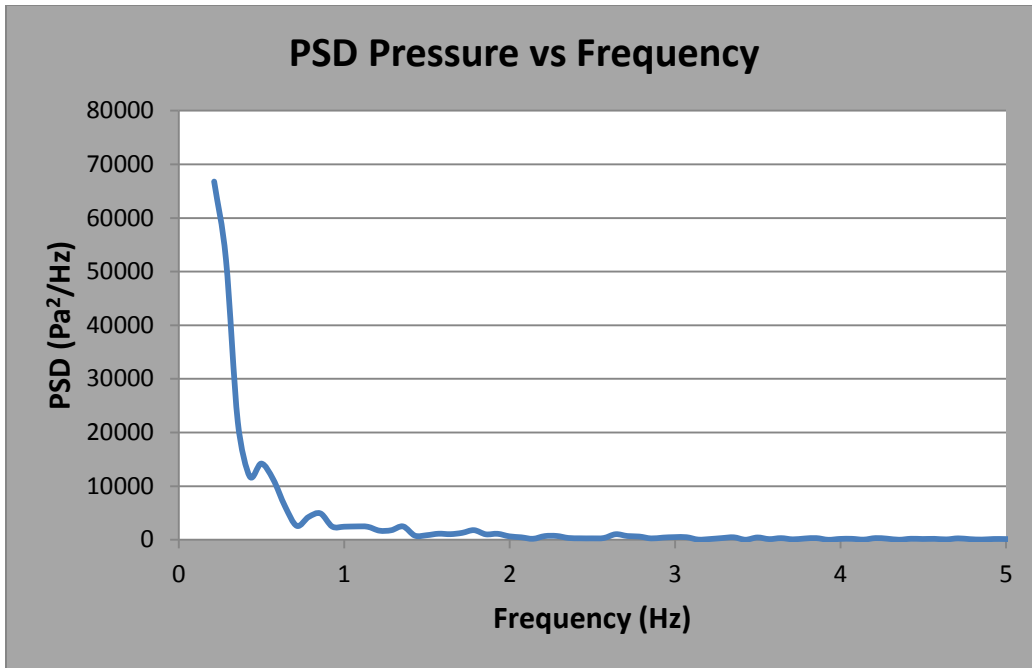


Figure 38. PSD of Pressure Signatures at the 4th Bend for Case 3

Table 12. PSD Pressure Response Frequencies of two-phase flow cases

Velocity	1m/s			2m/s		
	0.2	0.5	0.8	0.2	0.5	0.8
1st Frequency (highest)	0.74	0.07	-	0.625	0.416	0.304
2nd Frequency	2.87	-	-	0.174	7.58	0.167
3rd Frequency (lowest)	1.17	-	-	-	-	0.25
Broadband Frequency range (Hz)	0–5	0–3	0–2	0–6	0–10	0–9

10.3. Oil-Gas-Water Flow

Adding a third phase to the flow in the jumper might differ the results significantly. Besides oil and gas, production fluid comes with substantial amount of water that could modify the vibration response of the structure. Assuming mid-life production conditions where the volume fraction of gas is between 50% and 60% and induced forces are much significant, case 2 and case 5 from two-phase flow were considered to analyze three-phase flow as follows:

- Case 7: 50% Gas, 40% Oil, 10% Water, Inlet velocity = 1 m/s
- Case 8: 50% Gas, 40% Oil, 10% Water, Inlet velocity = 2.0 m/s

10.3.1. Volume Fraction

Similar to the two-phase flow, the oil-gas-water is initialized at the inlet as a stratified flow with water at the bottom followed by oil and gas in the top as shown in Figure 39. The flow patterns are very similar to the two-phase flow with the difference that the liquid is a mixture of oil and water. As the flow approaches to the first bend, the oil is squeezed by the accumulated water (See Figure 40). The gas is then pushed or squeezed simultaneously by the two liquids such that the gas accelerates due to the reduction of its area and it releases upwards at a high velocity. The high momentum of the gas tends to create an annular flow at some time and portion of the vertical section.

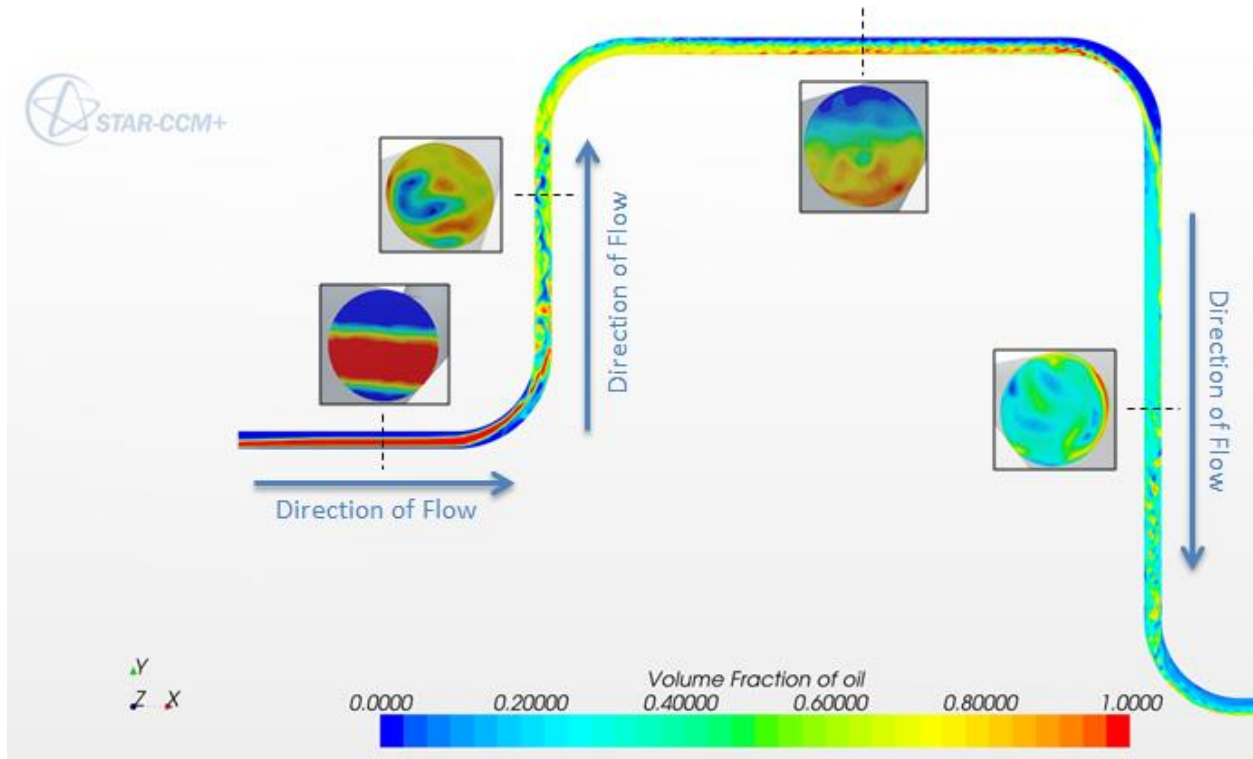


Figure 39. Contour of Volume Fraction of Oil for Oil-gas-water Flow in First Half of the Jumper for Case 7

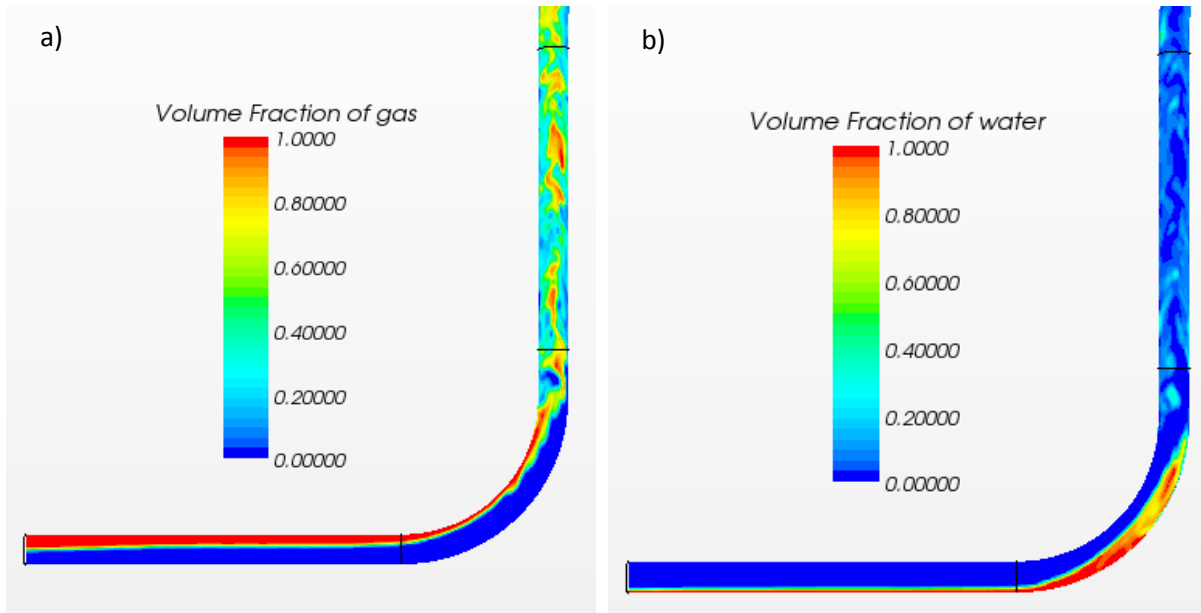


Figure 40. Contour of Volume Fraction of a) Gas, b) Water for the First Section of the Jumper for Case 7

Churn flow is still the regime that dominates the vertical sections with some small elongated bubbles rising up in the pipe, also known as dispersed bubble-oil continuous (DB-OC) while it is observed stratified-stratified (ST-ST) or stratified-wavy flow in the horizontal section of the jumper. In the second half of the jumper, the flow patterns are identically to the ones observed in the first half as shown in Figure 41.

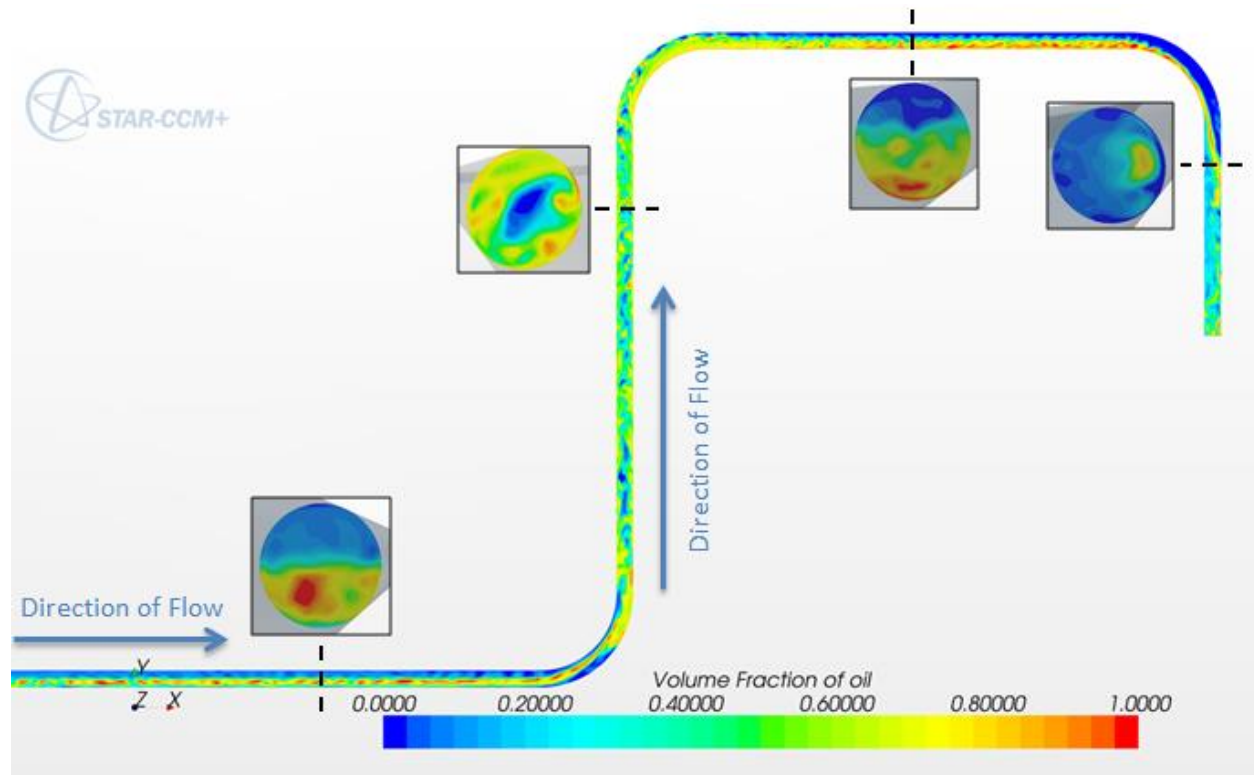


Figure 41. Contour of Volume Fraction of Oil for Oil-gas-water Flow in Second Half of the Jumper for Case 7

It is expected that the percentage of oil is about 40% along the length of the pipe as indicated in Table 13. In fact, the volume fraction of oil ranges approximately from 0.30 to 0.60 for both cases (See Figure 42). Table 13 shows that the range of oil fraction is much higher at a low velocity (1m/s) while it is reduced to a minimum of 0.22 when the velocity is 2.0 m/s.

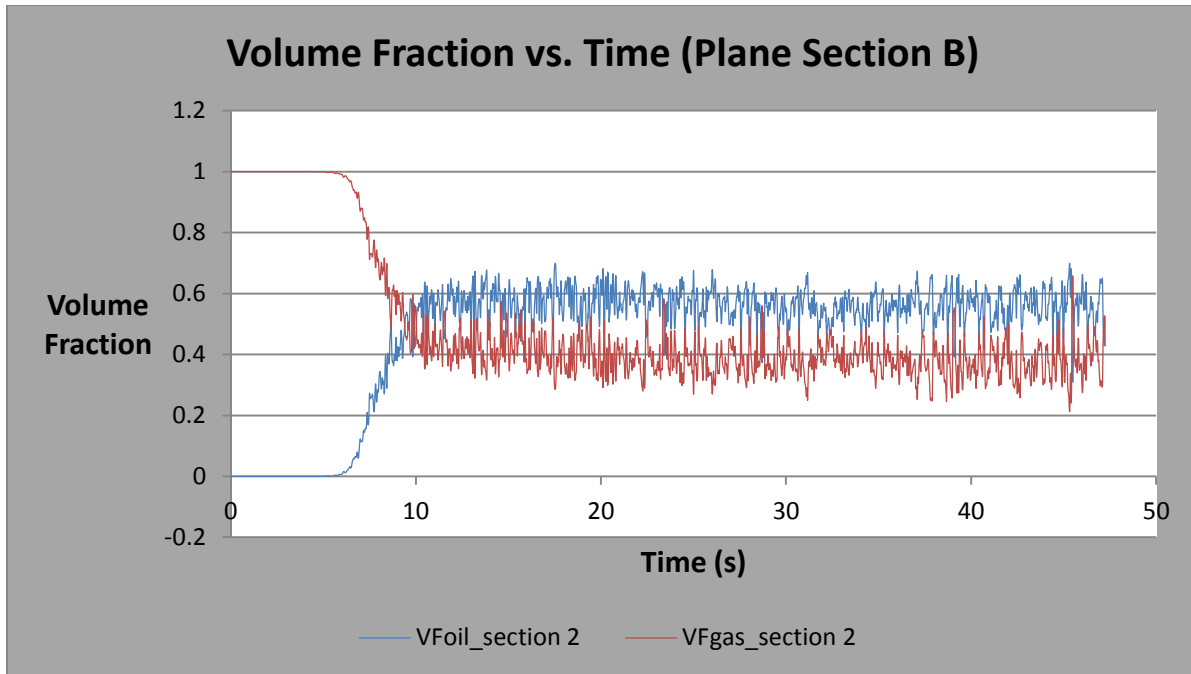


Figure 42. Time History of Volume Fraction for Case 7 – Cross-section Plane B

Table 13. Range of Volume Fraction of Oil for Three-phase Flow Cases

Ranges for Volume Fraction of Oil – Three-phase flow							
Cases	Section A	Section B	Section C	Section D	Section E	Section F	Section G
7	0.32-0.40	0.47-0.62	0.30-0.41	0.25-0.40	0.38-0.44	0.42-0.57	0.42-0.56
8	0.43-0.55	0.45-0.60	0.26-0.34	0.22-0.35	0.27-0.38	0.33-0.42	0.31-0.43

The fluid frequencies are extracted in terms of the time histogram of the volume fraction of oil since this is the main parameter that dominates the flow regime besides the velocity. The PSD of the volume fraction shows that the energy content of the fluid is distributed as a broadband signal with two or more significant frequencies as illustrated in Figure 43. Some of the frequencies excite one or more of the structural modes such that the amplitude of the vibrations might reduce the life of the jumper. As indicated in Table 14, there is a high risk for both cases 7 and 8 since the fluid (slug) frequencies fall within 10% of the natural frequencies. Therefore, it is recommended for future work to analyze in detail the consequences of having three-phase flow in a jumper by performing a two-way coupling simulation in which the time history location of stress reveals the life of the structure based on the actual flow conditions.

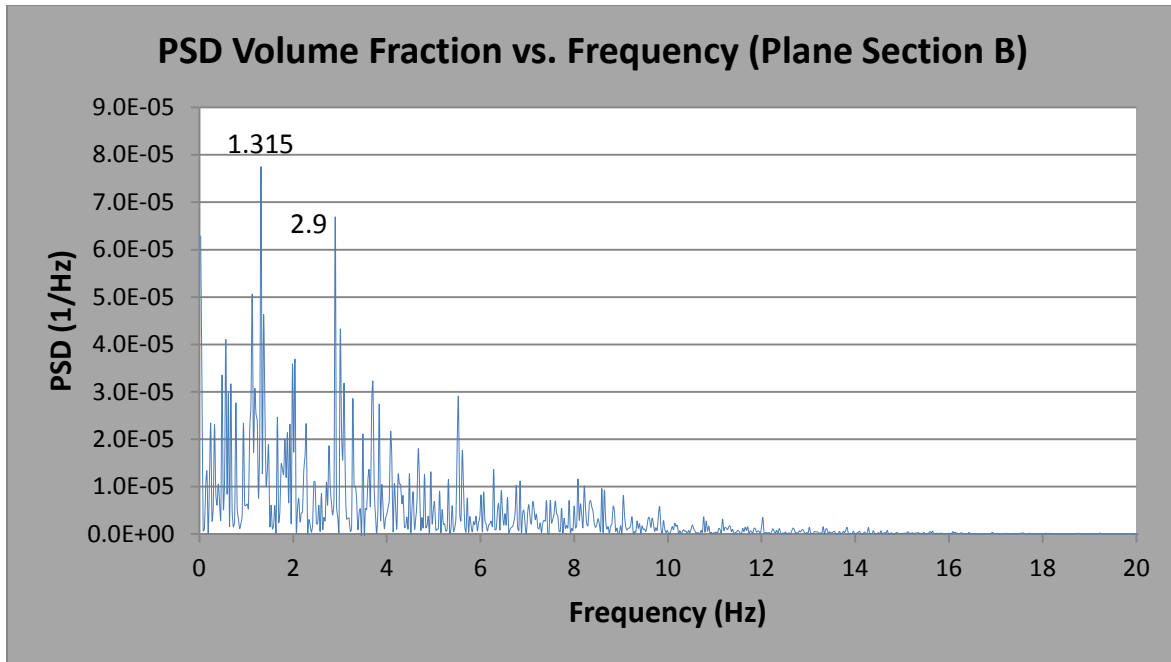


Figure 43. PSD of Volume Fraction of Oil for Case 7 – Plane Section B

HIGH RISK	
LOW RISK	

Table 14. PSD Volume Fraction Frequencies for Case 7 & Case 8

PSD for three-phase flow cases							
Case 7	Section A	Section B	Section C	Section D	Section E	Section F	Section G
1 st Frequency	0.213	1.315	0.264	0.11	1.39	0.408	1.93
2 nd Frequency	0.284	2.9	0.364	0.514	0.232	2.611	3.86
Case 8	Section A	Section B	Section C	Section D	Section E	Section F	Section G
1 st Frequency	10.97	0.818	0.08	0.08	0.1	1.187	0.214
2 nd Frequency	10.75	0.0606	0.48	0.56	7.797	1.375	0.357

10.3.2. Pressure Fluctuations

For FIV, pressure or forces on the bends dictates the vibration of the structure because it also can agitate the flow and then change the behavior of the flow regime if the deformation of the pipe wall is significant. From the momentum equation, the resultant force is dependent on the change in velocity and the pressure in the region of interest. It was found that the forces increases as the velocity of the flow increases at different locations as indicated in Table 15. Similar to the two-phase flow, the 3rd bend and 4th bend are the locations where the maximum pressures occur.

The velocity dominates the response of the structure for either two-phase flow or three-phase flow. However, it was noticed that the three-phase flow induces higher forces than the two-phase flow for the same volume fraction of gas (50 percent) which is the case for mid-life production.

Table 15. Maximum Pressure on Bends for Three-phase Flow Cases

Velocity (m/s)	Max. Pressure 3 rd Bend (Pa)	Max. Pressure 4 th bend (Pa)	Max. Pressure 5 th bend (Pa)	Max. Pressure 6 th bend (Pa)
0.7	17810	34240	31115	2436
1.0	19780	38760	35770	4350
2.0	23290	43890	40670	12100

Pressure on the bends fluctuates approximately from 1000 Pa to 1500 Pa range as shown in Figure 44. This starts happening after 30 seconds when the three phases reach the 4th and 5th bend of the jumper and consequently more stable flow conditions are achieved after 42 seconds.

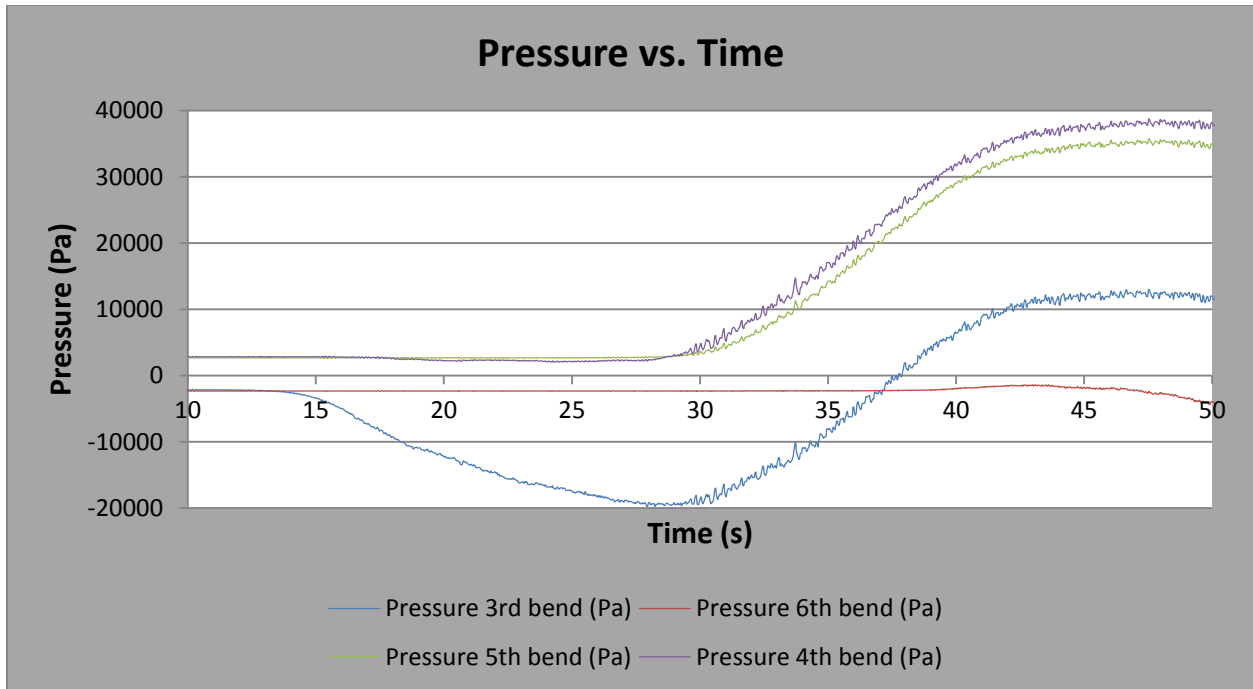


Figure 44. Time History of the Pressure for the Bends of the Jumper (Case 7)

Pressure fluctuations were found to have a broadband response from 0 Hz to 10 Hz for case 7 and case 8 such that the energy content from the fluid has a random frequency due to the transient behavior of the flow (See Figure 45). Case 8 has about 7 or 8 peaks where the fluid frequency falls within this 10 Hz spectrum range. This indicates that there is a moderate risk of the fluid exciting one of the modes of the structure, and therefore some potential vibration might damage the pipe. Table 16 summarizes the power spectral density of the pressure time signatures for case 7 and case 8.

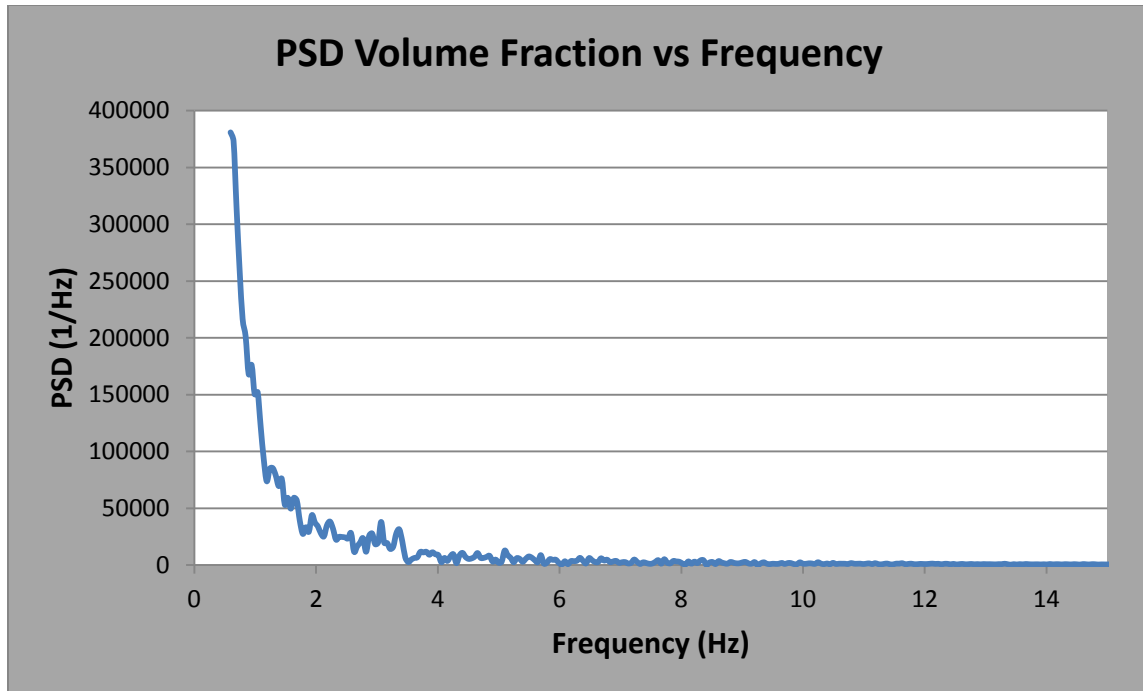


Figure 45. PSD of Pressure Signatures at the 4th Bend for Case 7

Table 16. PSD Pressure Response Frequencies of Three-phase Flow Cases

Response Frequency	Velocity (m/s)	
	1 (Case 7)	2.0 (Case 8)
1 st Frequency (highest)	–	6.08
2 nd Frequency	–	1.33
3 rd Frequency (lowest)	–	–
Broadband Frequency range (Hz)	0 – 10	0 – 10

10.4. Oil-Gas-Water Flow with Sand Production

For the same jumper model, sand particles were simulated to flow from a distributed grid at the inlet as shown in Figure 46 . The purpose of this analysis is to assess the effect of having sand particles in the pipe and to identify if four phases can be modeled and treated as a three-phase flow or two-phase flow. The locations where deposition of particles or blockage of the pipe occurs will be analyzed based on the velocity and pressure accordingly. Table 17 indicates the cases that were studied.

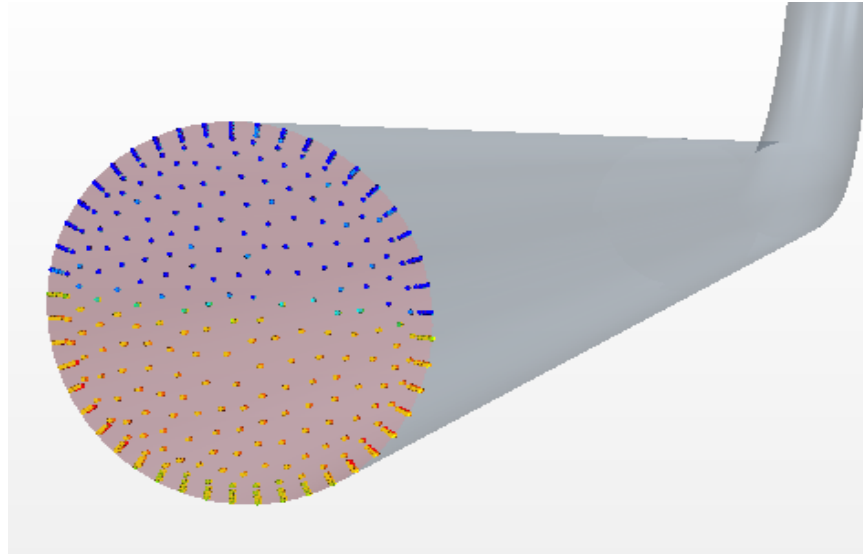


Figure 46. Contour of Sand Particles Traveling along the Pipe from Inlet of the Jumper

Table 17. CFD Simulation Cases for Four-phase Flow

Cases	Inlet Velocity (m/s)	Volume Fraction of Oil	Volume Fraction of Gas	Volume Fraction of Water	Sand Particles per second
9	2.0	0.40	0.50	0.10	150
10	2.0	0.40	0.50	0.10	300

10.4.1. Volume Fraction, Velocity, and Tracking of Sand Particles

It was assumed that the particles are stationary as initial condition, so the motion of these solids is generated due to the drag from the continuous oil-gas-water flow. The presence of sand might modify the flow patterns in particular the first bend and fifth bend where the solids might accumulate in significant amount because of the decreasing in the velocity as shown in Figure 47. The main flow patterns developed with three phases are still dominating the flow; however, adding particles changes the direction and behavior of the flow traveling upwards in the vertical section as shown in Figure 48, which can affect severely the response of the structure.

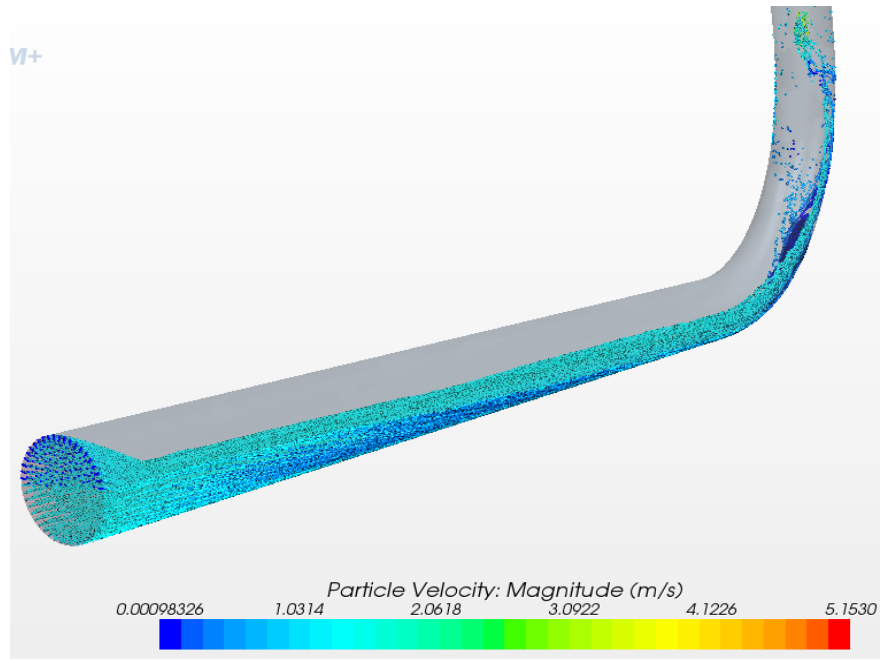


Figure 47. Initial Accumulation of Sand Particles at First Bend of the jumper

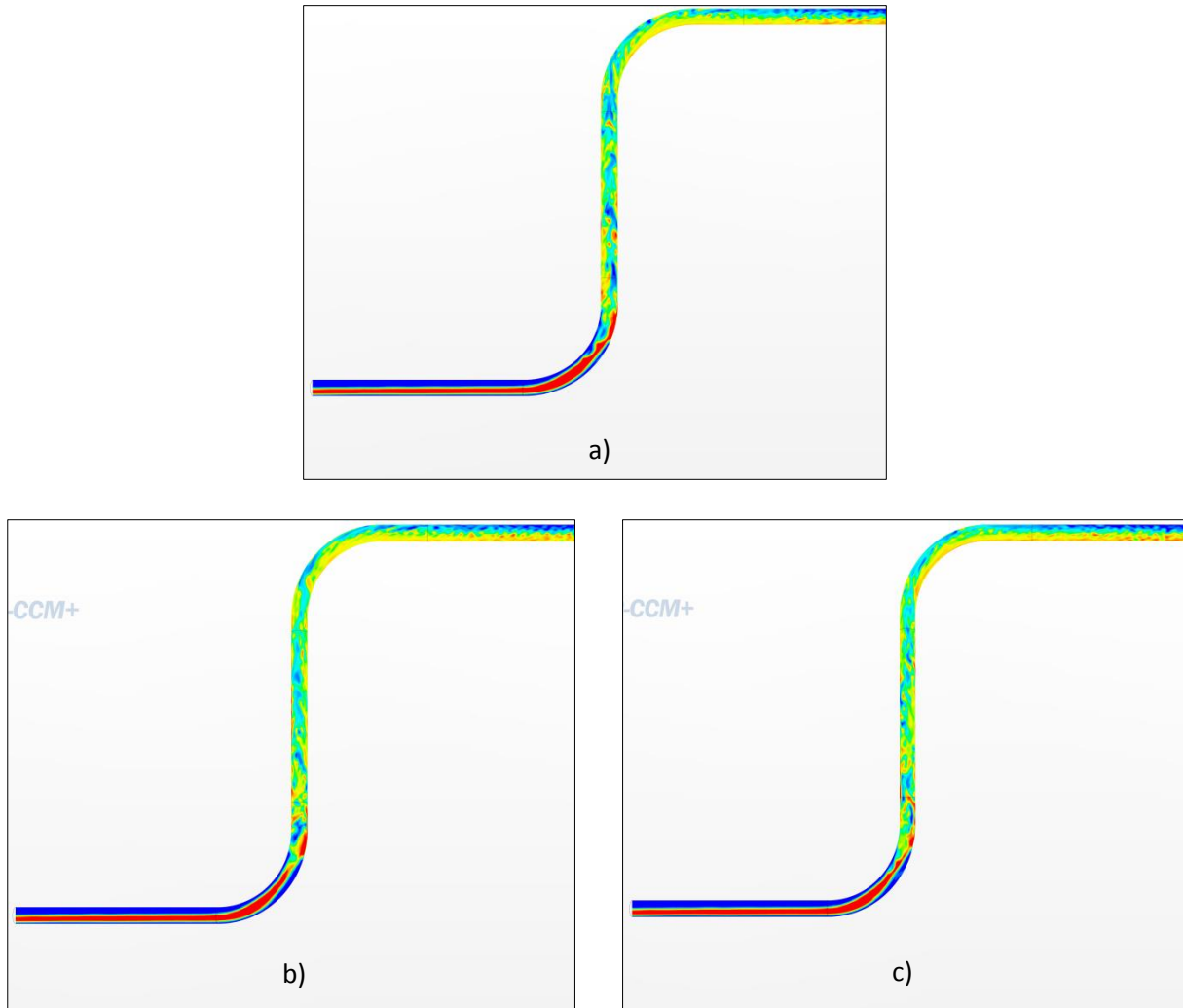


Figure 48. Contour of Volume Fraction of Oil in Jumper for a) Case 8, b) Case 9 and c) Case 10 after 20 Seconds of Flow

Large fraction of sand and low inlet velocity might induce particles to start accumulating in the first bend due to the friction. Sand will deposit at the bottom of the pipe and then the pressure builds up due to the blockage. If buildup occurs, the cross-sectional area for the continuous flow is reduced leading to an increase in the velocity and some of the sand particles are flushed upwards due to the drag of the flow. This process may occur several times. Figure 49 shows the cross-section of the region at the bend where the velocity increases since the area is reduced due to the accumulation of water-oil plus particles. There is only a slight increase in velocity by changing the flow rate from 150 particles per second to 300 particles per second.

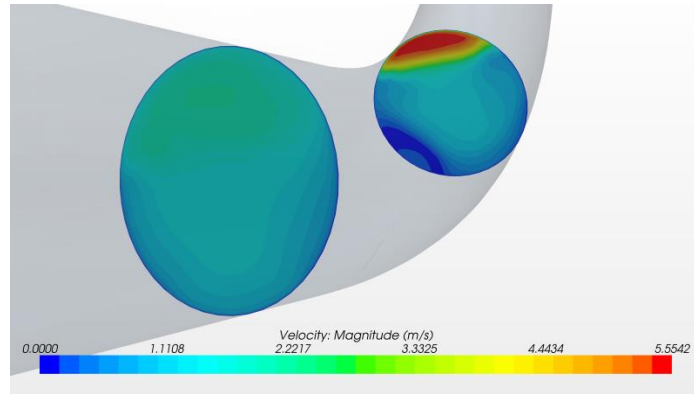


Figure 49. Contour of Velocity for Cross-section Area at the First Bend of the Jumper

The particles will reach the top of the jumper if the drag force is larger than the weight of the particle. Some of them will have enough velocity to impact the second bend with a potential to cause erosion in this section over time (See Figure 50).

The flow at the horizontal section of the jumper after the second bend is a stratified flow that drags the particles along the pipe with some of them being suspended by the friction from the wall. The gravity forces the particles to drop and they become more sensitive to seat at the bottom of the pipe as illustrated in Figure 51. Once the particles reach the third bend, it is much easier to flush them down due to the gravitational force and turbulent motion. They will keep flowing along the jumper with potential accumulation of particles on the fifth bend due to the vertical section where there is a resistance for the continuous flow to move upwards.

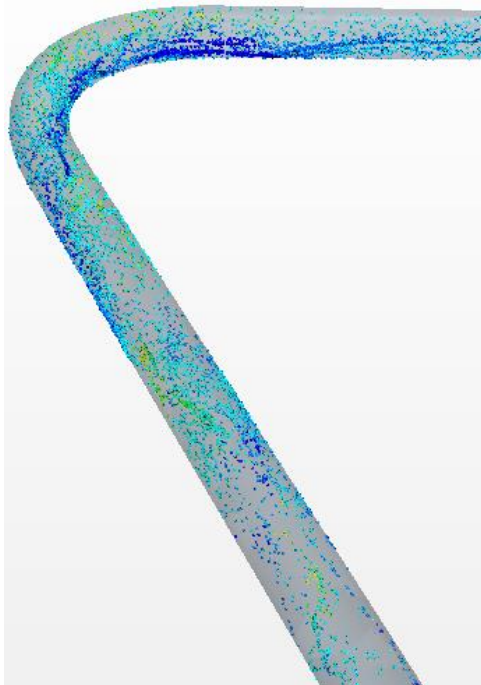


Figure 50. Tracking Sand Particles Flowing into 1st Vertical Section of the Jumper

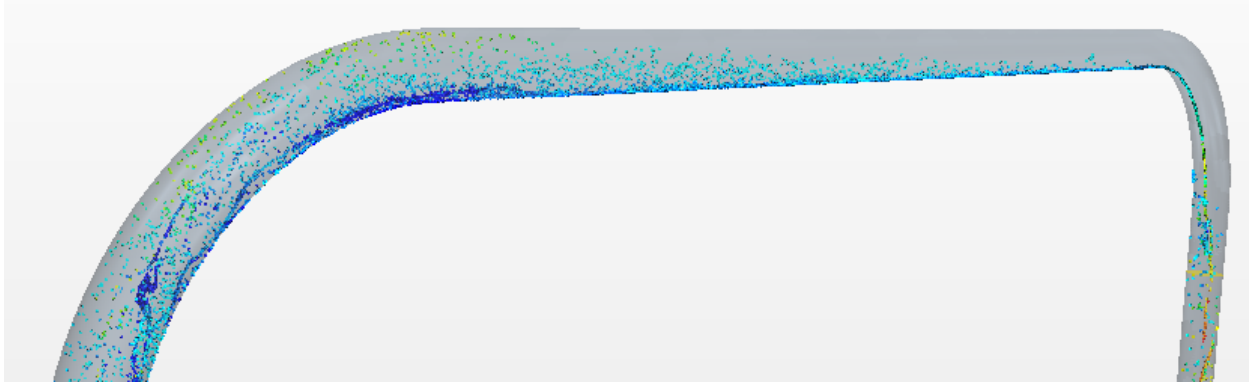


Figure 51. Tracking Sand Particles Flowing into First Top Horizontal Section of the Jumper

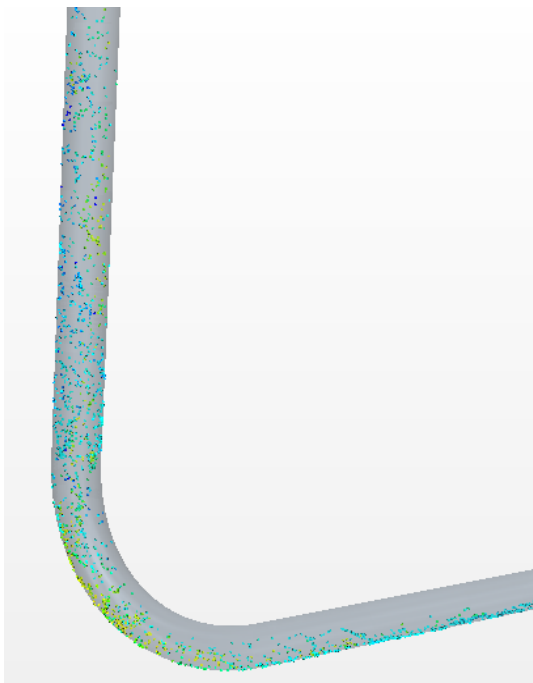


Figure 52. Tracking Sand Particles Flowing towards the Fourth Bend of the Jumper

For screening purposes, the fluid frequencies for these cases were compared with case 8 in which no solid particles are introduced. For all cases, the excitation energy of the fluid is spread over 10Hz – 15Hz frequency range, so there is a probability that some energy of the fluid will input at the system’s natural frequency. Table 18 shows some of the frequencies falling within $\pm 20\%$ of the natural frequencies as observed by the highlighted cases. It was also found that the highest volume fraction frequency varies significantly with introducing sand particles into the pipe even though a slight variation in velocity and volume fraction of oil occurs.

HIGH RISK	
LOW RISK	

Table 18. PSD Volume Fraction Frequencies for Case 8, Case 9, & Case 10

PSD Frequencies for cases with inlet velocity = 2.0 m/s							
Case	Section A	Section B	Section C	Section D	Section E	Section F	Section G
8	10.97	0.82	0.08	0.08	0.1	1.19	0.214
9	0.79	0.85	0.606	1.09	6.7	1.25	4.7
10	0.78	0.26	0.26	2.34	6.8	1.7	3.23

10.4.2. Pressure

The maximum pressures on the bends were estimated to assess if sand particles cause a major effect on the jumper. It was found that the flow induced forces are much higher when oil-gas-water is flowing without introducing any solid particle (See Table 19). The pressure is almost the same for the cases with the presence of sand. The 4th bend and the 5th bend are still the locations with the maximum pressures having fluctuations of approximately 1000 Pa.

Table 19. Maximum Pressure on Bends for Oil-water-gas Flow with and without Sand Particles

Case	Max. Pressure 3 rd Bend (Pa)	Max. Pressure 4 th bend (Pa)	Max. Pressure 5 th bend (Pa)	Max. Pressure 6 th bend (Pa)
8	23290	43890	40670	12100
9	17868	43791	40616	3721
10	16999	42734	39571	2422

The excitation energy for case 9 and case 10 was distributed from 0Hz to 10Hz such that these response frequencies might excite one of the natural frequencies of the jumper. In fact, there is an important response of the energy content at 1.63Hz and 2.0Hz for case 9 that can generate some vibration in the system. A fluid structure interaction analysis can determine if the magnitude of this response affects the structure.

10.5. Summary of CFD Results

Table 20 summarizes the results for the different multiphase configurations of oil-gas-water with sand particles from Section 10.2 to Section 10.4.

Table 20. Summary of CFD Results for Multiphase Flow

Parameter	Two Phases	Three Phases	Four Phases
Volume Fraction (Flow Patterns)	<u>Horizontal Sections:</u> Stratified or Wavy Flow <u>Vertical Sections:</u> Dispersed Flow, Churn Flow, tiny slugs for 0.8 oil fraction	<u>Horizontal Sections:</u> Stratified or Wavy Flow <u>Vertical Sections:</u> Dispersed Flow, Churn Flow	<u>Horizontal Sections:</u> Stratified or Wavy Flow <u>Vertical Sections:</u> Dispersed Flow, Churn Flow
Pressure or Forces	Low	High	Significant but not as high as three-phase flow
Location of Maximum Pressures	4 th bend and 5 th bend	4 th bend and 5 th bend	4 th bend and 5 th bend
Pressure vs. Volume Fraction of Oil	Pressure increases as the volume fraction of oil increases	Not Applicable	Not Applicable
Force vs. Velocity	Force increases with an increase in inlet velocity	Force increases with an increase in inlet velocity	Not Applicable
PSD Volume Fraction	Broadband energy content (within 10% of natural frequencies)	Broadband energy content (within 10% of natural frequencies)	Broadband energy content (within 20% of natural frequencies)
PSD Pressure	<u>Broadband excitation</u> 0Hz – 5Hz for $v = 1\text{m/s}$ 0Hz – 10Hz for $v = 2\text{m/s}$	<u>Broadband excitation</u> 0Hz – 10Hz for $v = 1\text{m/s}$ 0Hz – 10Hz for $v = 2.0\text{m/s}$	<u>Broadband excitation</u> 0Hz – 10Hz for both particles flow rate cases

11. Phase II – FIV Results

For Phase II of the FIV methodology, the midlife production cases (case 5 and case 8) were selected to estimate the response of the pipe and to verify the results of the screening performed in Phase I of the FIV methodology.

Having the same assumptions for phase I of the methodology, a FSI analysis was performed to study the response of the jumper when subjected to multiphase flow. It is of interest to find the maximum and time history of the displacements and stresses of the jumper. After that, the frequency spectra of both responses are obtained and compared to the natural frequencies to determine if the multiphase flow is excited one of the modes of the jumper.

11.1. Oil-Gas Flow (Case 5)

When the production fluid is injected into the jumper at the initial stage, the maximum amplitude of vibration (approximately 0.4 m) occurs due to the high momentum of the fluid hitting the wall on the bends as shown in Figure 53. It was found previously that the maximum forces occur at the 4th bend; thus, it is expected to exhibit the maximum displacements at this location and surroundings as indicated in Figure 54 and Figure 55. A sinusoidal uniform displacement is reduced as the jumper is filled with oil since the system reaches steady state within this transient dynamic behavior. Also, it was found that the motion is in-line with the plane of the jumper.

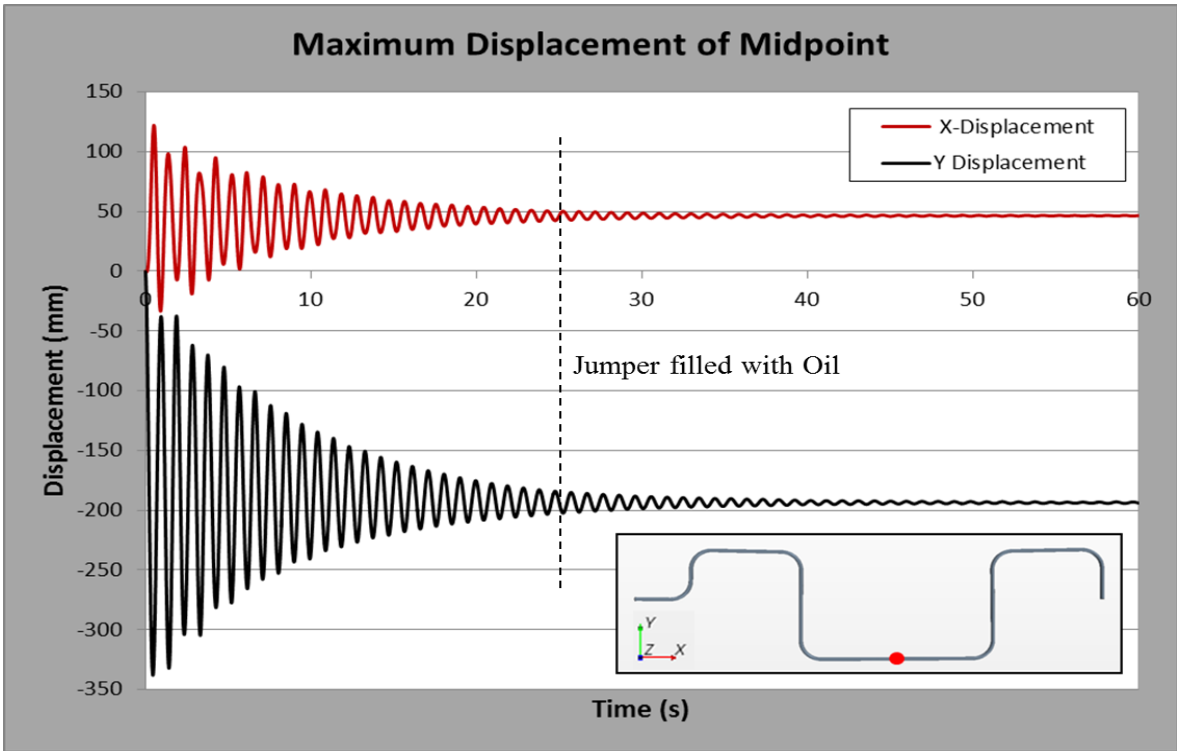


Figure 53. Maximum Displacement of Jumper at Midpoint for Case 5

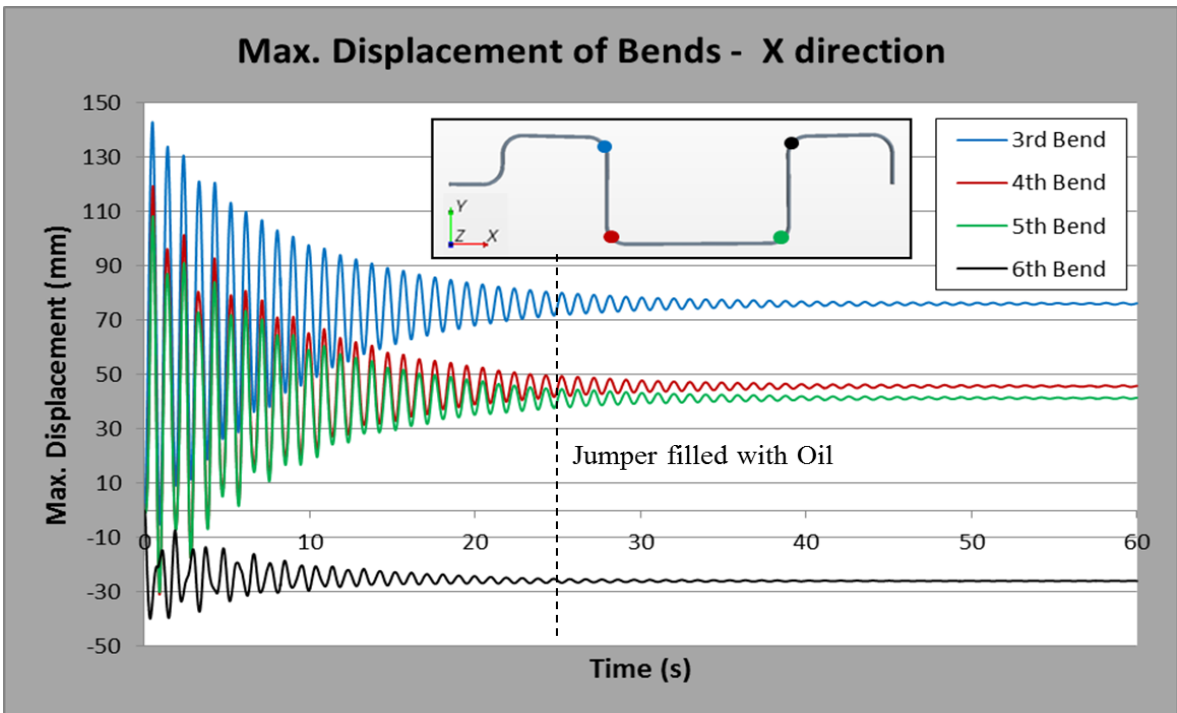


Figure 54. Maximum Displacement (in X direction) at Bends for Case 5

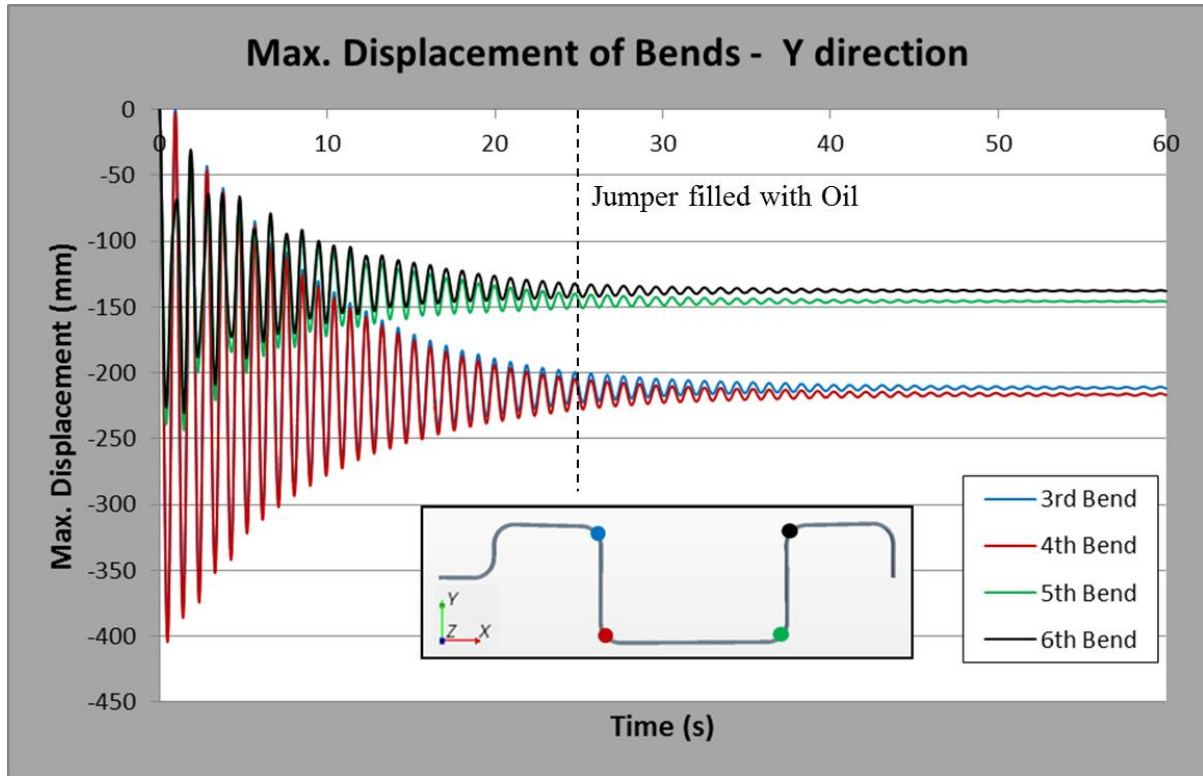


Figure 55. Maximum Displacement (in Y direction) at Bends for Case 5

Similarly, the maximum principal stresses were extracted at the two fixed ends of the jumper at which the stress range is estimated to have the maximum amplitude of 400 MPa when production starts and then it reduces to 20 MPa after the jumper is filled with oil as shown in Figure 56. The magnitude of the stress was kept below the elastic limit of 448 MPa during the entire analysis.

The time history of stress was taken at three locations of the thickness (Outer Diameter, Inner Diameter, and middle of the thickness) for 12 o'clock position and 3 o'clock position of pipe cross-section as indicated in Figure 56 and Figure 57 respectively. At the inlet-fixed end, the maximum stress of the jumper is located at the OD from the 12 o'clock cross section position. The maximum stress at the outlet-fixed end is very low (less than 1MPa) such that it is expected to have minor effect on fatigue of the jumper (See Figure 58).

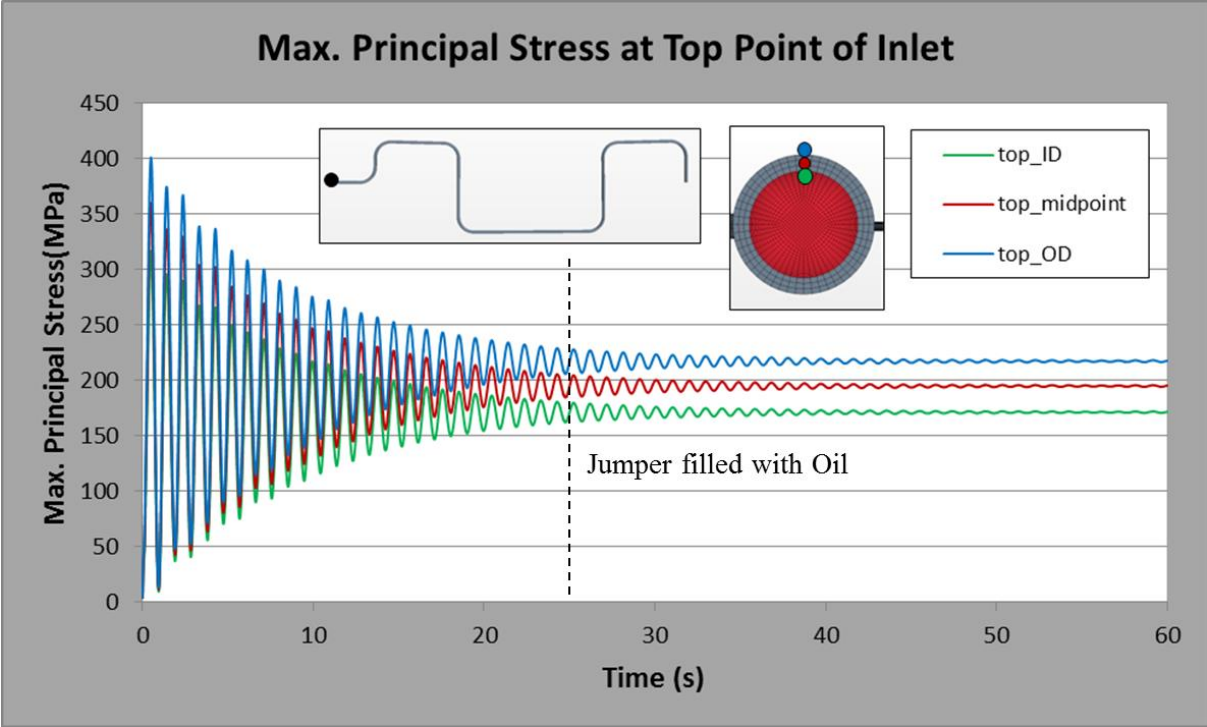


Figure 56. Maximum Principal Stress at Top Point of Inlet for Case 5

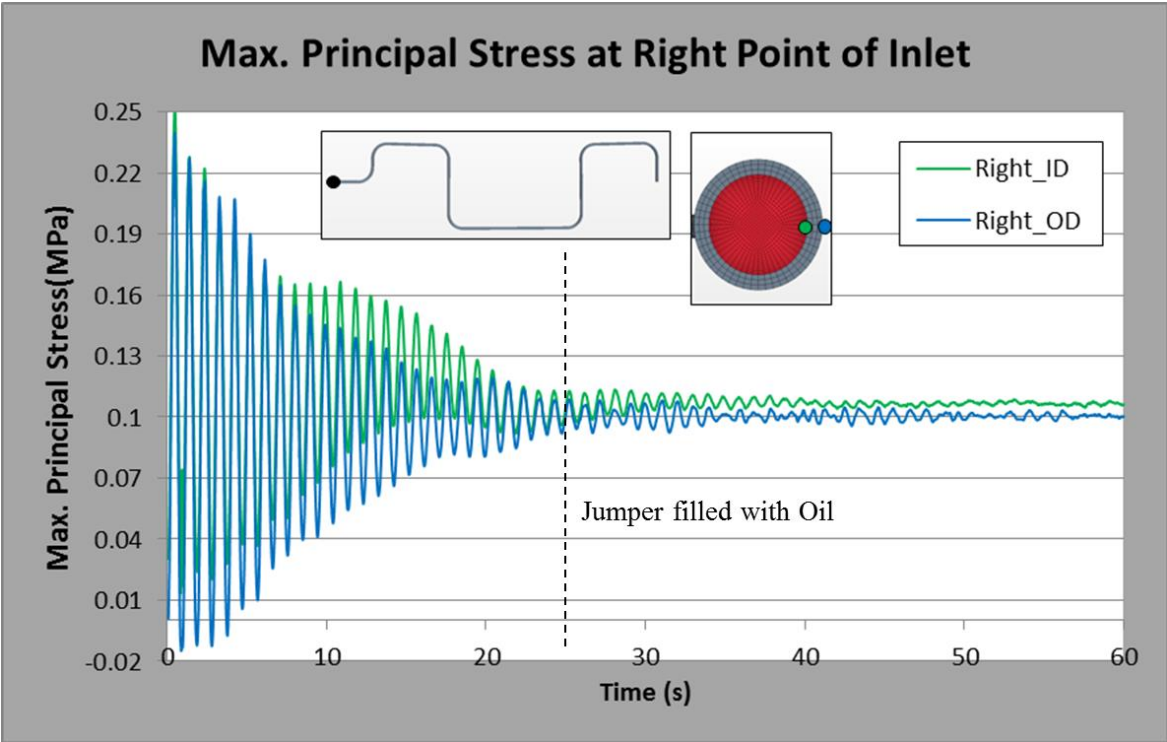


Figure 57. Maximum Principal Stress at Right Point of Inlet for Case 5

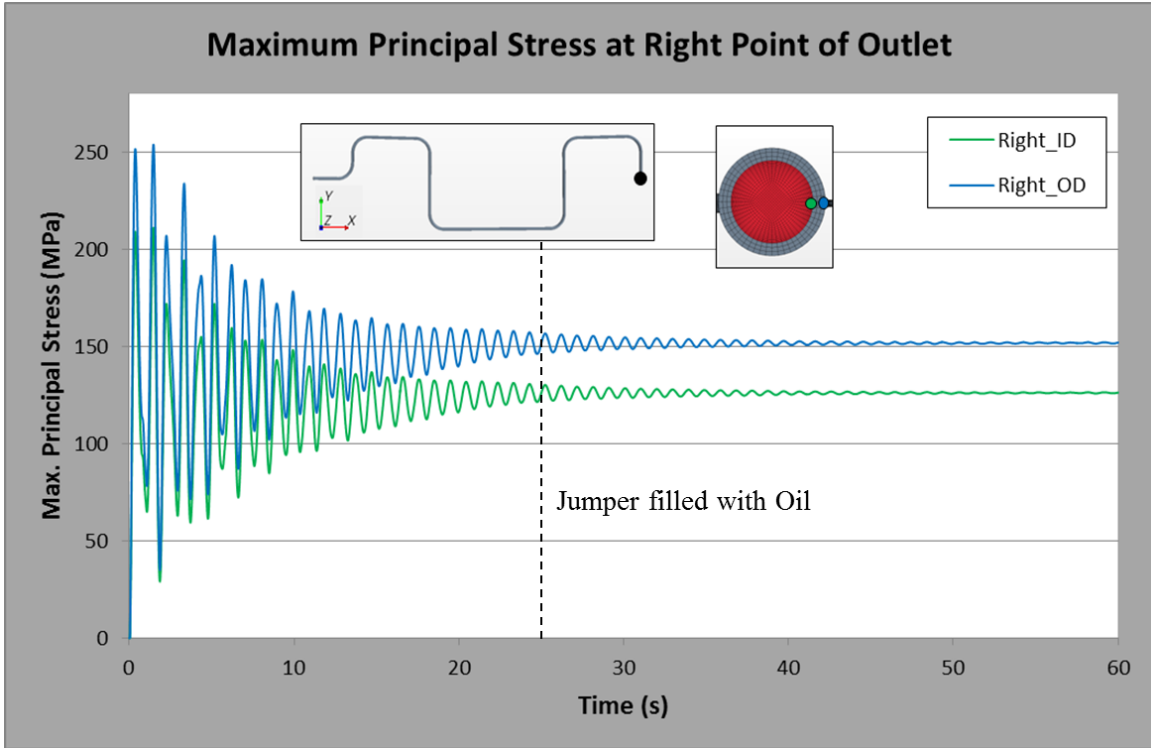


Figure 58. Maximum Principal Stress at Right Point of Outlet for Case 5

According to the PSD of the displacement and maximum principal stress (Figure 59 and Figure 60), it was found that the response frequency (1.04 Hz) falls within 6 % of the natural frequency of mode 2 (0.981 Hz) considering the added mass due to external flow. In fact, the deformation of the jumper has similar shape as the second mode of the jumper as shown in Figure 61. In other words, the oil-gas flow excites the second mode of the jumper.

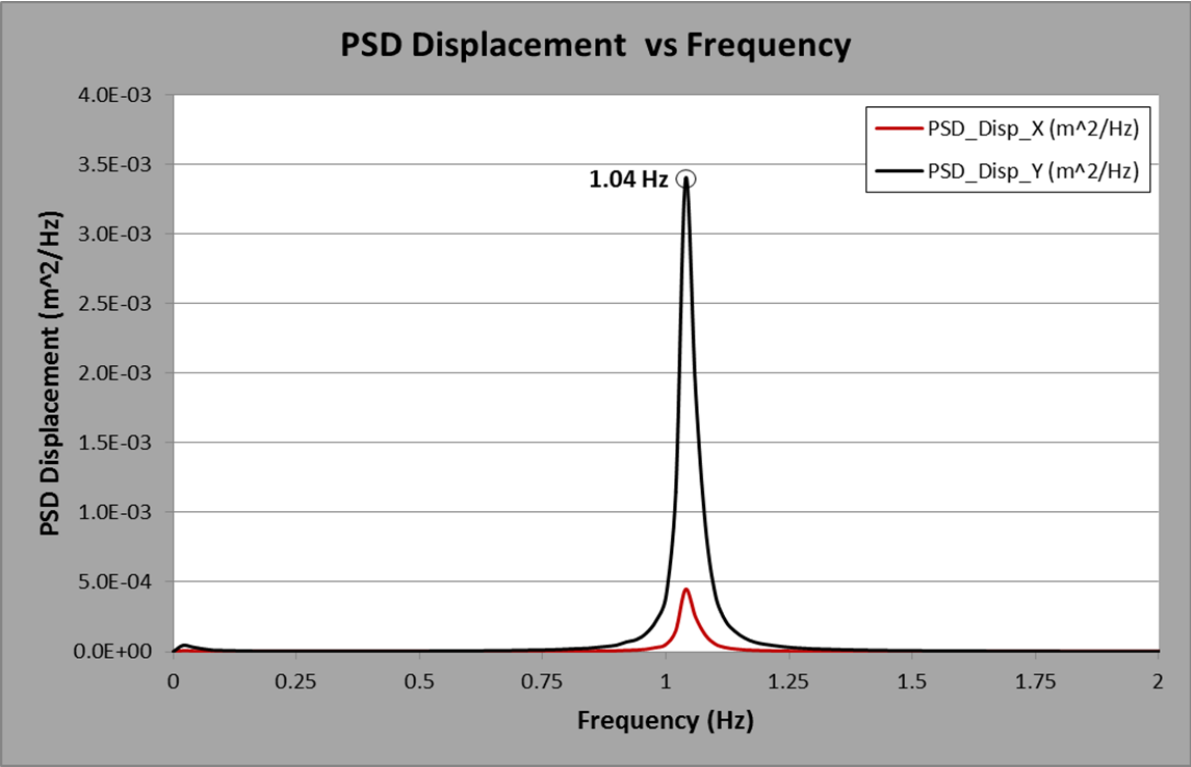


Figure 59. PSD of Displacement of Jumper for Case 5

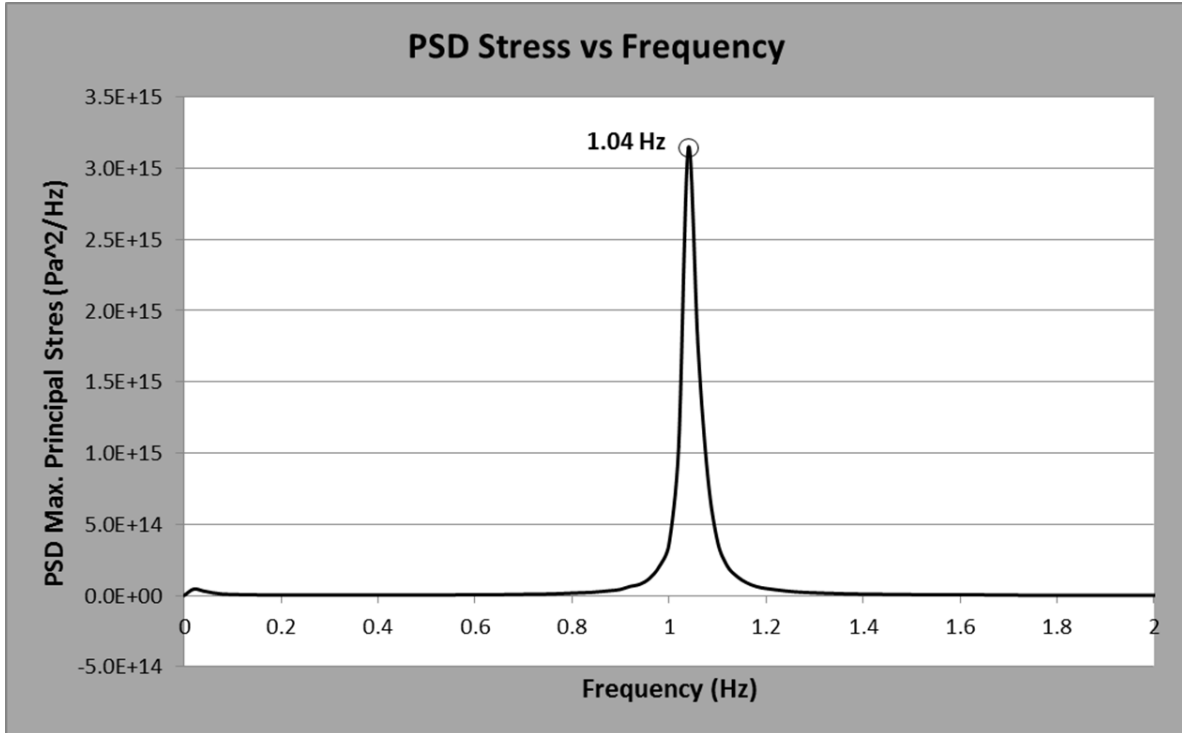


Figure 60. PSD of Max. Principal Stress of Jumper for Case 5

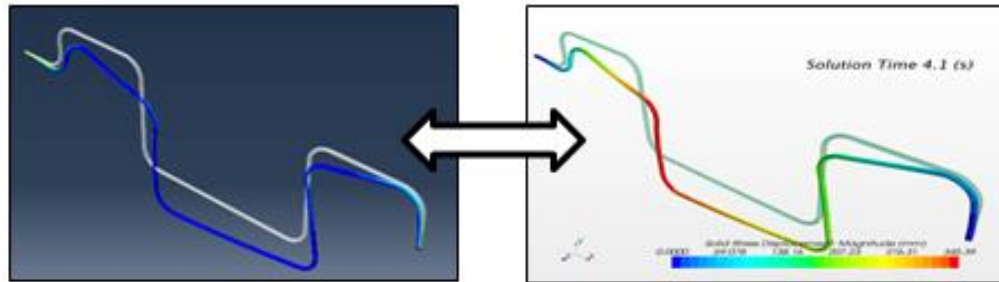


Figure 61. Comparison of the Deformation of the Jumper due to Oil-gas Flow and the Second Mode Shape

11.2. Oil-Gas-Water Flow (Case 8)

The FSI analysis of three-phase flow presents some similarities and differences with respect to the two-phase flow case. The maximum amplitude of displacement of 0.4 m occurs at the same location (bend 4 and bend 3) and keeps vibrating in-line with the plane of the jumper (Figure 62 and Figure 63). However, the amplitude of the vibration is 10 times higher than the two-phase flow case when the jumper is filled with oil (after 25 seconds of physical time).

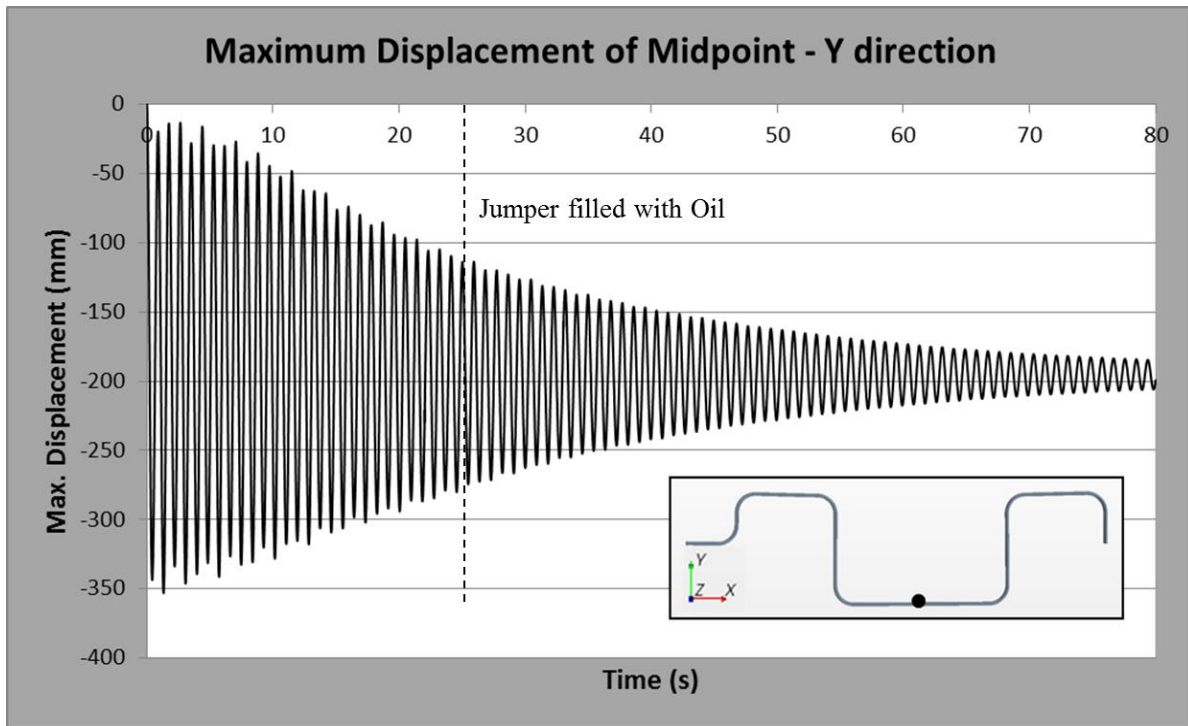


Figure 62. Maximum Displacement of Jumper at Midpoint for Case 8

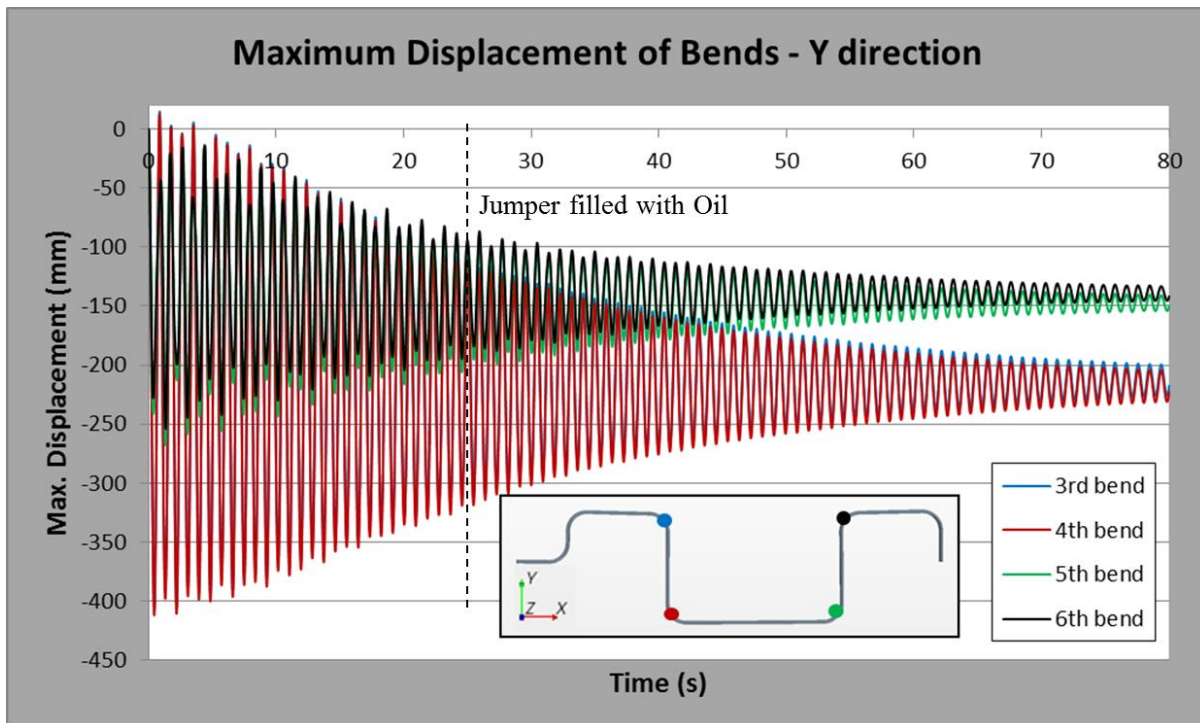


Figure 63. Maximum Displacement of Jumper at Bends for Case 8

The maximum stress increases slightly to 410 MPa, but it is still below the elastic yield limit. The stress range is approximately 400 MPa at the initial stage of the production and it decreases to 200 MPa after the jumper is filled with oil. The stress was measured at the same locations of the two-phase flow case and similar trends were found regarding the magnitude and location of maximum stresses. Figure 64 and Figure 65 show the history of the maximum principal stress at inlet-fixed end and outlet-fixed end respectively.

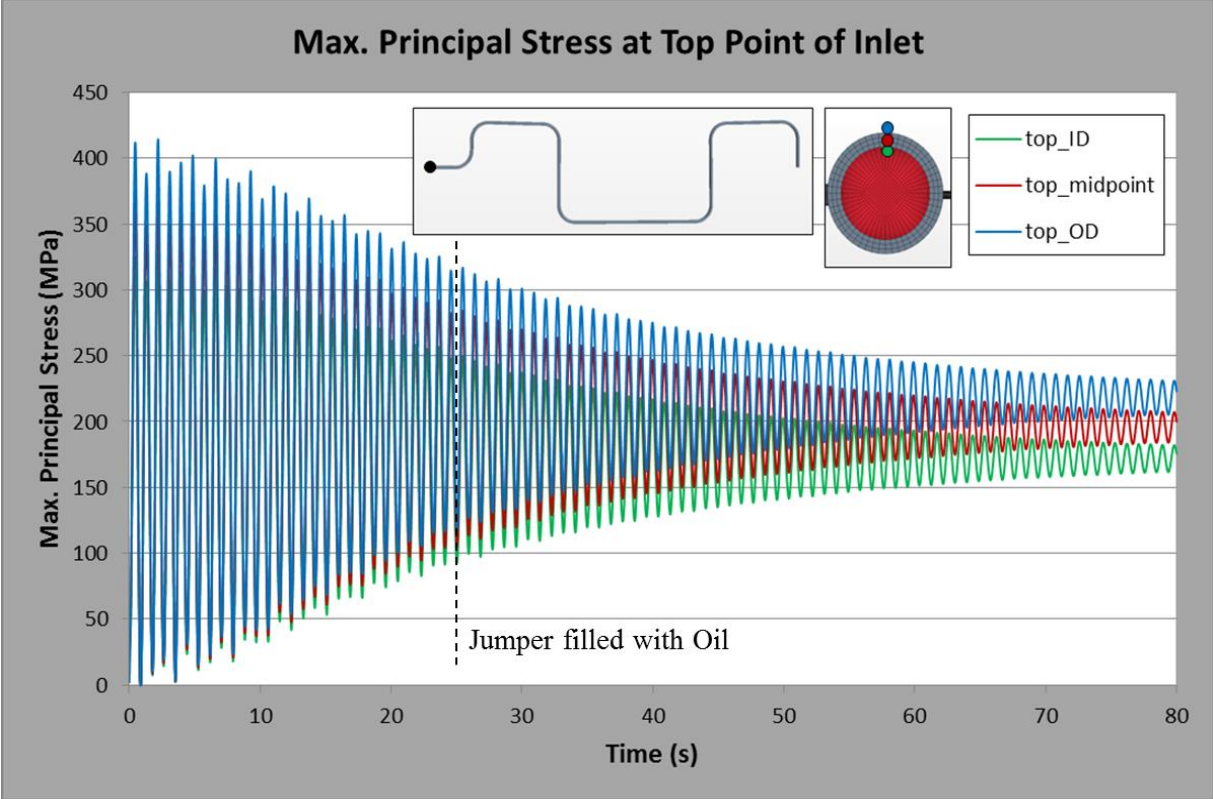


Figure 64. Maximum Principal Stress at Top Point of Inlet for Case 8

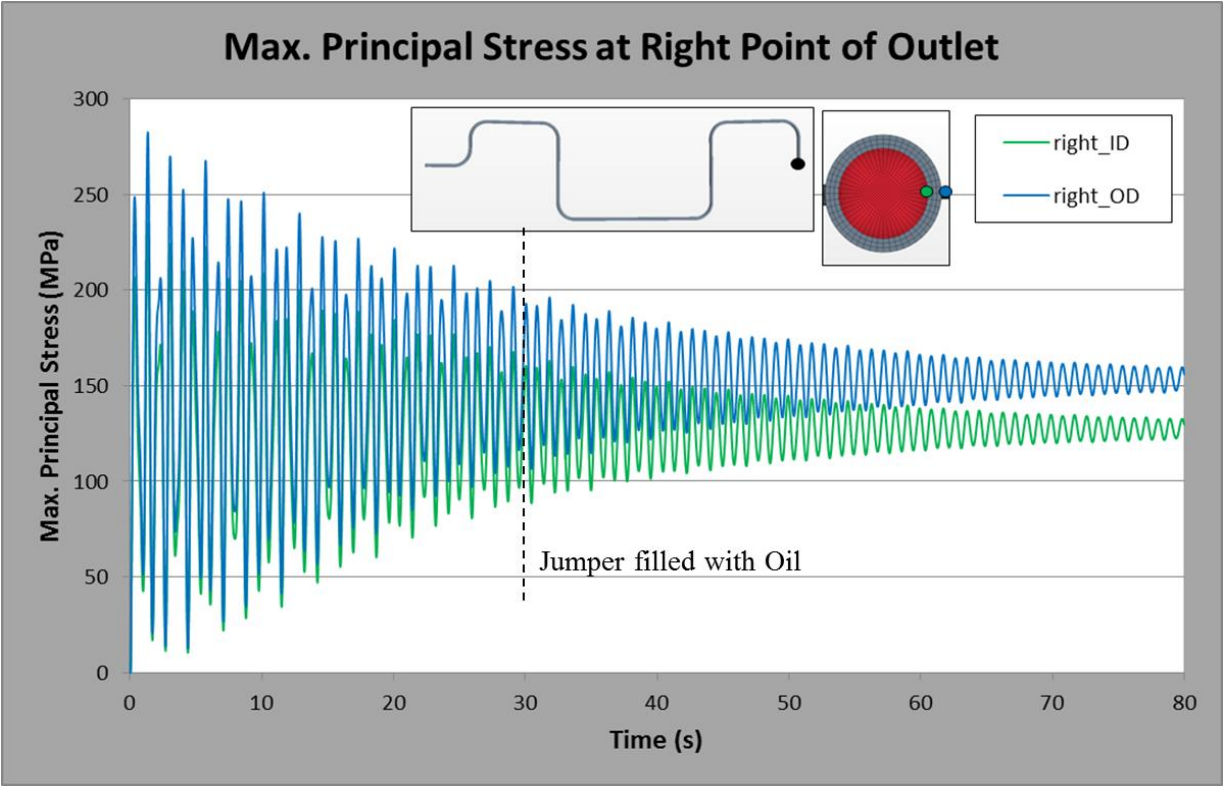


Figure 65. Maximum Principal Stress at Right Point of Outlet for Case 8

Similar to the two-phase flow case where the second mode was excited by the multiphase flow, the three-phase flow has similar results since the jumper can vibrate at the second mode of the jumper. The PSD of the displacement and stress of the jumper indicates that the response frequency of 1.1 Hz (refer to Figure 66 and Figure 67) falls approximately within 12 % of the natural frequency of the second mode if the added mass included. Otherwise, only 2 % of difference to the resonance case would be the result considering only the mass of the carbon X65 steel.

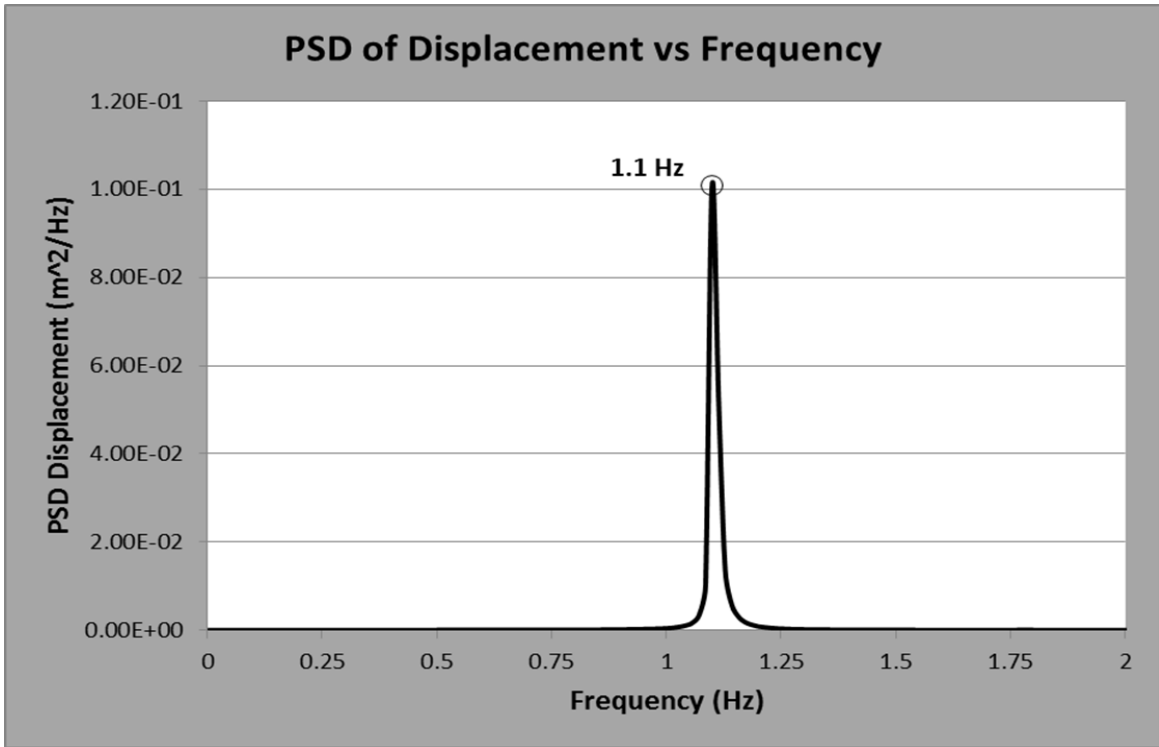


Figure 66. PSD of Displacement of Jumper for Case 8

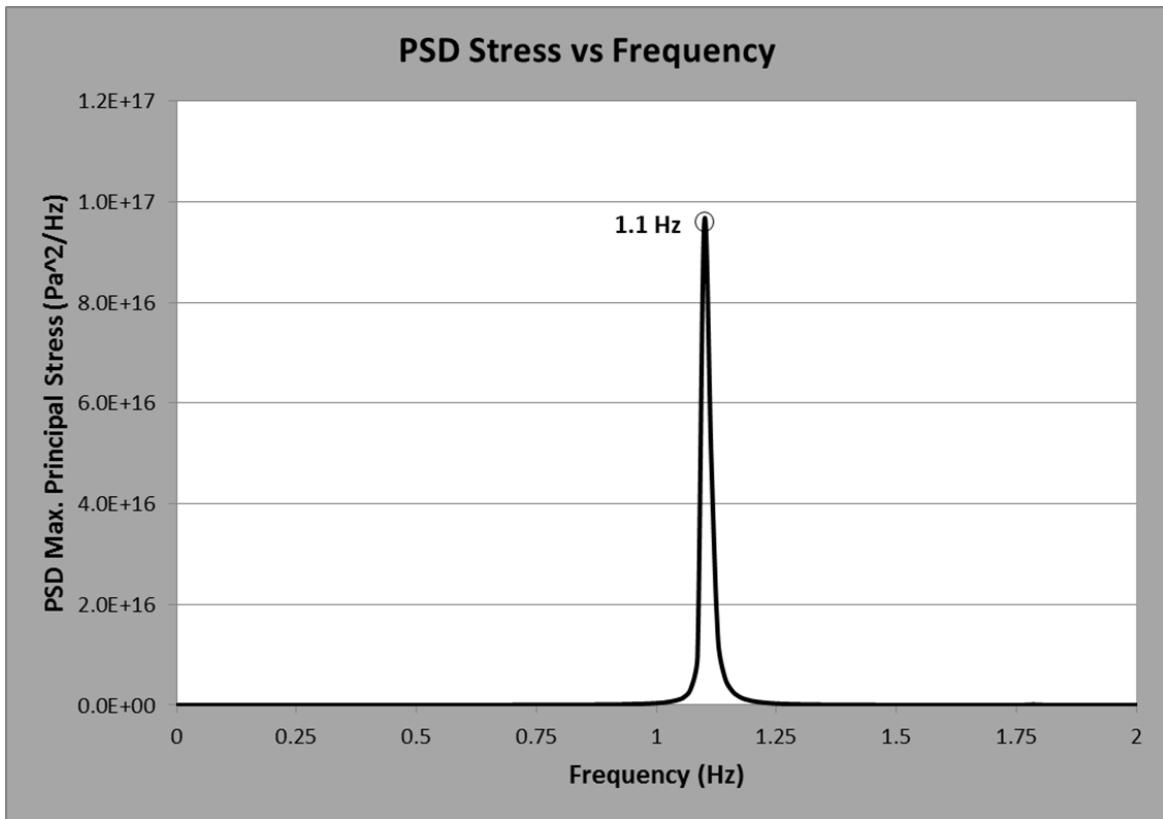


Figure 67. PSD of Max. Principal Stress of Jumper for Case 8

12. Conclusions

A methodology for assessing Flow Induced Vibration (FIV) due to multi-phase flow is missing for rigid subsea pipelines such as jumpers, manifolds, and other subsea piping components. A FIV methodology, which consists of two phases, was presented to solve this fluid structure interaction phenomenon.

According to the results of the FIV Methodology Phase I, fluid frequencies fall within 10% of the natural frequencies. Therefore, the jumper is in risk of damage under the current flow conditions based on the phase I screening methodology presented in this thesis.

The fluid or slug frequency results in a random value that varies with geometry, superficial velocity of each phase, and properties of the fluids. In fact, fluid frequency changes more than 100% along the length of the jumper; it is then over conservative to input the slug/fluid frequency such that it matches the natural frequency. It was also observed that slugs are hardly developed along the pipe, and flow regimes such as stratified flow and churn flow dominate the jumper.

It was demonstrated that the response of the jumper and behavior of the flow is at least 10% different between two-phase flow (oil-gas) and three phase flow (oil-gas-water). The fluid frequency changes by greater than 50% if a third phase is added to the oil-gas flow. Forces on the bends increase by 22% from two-phase flow to three-phase flow.

According to the results of the FIV Methodology Phase II, three-phase flow case has a higher stress range (200 MPa) than two-phase flow (10 MPa) after the jumper is filled with oil (after 25 seconds of physical time). The PSD of the displacement and stress suggested that mode 2 of the jumper is excited as the response frequency vibrates within 6% and 11% of the natural frequency of this mode for two-phase flow and three-phase flow respectively.

For both two-phase and three-phase flows, it was also found that the magnitude of the forces increases with increasing the flow rate and the percentage of oil. However, a similar trend was not found with the number of phases. Adding sand particles to the oil-gas-water flow decreases the maximum pressure on the bends, which is possible if the sand volume fraction is relatively low to accumulate in the pipe, and the resistance from the particles causes a slight or major pressure loss.

13. Recommendations and Future Work

Based on the results obtained from Phase I of the FIV methodology, it is recommended to perform a FSI analysis for the entire jumper by coupling the stress solver with the fluid solver such that the maximum principal stresses and displacements are obtained. The S-N curve will then be specified based on the environmental conditions and material of the steel pipe to finally determine the fatigue life of the jumper.

It is recommended to model and analyze the three phase flow in a jumper independently from a two-phase flow since both generate a different response on the structure. Given the actual results of the screening methodology, it is suggested to modify the flow rate of the production fluid to prevent the fluid frequency falls within 10% of the natural frequencies.

There is limited research and work in FIV of multiphase flow in subsea pipes. A small scale prototype of the jumper should be manufactured to validate and compare with the numerical results for the two-phase flow and three-phase flow configurations.

There are a lot of parameters that can be studied in the fluid and geometry. Therefore, it is recommended to perform a design of experiments to identify the parameters or interaction of parameters that have more effect on the life of the pipe. Additional CFD simulations are recommended to study the effect of varying:

- the volume fraction of each phase within the three-phase flow
- the particle diameter for oil-gas-water flow with sand particles
- the initial velocity for the oil-gas-water flow with sand production using the same particle flow rate and volume fraction of the phases

It is also understood that the internal flow is not the only source of vibration. External flow due to current or waves can induce significant vibrations on the structure, also known as Vortex Induced Vibration (VIV), so this phenomenon can be considered for future work to simulate a more realistic interaction scenario.

14. Bibliography

- Al-lababidi, S., Yan, W., & Yeung, H. (2012). Sand Transportations and Deposition Characteristics in Multiphase Flows in Pipelines. *Journal of Energy Resources Technology*, 134.
- Been, J. (2011). *Comparison of the Corrosivity of Dilbit and Conventional Crude*. Alberta Innovates Technology Futures.
- Bello, O., Reinicke, K., & Teodoriu, C. (2005). Particle Holdup Profiles in Horizontal Gas-liquid-solid Multiphase Flow Pipeline. *Chemical Engineering & Technology*, 1546-1553.
- Bello, O. (2008). *Modelling Particle Transport in Gas-oil-sand multiphase flows and its applications to production operations*. Clausthal University of Technology.
- Bratland, O. (2010). *Pipe Flow 2: Multi-phase Flow Assurance*.
- Chica, L. (2011). *Jumper Analysis with Interacting Internal Two-Phase Flow*. Houston: College of Technology.
- Clough, R. W., & Penzien, J. (1993). *Dynamics of Structures* (2nd ed.). New York: McGraw-Hill Publishing Company.
- Cooper, P., Burnett, C., & Nash, I. (2009). Fatigue Design of Flowline Systems with Slug Flow. *Proceedings of the ASME 2009 28th International Conference on Ocean, Offshore and Arctic Engineering*. Honolulu.
- Encyclopedia, T. G. (1979). *The Free Dictionary by Farlex*. Retrieved August 3, 2013, from <http://encyclopedia2.thefreedictionary.com/Gas-Oil+Ratio>
- Energy Institute. (2008). *Guidelines for the avoidance of vibration induced fatigue failure in process pipework*. London: Energy Institute.
- Ersoy, G., Sarica, C., Al-Safran, E., & Zhang, H. (2011). Experimental Investigation of Three-Phase Gas-Oil-Water Slug Flow Evolution in Hilly-terrain Pipelines. *SPE Annual Technical Conference*. Denver.
- Hirt, C., & D., N. B. (1981). Volume of Fluid (VOF) Method for the Dynamocs of Free Boundaries. *Journal of Computational Physics*, 201-225.
- Izarra, R. (2009). *Second Moment Modelling for the Numerical Simulation of Passive Scalar Dispersion of Air Pollutants in Urban Environments*. Siegen.
- Jia, D. (2012). Slug Flow Induced Vibration in a Pipeline Span, a Jumper, and a Riser Section. *Offshore Technology Conference*. Houston.

- Keskin, C., Zhang, H.-Q., & Sarica, C. (2007). Identification and Classification of New Three-Phase Gas/Oil/Water Flow Patterns. *SPE Annual Technical Conference and Exhibition*. Anaheim, California.
- McMurtry, P. (n.d.). Length and Time Scales in Turbulent Flows. Salt Lake City, Utah, United States. Retrieved from www.eng.utah.edu/~mcmurtry/Turbulence/turbflt.pdf
- National Aeronautics and Space Administration. (2008). *Navier-Stokes Equations: 3-dimensional-unsteady*.
- Pontaza, J., & Menon, R. (2011). Flow-Induced Vibrations of Subsea Jumpers due to Internal Multi-phase flow. *30th International Conference on Offshore Mechanics and Arctic Engineering*. Rotterdam.
- Pontaza, J., & al, e. (2013). Flow-induced Vibrations of High gas rate Well Jumpers: Tees vs. Bends. *Proceedings of the ASME 2013 32nd International Conference on Ocean, Offshore and Arctic Engineering*. Nantes.
- Ramdin, M., & Henkes, R. (2011). CFD for Multiphase Flow Transport in Pipelines. *Proceedings of the ASME 2011 30th International Conference on Ocean, Offshore and Arctic Engineering*.
- Riverin, J., de Langre, E., & Pettigrew, M. (2006). Fluctuating forces caused by internal two-phase flow on bends and tees. *Journal of Sound and Vibration*, 1088-1098.
- Riverin, J., & Pettigrew, M. (2007). Vibration Excitation Forces due to Two-phase Flow in Piping Elements. *Journal of Pressure Vessel Technology*, 7-13.
- Science Flow. (2013). *Flow-3D*. Retrieved October 20, 2013, from Flow Science: <http://www.flow3d.com/cfd-101/cfd-101-implicit-explicit-schemes.html>
- Soviet State. (1979). *The Free Dictionary*. Retrieved August 25, 2013, from The Great Soviet Encyclopedia: <http://encyclopedia2.thefreedictionary.com/Gas-Oil+Ratio>
- STAR CCM+. (2013). *CD-adapco Star-CCM+*. Retrieved October 10, 2013, from C:\Program Files\CD-adapco\STAR-CCM+8.04.007\doc\online\wwhelp\wwhimpl\js\html\wwhelp.htm
- Stour, P. (1988, October). *Rhode Island Sea Grant Fact Sheet*. Retrieved August 14, 2013, from <http://seagrant.gso.uri.edu/factsheets/sand.html>
- Swindell, R. (2011, September 01). *Hidden integrity threat looms in subsea pipework vibrations*. (Xodus Group) Retrieved October 15, 2012, from Offshore: <http://www.offshore-mag.com/articles/print/volume-71/issue-9/production-operations/hidden-integrity-threat-looms-in-subsea.html>

Timoshenko, S., & Goodie, J. (1970). *Theory of Elasticity* (3rd ed. ed.). New York: McGraw-Hill.

Appendices

Appendix A: Modes Shapes of the Jumper from ABAQUS

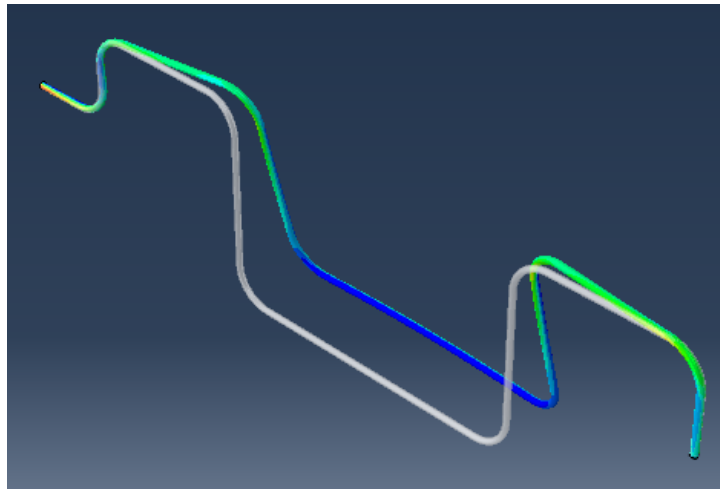


Figure 68. Mode-1 for M-shaped Jumper - Isometric View

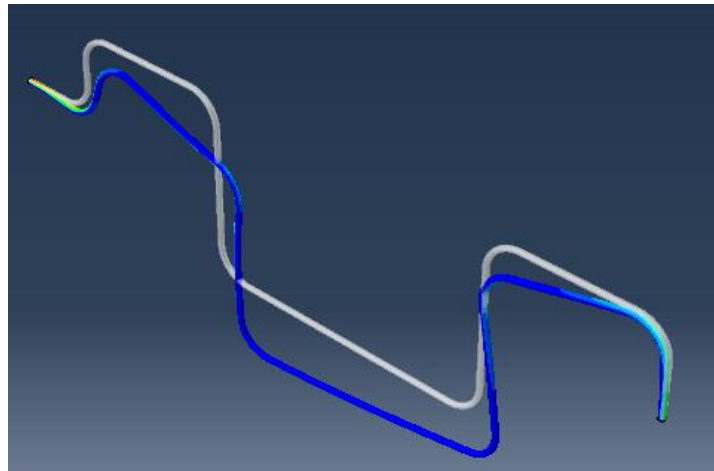


Figure 69. Mode-2 for M-shaped Jumper - Isometric View

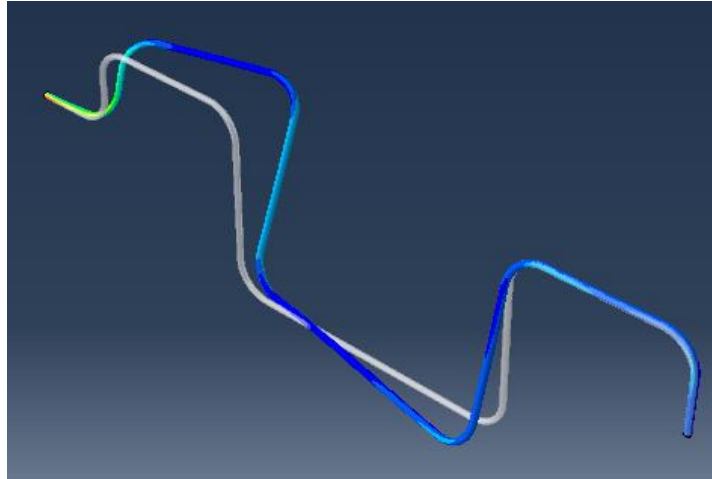


Figure 70. Mode-3 for M-shaped Jumper - Isometric View

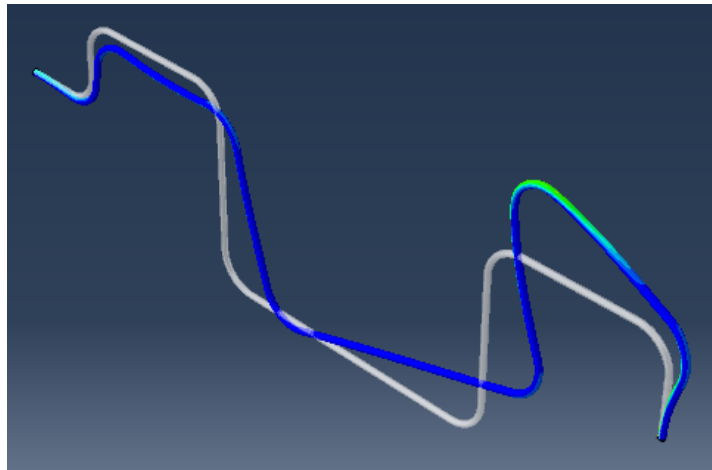


Figure 71. Mode-4 for M-shaped Jumper - Isometric View

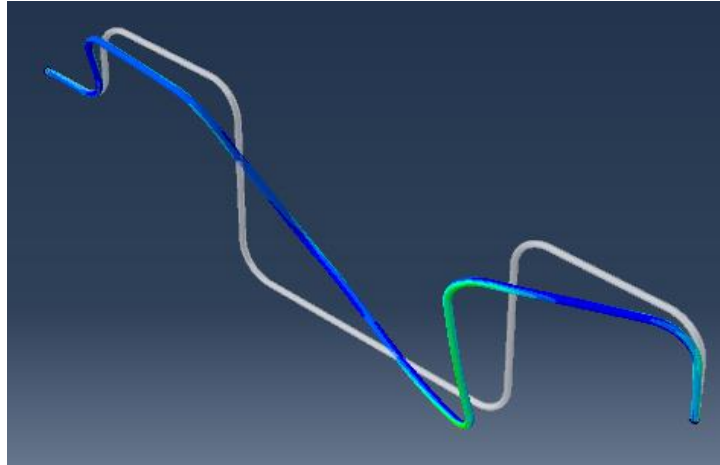


Figure 72. Mode-5 for M-shaped Jumper - Isometric View

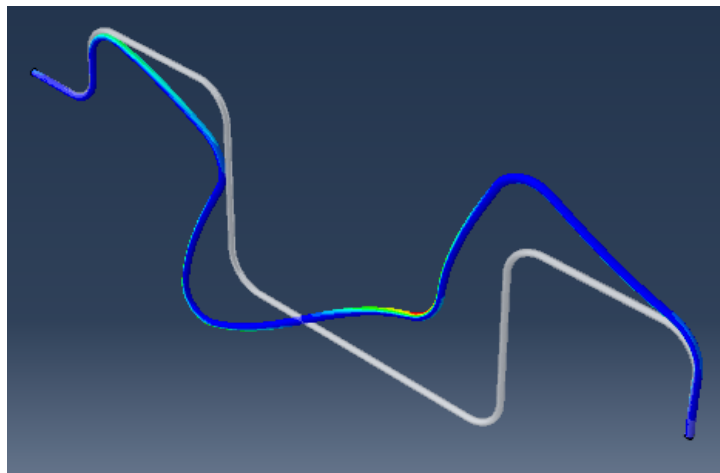


Figure 73. Mode-6 for M-shaped Jumper - Isometric View

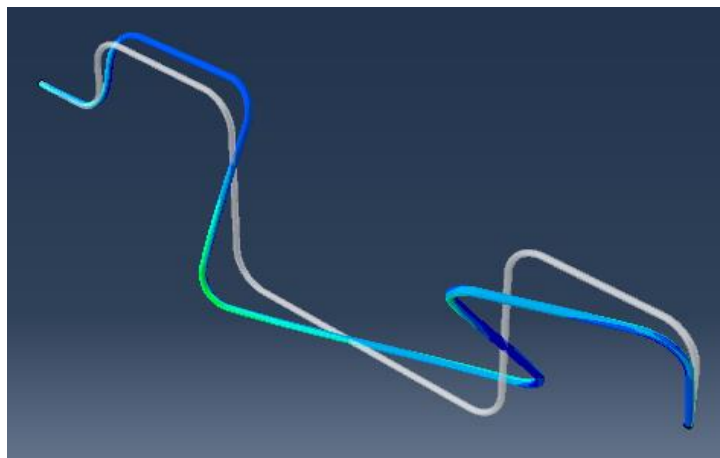


Figure 74. Mode-7 for M-shaped Jumper - Isometric View

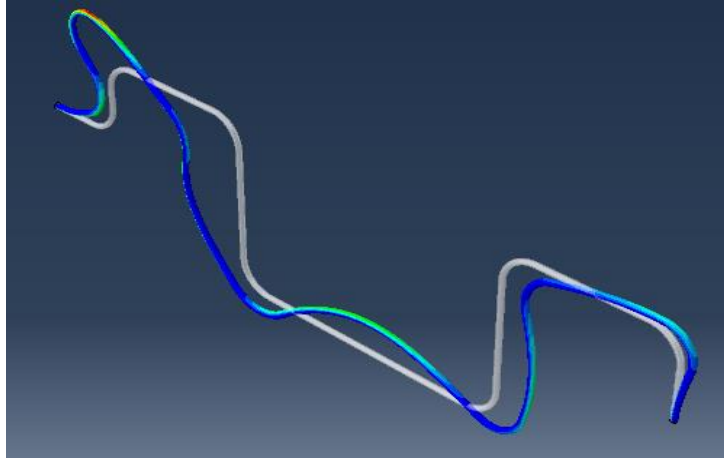


Figure 75. Mode-8 for M-shaped Jumper - Isometric View

Appendix B: Computational Performance

Computational efficiency is one of the important aspects when dealing with high-intensive CFD simulations. It is then a need to have enough computing power available such that the results are obtained in an efficiency way with the appropriate accuracy. Solving complex engineering problems in CFD programs requires computational machines with excellent processor speed, enough number of cores, high RAM memory, and compatible operating system. For example, some simulations performed using a Intel (R) Core (TM) 2.4 GHz processor with 8GB RAM took from 2 days to 6 days to complete a 20 second two-phase flow (air and water) running through a one bend model (Chica, 2011). Those simulations were submitted in series or 2 parallel processors using only StarCCM+ (Refer to Table 21). This type of simulations requires a minimum physical time of 25 seconds to have a real representation of the flow in a pipe.

Table 21. Computational Demand for a Simulation with Different Mesh and Time Step using a Local Machine (Intel (R) Core (TM) 2.4 GHz Processor and 8GB RAM Memory)

Time step (s)	No. of cells	Computational time	Physical time (s)	No local processors
0.01	186600	29 hours	20	1
0.004	295000	2 days 4 hours	25	2
0.003	445500	3 days 13 hours	20	2
0.001	230750	6 days	6	1

If another two phases are added to the flow (i.e. oil and sand particles) and the CFD tool is coupled with a FEA program, then it would be computational unfeasible to complete those analyses at least in a few days. For this reason, there was a need to look for options to improve the computational time by using a cluster or a high speed computer processor. Two resources were available at the college:

- Desktop Windows Machine Intel (R) Core (TM) i7-2600 CPU @3.40 GHz, 4 cores, 8 processors, 64-bit OS
- Maxwell AMD Opteron based Linux cluster)

Maxwell is an AMD based cluster with approximately 3,600 processing cores running 2.2GHz and 2.3GHz processors. It uses gigabit Ethernet for its interconnect. System nodes are

from 4 to 32 cores with memory between 8GB and 128GB. Maxwell also includes 30 workstations to provide GPU processing with 22 GTX 580 cards and 8 Tesla cards in an 8-node Infiniband network.

Table 22 describes how the computing nodes are distributed in the cluster. There are seven computing node types: three are AMD Quad core processors, one AMD dual core, one AMD 16 core, and two Intel Xeon dual core processors. Each computing node type has a particular amount of nodes and memory capacity. The node count is how many of that particular kind of node there is in the cluster. The queuing system decides where the best compute node to run on based on number of processors requested, the amount of memory and how long wall time is listed.

Table 22. Hardware Specifications of AMD Opteron based Linux Cluster

Node Type	CPU Type	CPU Count	Total Cores	Memory	Node Count
login Sun Fire X2200	AMD Quad Core Opteron 2.2GHz	2	8	16GB	1
compute Sun Fire X4600	AMD Quad Core Opteron 2.3GHz	8	32	64GB	4
compute Sun Fire X2200	AMD Quad Core Opteron 2.2GHz	2	8	16GB	124
compute Western Scientific	AMD Dual Core Opteron 2.2GHz	2	4	8GB	114
compute SuperMicro	AMD 16 Core Opteron 2.2GHz	2	32	64GB	28
compute Dell	Intel Xeon Dual Core 3.0GHz GPU GTK 570	2	4	32GB	22
compute Dell	Intel Xeon Dual Core 3.0GHz GPU TeslaC2075	2	4	32GB	8

A simulation was set up to compare the efficiency of the local machine and cluster with the number of cpus specified. The purpose was to calibrate the model at an optimum number of

processors. This analysis was a short simulation of three-phase flow in a jumper for 10 steps of 0.005 seconds at each step. Each processor takes one license of Star CCM+ and the department is limited to 25 licenses.

According to the results shown in Figure 76 of the computational time, the same analysis is completed in a shorter period of time by increasing the number of processors. In fact, there is a 94 percent fit of the points to follow a quadratic relationship between the number of cpus and the computational time. The maximum efficiency is achieved when the analysis is run using 16 processors. After this point, a greater number of processors would take more computational time due to delays in the communication between cpus. It is also better to specify all the processors in one single node; otherwise, the job would take more time for completion.

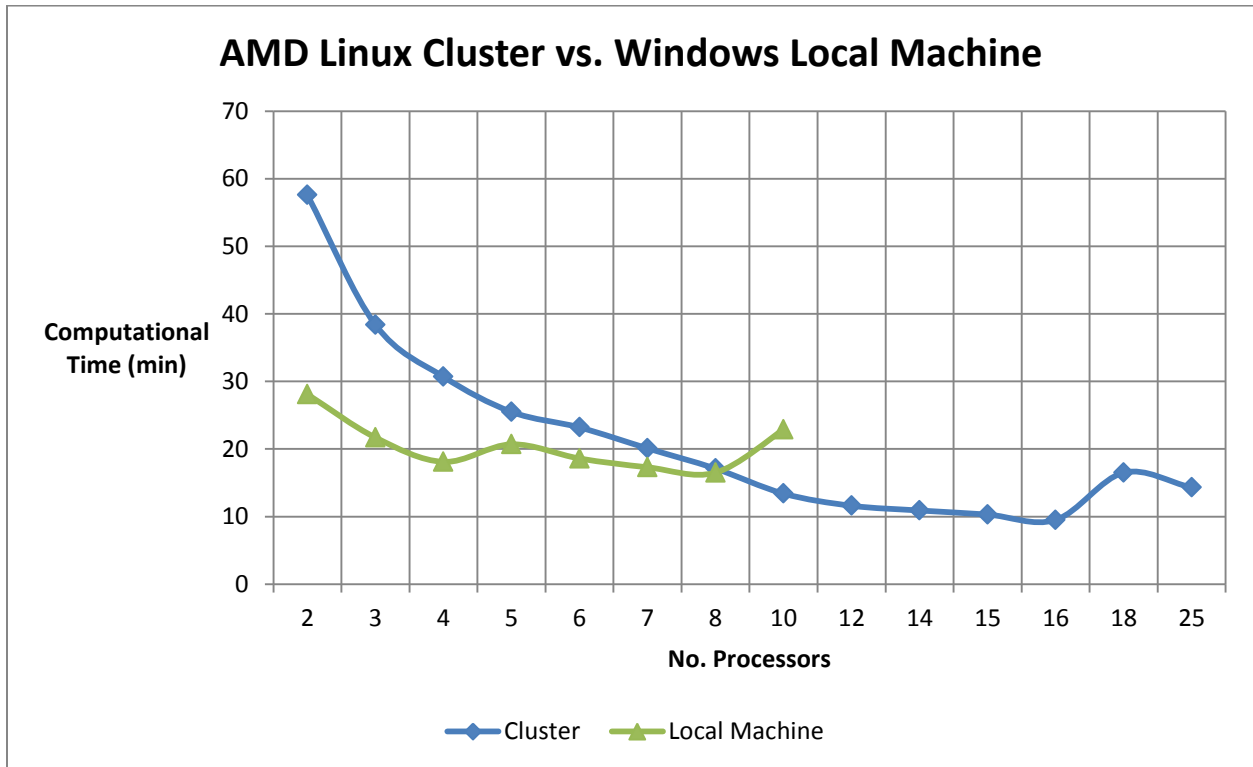


Figure 76. Computational Demanding using a AMD Linux Cluster versus a Windows Machine Intel (R) Core (TM) i7-2600, 64-bit OS

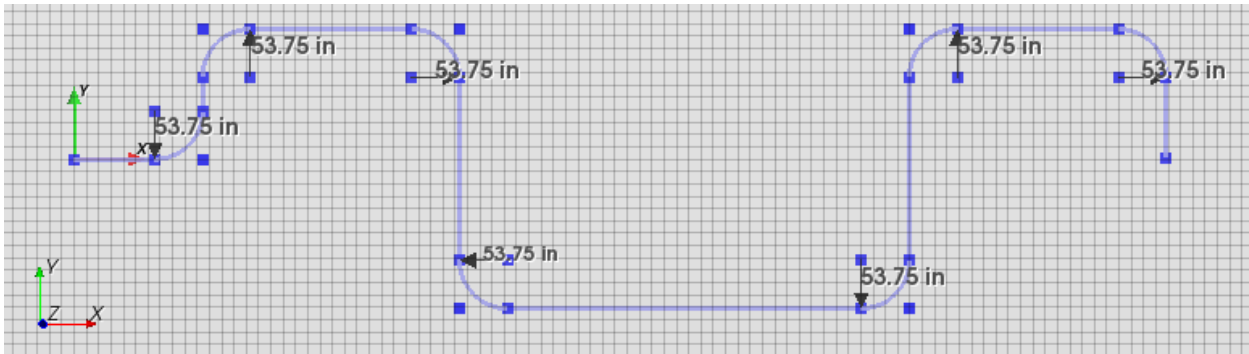
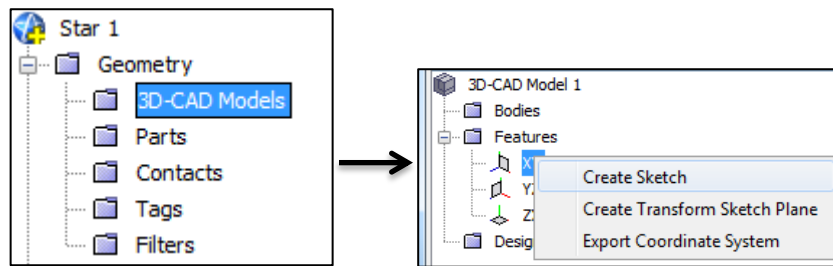
A significant difference is observed when comparing the time of a simulation in the cluster versus in the local machine. Using the same number of processors, a job in the desktop machine takes less time than the same job submitted at the cluster. However, the machine is limited to 8 cpus; it would then decrease its efficiency if more than 8 cpus are specified.

Another peculiar condition that occurs in both cluster and local machine is the presence of a small peak in which the job takes more time for a particular number of cpus specified, and then it starts running faster again after increasing the number of cpus.

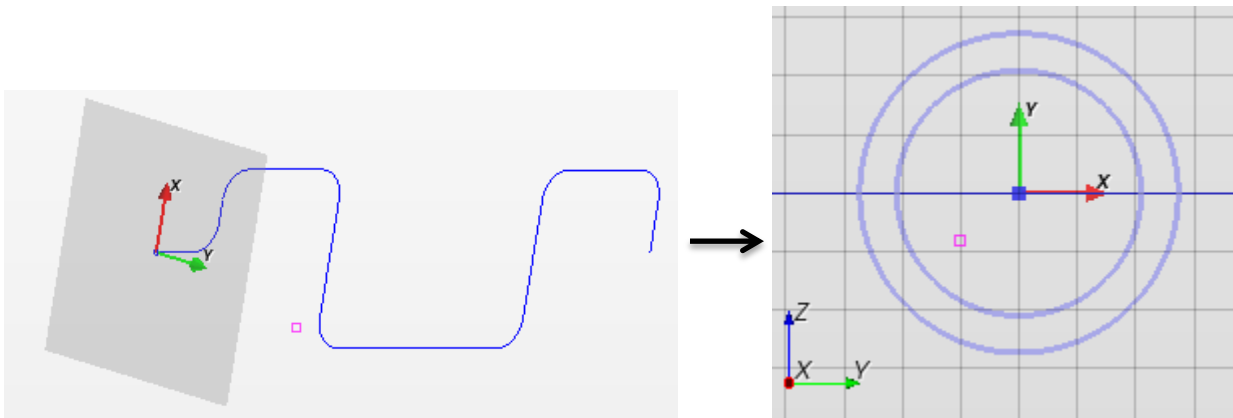
Based on the results of this assessment, it is useful to perform sensitivity studies to calibrate the number of cpus per simulation since the processing time would differ with mesh, time step, complexity of the model, numerical models or methods, and size of the model.

Appendix C: Setting up the Mesh in Star-CCM+ for Sensitivity Analysis

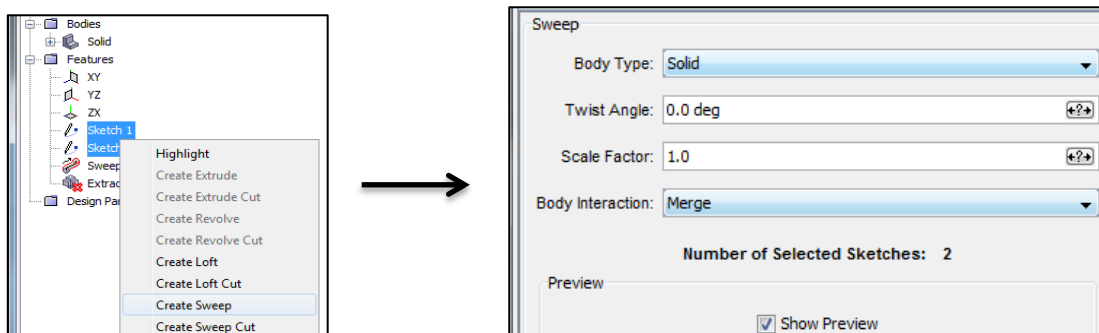
1. Create the 3D-CAD model of the jumper – sketch the path of the jumper in X-Y plane

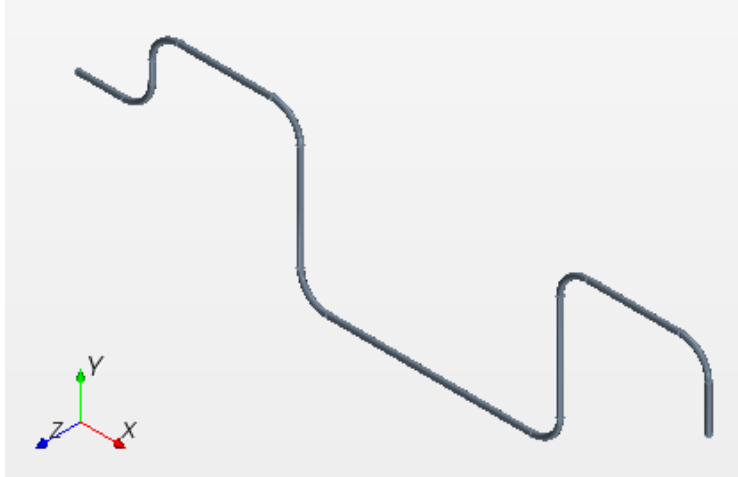


2. Create the 3D-CAD model of the jumper – sketch the cross-section of the pipe in X-Z plane



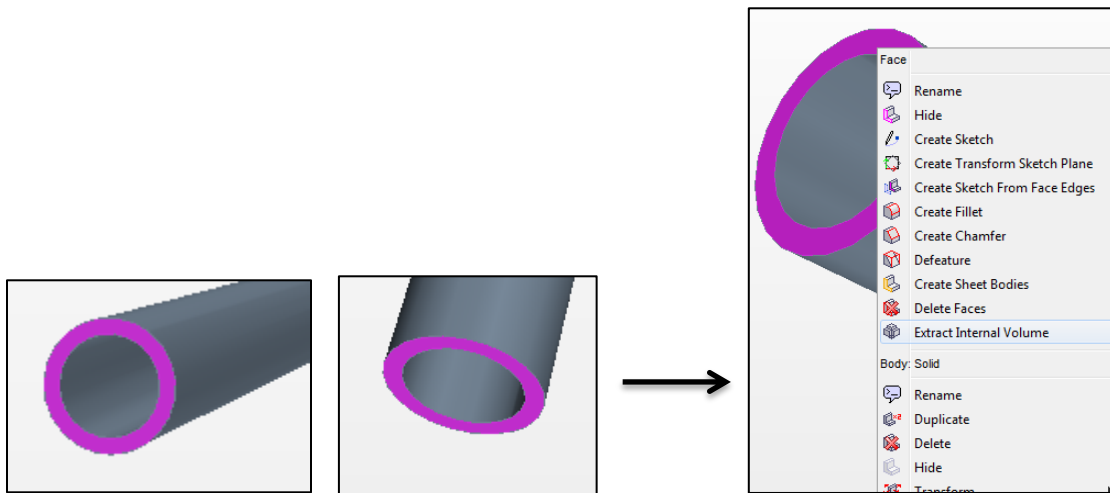
3. Perform a sweep operation from the two sections



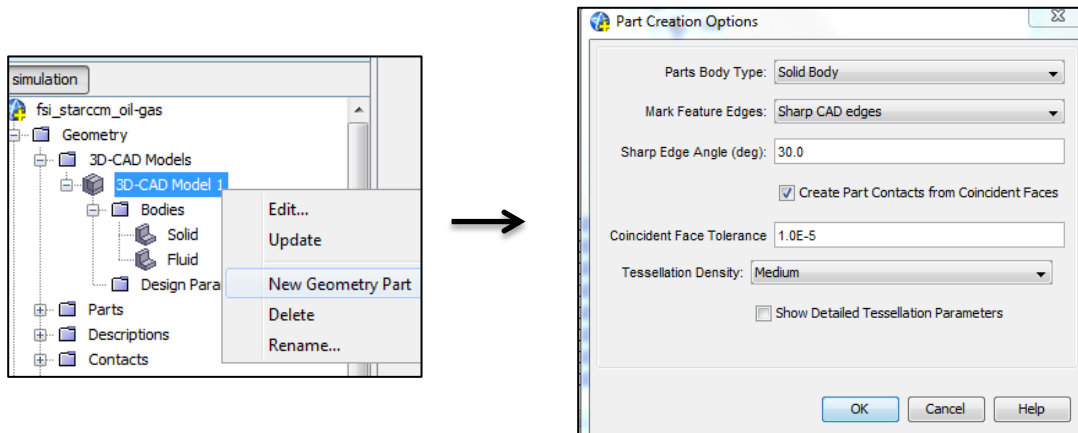


4. Extract internal volume of the jumper for meshing of the fluid domain

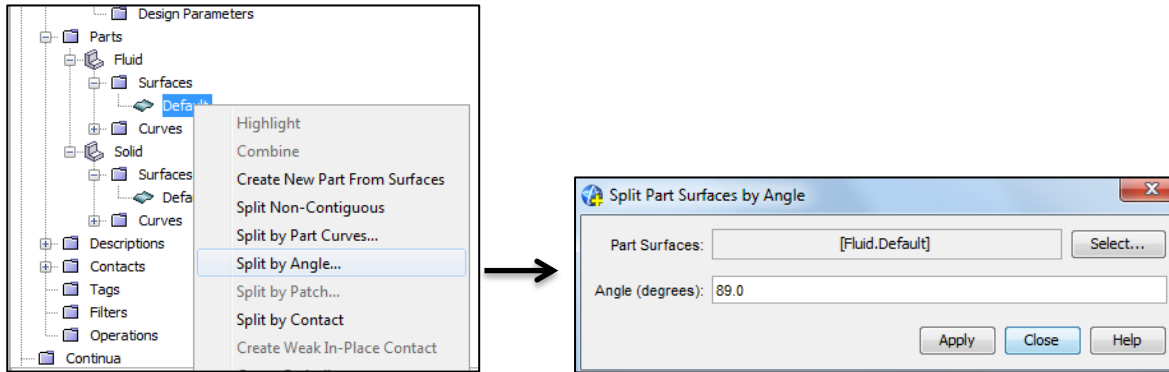
- Select the two surfaces of the ends of the jumper
- Extract Internal Volume option



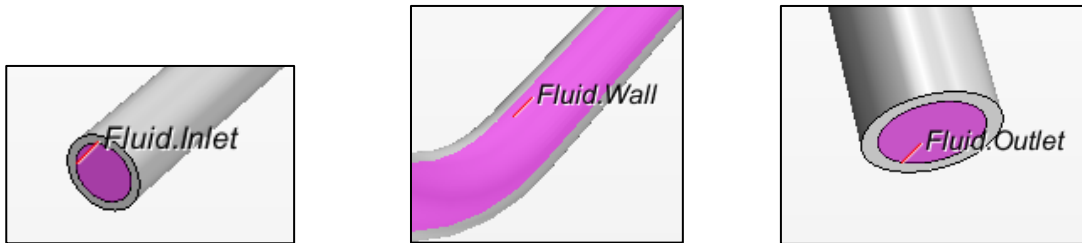
5. Create New Geometry Part



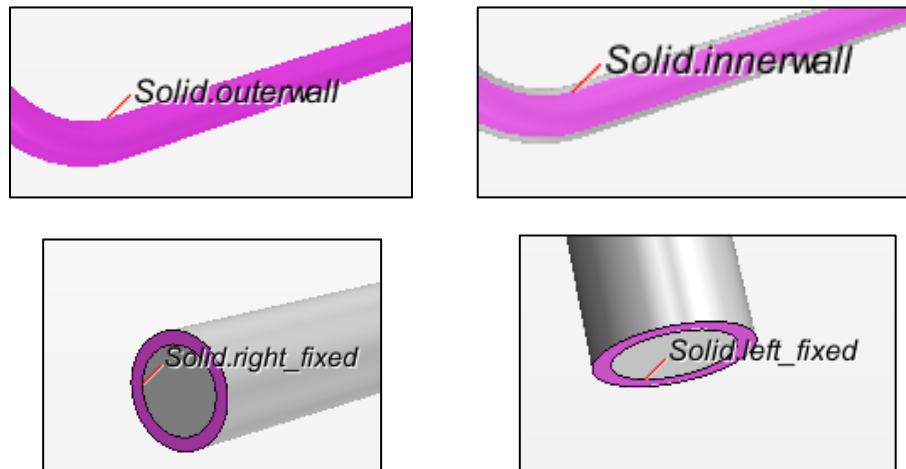
6. Split the surfaces of the two parts (fluid and solid)



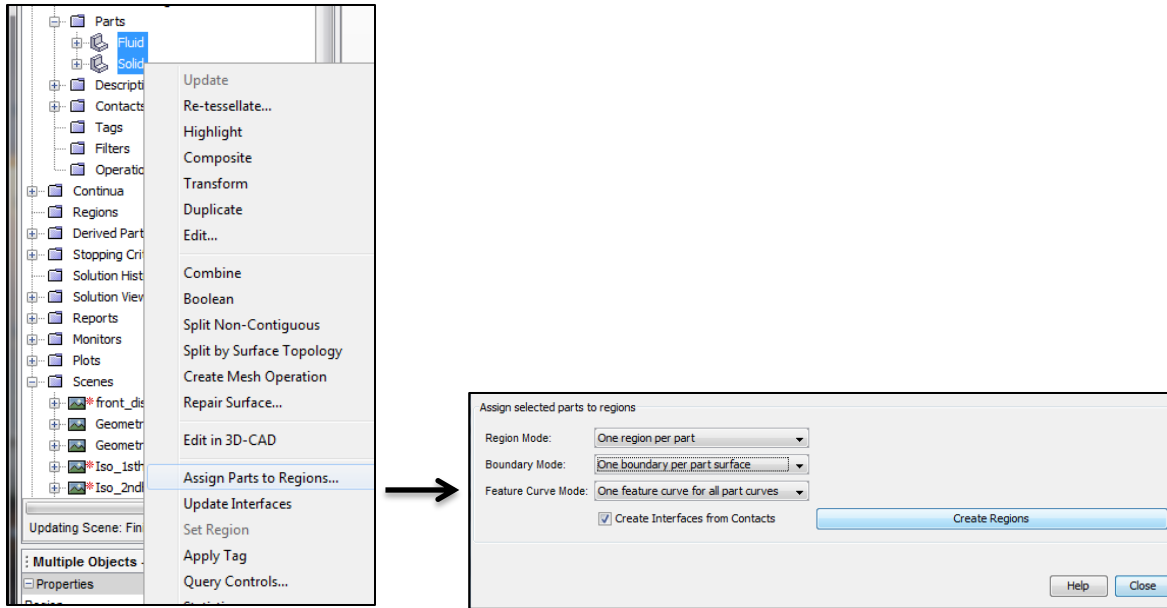
Fluid Surfaces



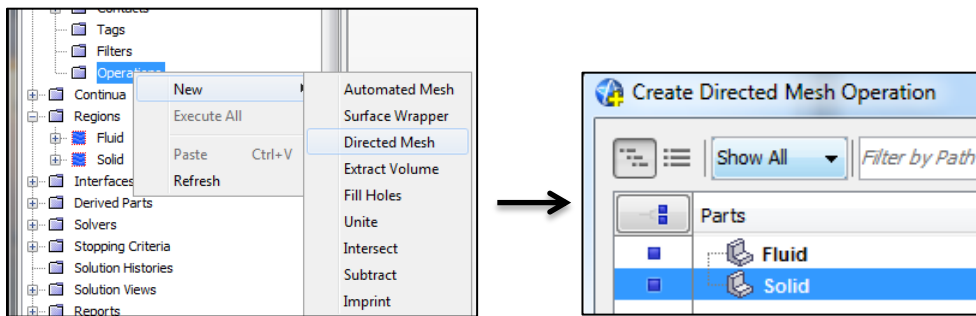
Solid Surfaces



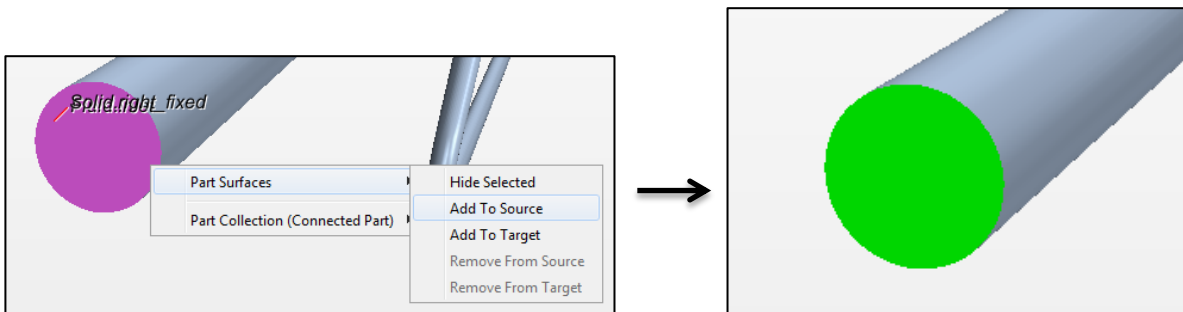
7. Assign Parts to Regions



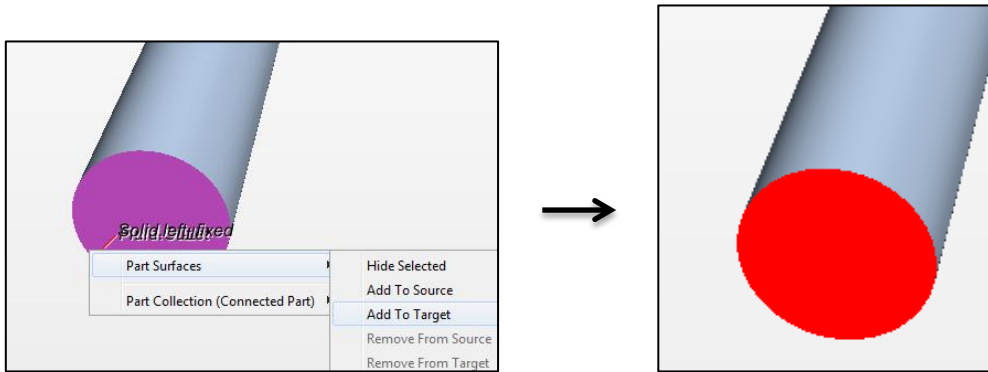
8. Create a Directed Mesh for both fluid and solid domains



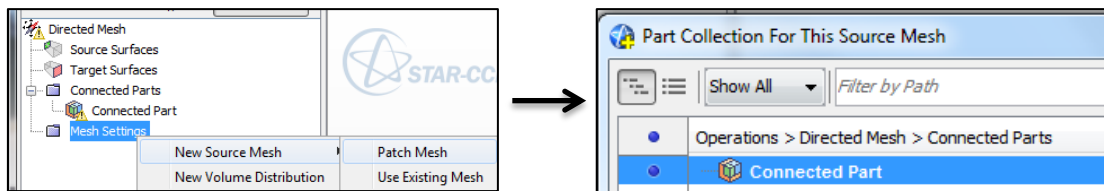
9. Select the inlet and solid left fixed end surfaces to add as the Source



10. Select the outlet and solid right fixed end surfaces to add as the Target





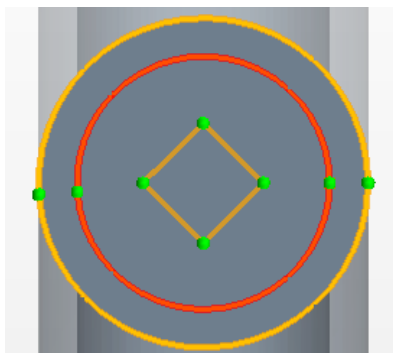
11. Create Patch Mesh



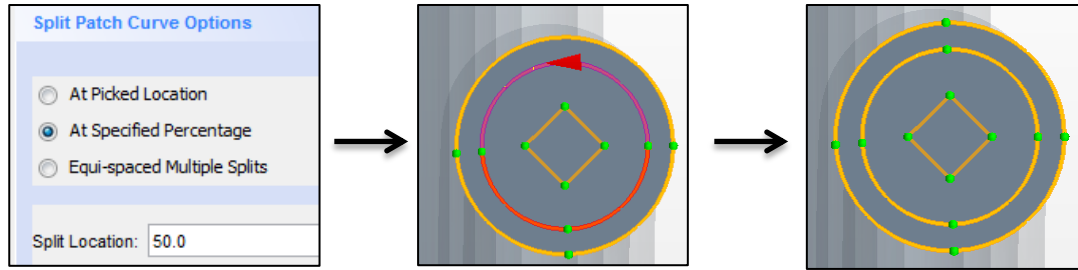
12. Create patch curve by drawing the points on the source surface



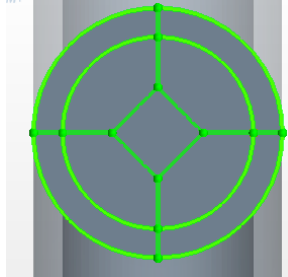
- Create patch curve by drawing the points on the source surface 
- Populate the feature edges with the patch curve as shown in figure below 



- Split orange and yellow patch curves to generate points at 90 degrees angles as shown below

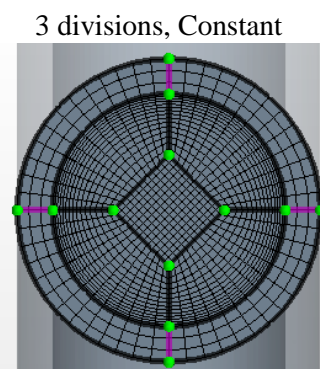
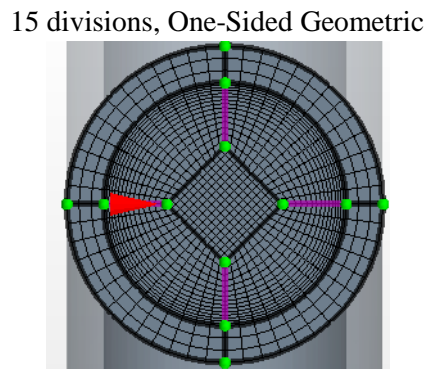
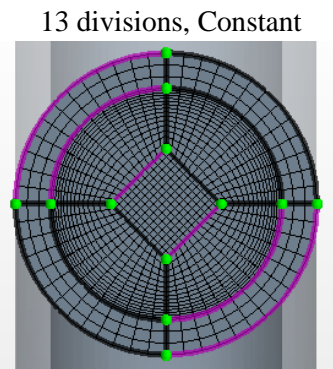
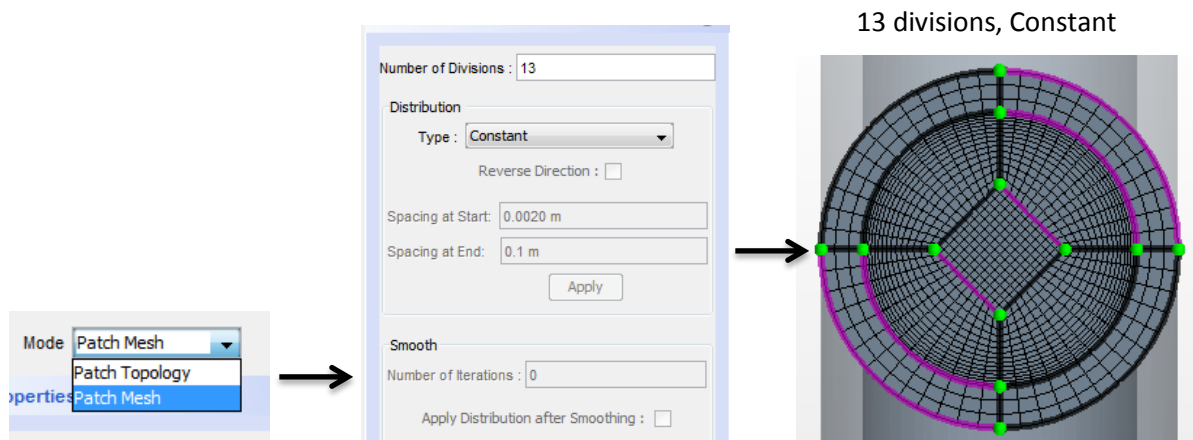


- Connect points to have a four-side polygon at each patch

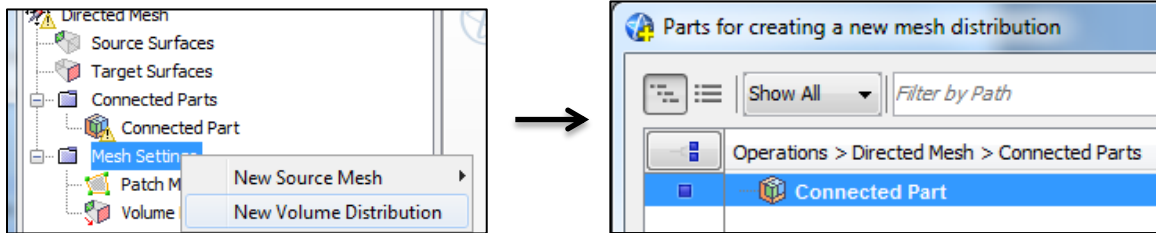


13. Divide the lines in a specific number of divisions and specify the distribution of each line

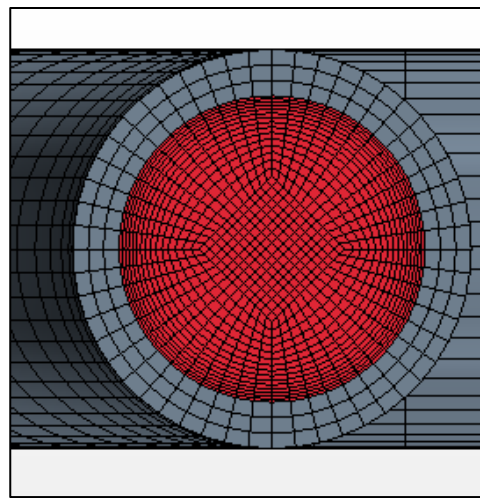
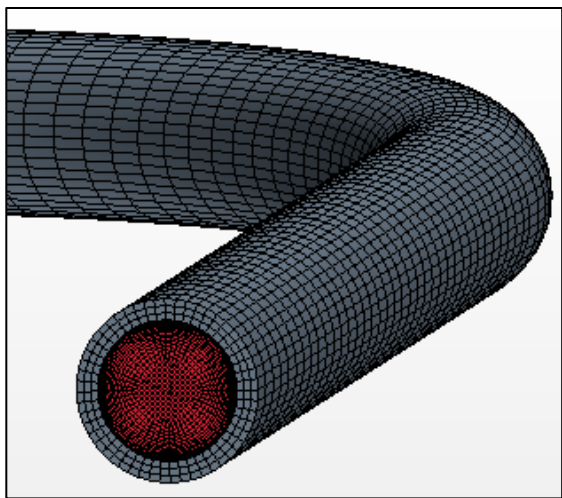
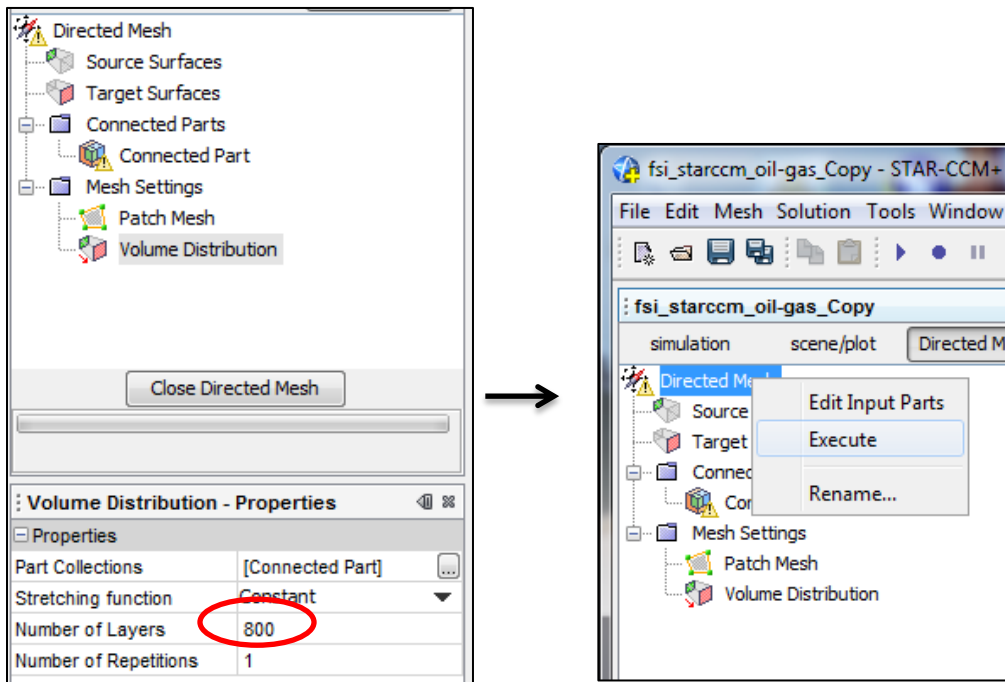
- Number of divisions
- Type of distribution: constant, One Sided Geometric, One Sided Hyperbolic, or Two Sided Hyperbolic



14. Create Volume Distribution to repeat the patch along the path of the jumper



15. Specify the number of layers of the patch along the length of the jumper



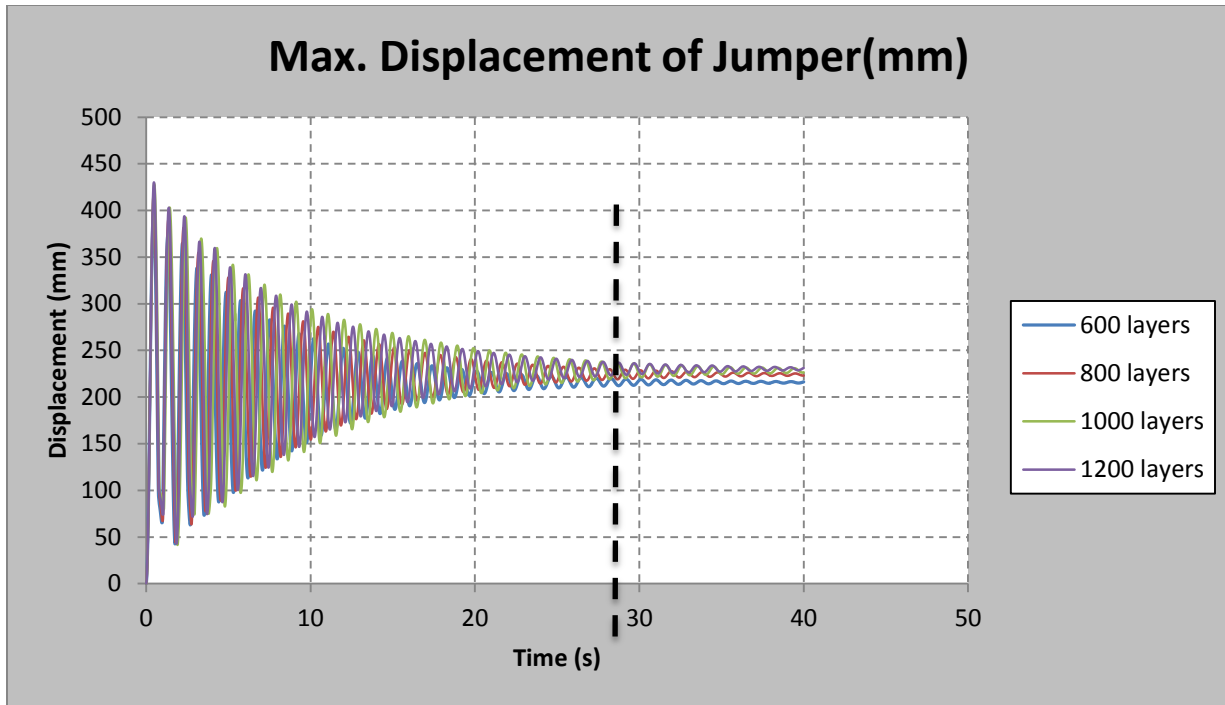


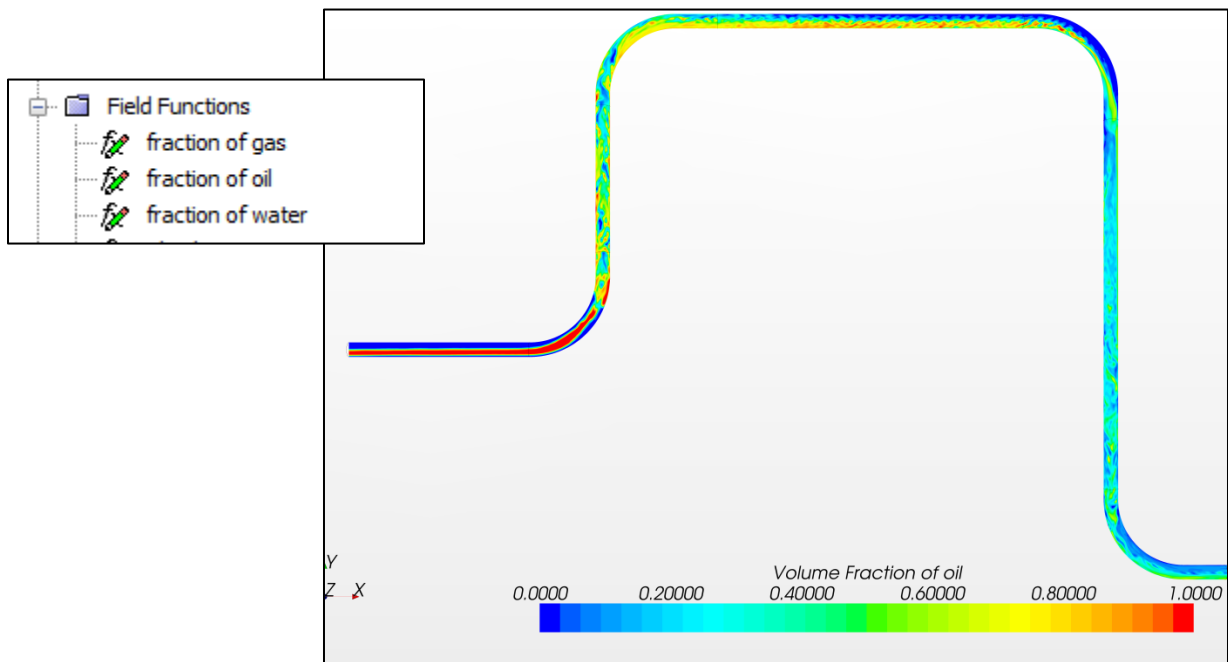
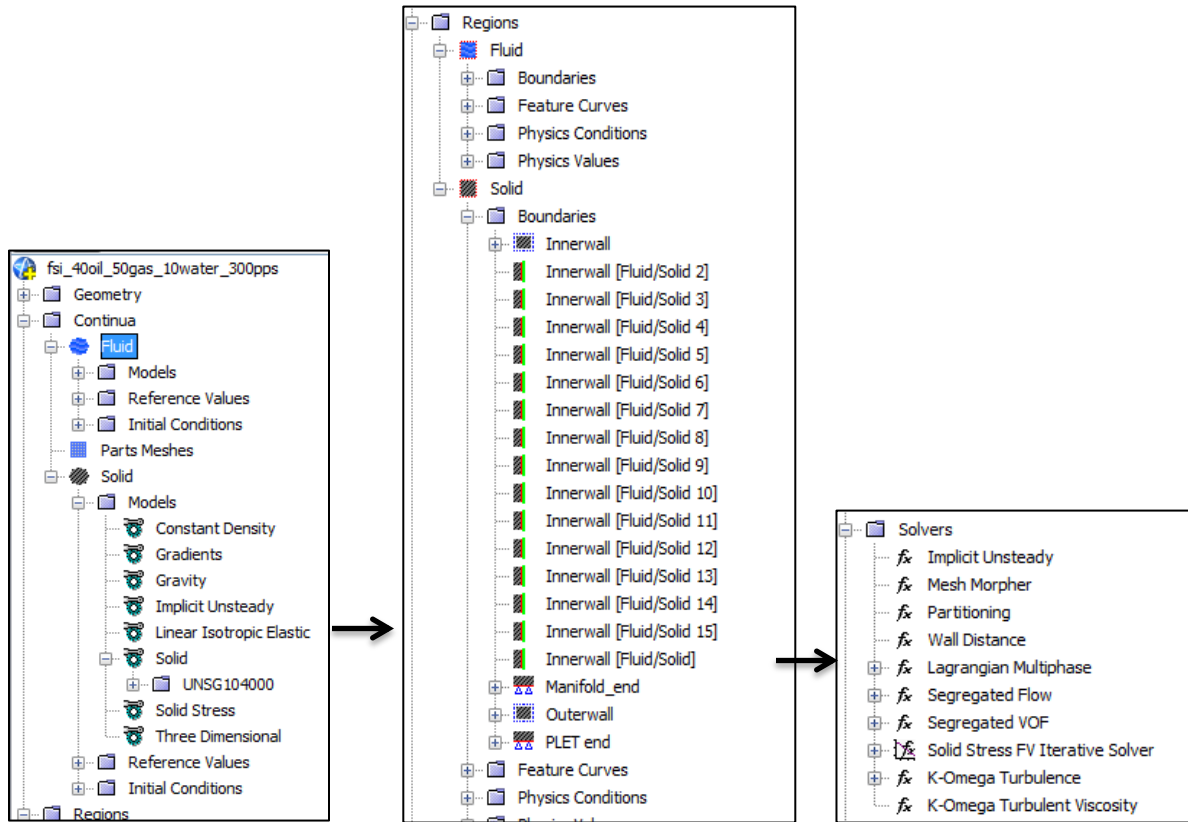
Figure 77. Comparison of Maximum Displacement using different number of mesh divisions along the jumper

Table 23. Mesh sensitivity results varying the number of mesh divisions along the jumper

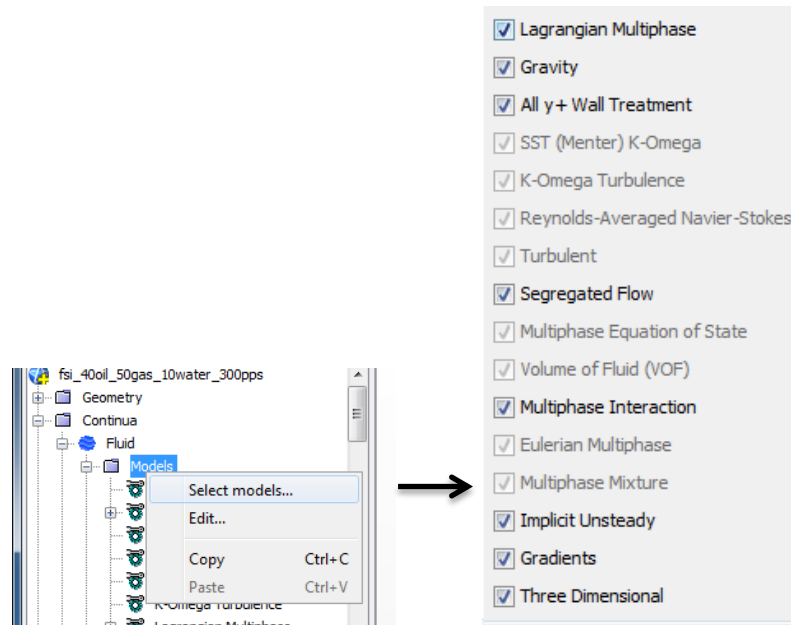
No. of Divisions	600	800	1000	1200	1500
Mean Displacement (mm)	213.0	221.2	225.3	227.3	229.0
% Difference in Displacement		3.80	1.81	0.89	0.75
Mean Stress (MPa)	199	208	214	217	NA
% Difference	4.80	2.84	1.32	0.89	NA

Appendix D: Setting up the Lagrangian Particles in STAR-CCM+

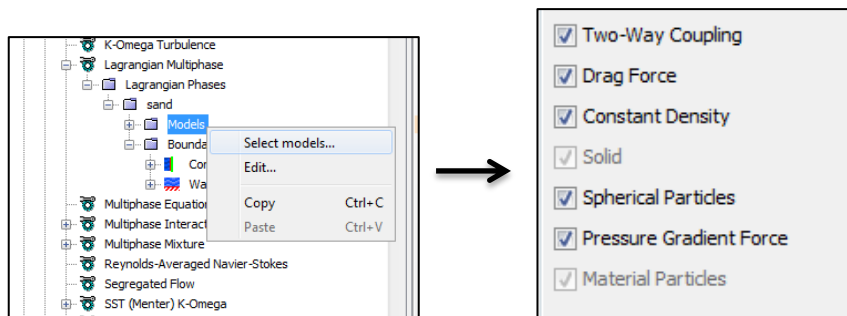
1. Set up three-phase flow with meshing, physics, monitors, stopping criteria, etc.



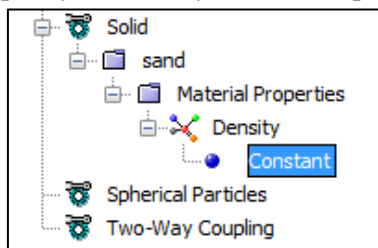
2. Select the physics models for 3-phase flow with solid particles



3. Create a lagrangian phase to specify the physics models of the solid

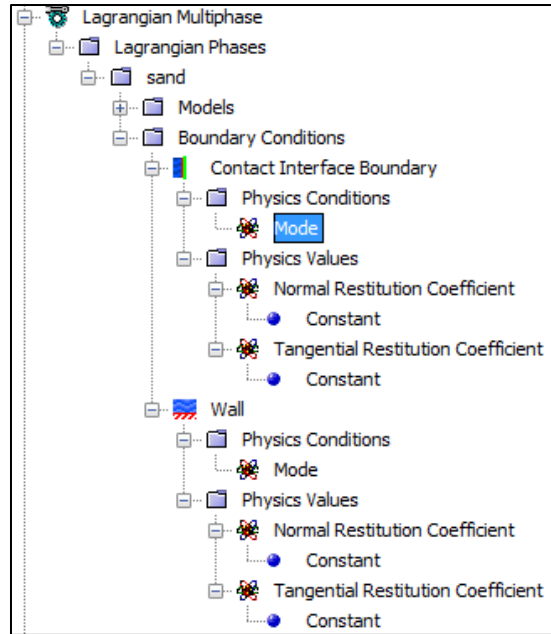


4. Specify the density of the sand particles to be 2650 kg/m³

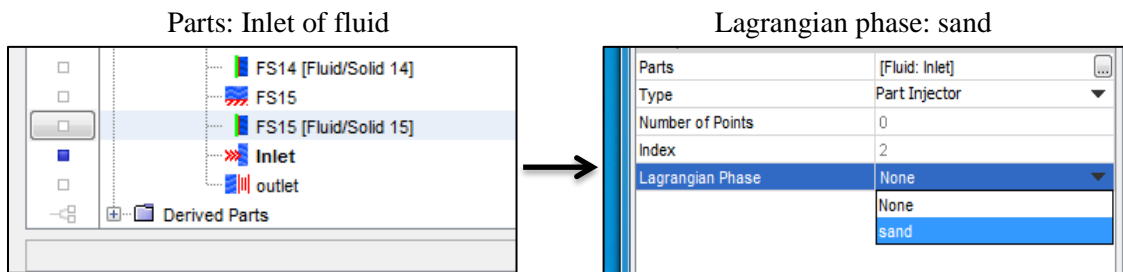
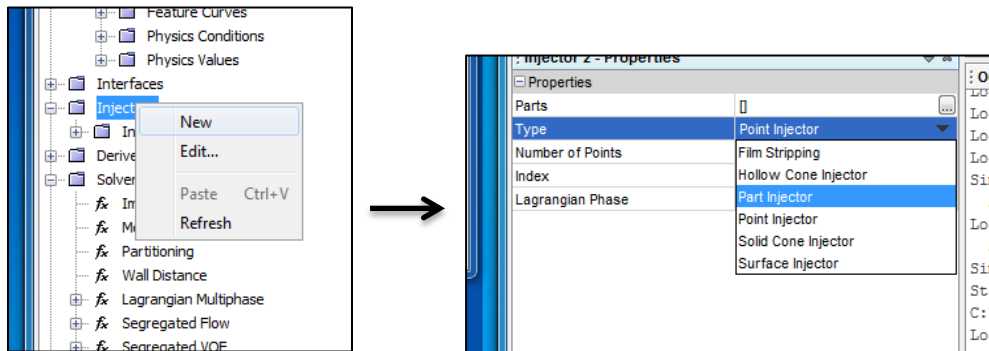


5. Specify the boundary conditions for the solid particles as follows:

- Mode: Rebound for both particle-particle interaction and wall-particles interaction
- Normal and Tangential Restitution Coefficient: 1.0 (Completely elastic)



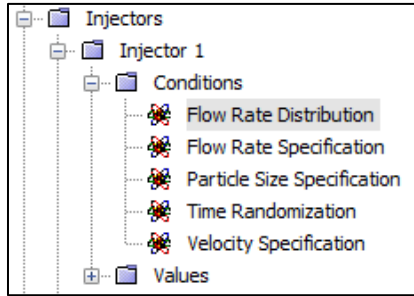
6. Create a “part injector” to introduce particles in the pipe



7. Physics conditions of the solid particles

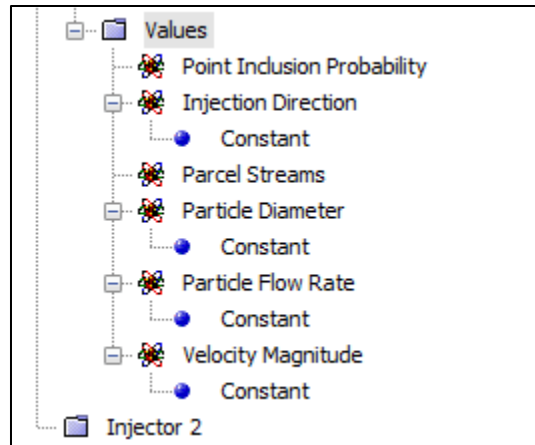
- Flow Rate Distribution: Per Injector
- Flow Rate Specification: Particle Flow Rate
- Particle Size Specification: Particle Size
- Time Randomization: uncheck

- Velocity Specification: Magnitude and direction

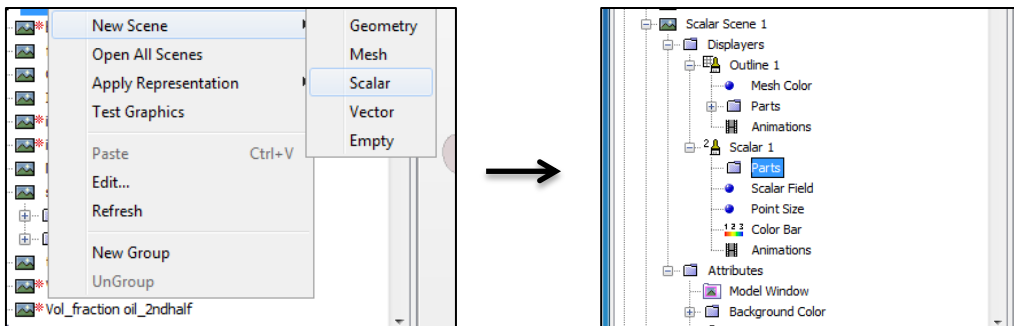


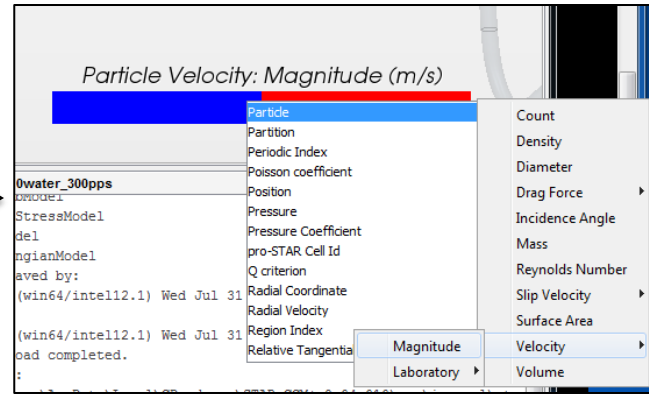
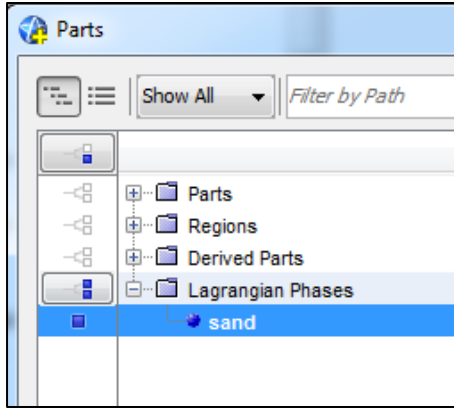
8. Specify the values of the flow conditions as follows:

- Injection Direction: [1.0, 0.0, 0.0]
- Particle Diameter: 6.0E-4 m
- Particle Flow Rate: 300.0 particles/second
- Velocity Magnitude: 0.0 m/s



9. Create a Scene to display flow of particles in post-processing





Check Surface in Outline to display the undeformed shape of the jumper

